

THESIS



3 1293 00383 8863

MICHIGAN STATE UNIVERSITY
LIBRARY



This is to certify that the

thesis entitled

AN INVESTIGATION OF ACOUSTIC EMISSION FROM COATED
AND UNCOATED IONIC CRYSTALS

presented by

ROBERT T. SEDGWICK

has been accepted towards fulfillment
of the requirements for

Ph.D. degree in Doctor of Philosophy
in Mechanics

Major Professor

Dr. T. Triffet

Date 14 October 1965

ADULT USE ONLY

[REDACTED]

MICHIGAN STATE UNIVERSITY
LIBRARY

[REDACTED]

[REDACTED]

ABSTRACT

AN INVESTIGATION OF ACOUSTIC EMISSION FROM COATED AND UNCOATED IONIC CRYSTALS

by Robert T. Sedgwick

Single crystals of LiF and KCl, some of which were coated with either NaCl or CaF₂, were subjected to incremental compressive stress along a $[100]$ direction. A continuous record of stress and strain was kept together with data from ultrasonic damping and acoustic emission measurements. The experimental techniques and the electronic equipment used are discussed in detail.

It was found that the presence of a thin surface film (500 Å) raised the entire stress-strain curve for KCl and increased the slope of the linear portion of the elastic range of the curve for LiF. This phenomenon, called the Roscoe effect, is attributed to dislocation pile-ups created when leading dislocations emanating from active sources are prevented by the film from leaving the crystal through the surface. The release of these pile-ups was evidenced by the large number of acoustic emission bursts following the removal of a film from its strained substrate crystal.

Both coated and uncoated specimens of LiF exhibited acoustic emission peaks in the macroscopic elastic range having their maximums at a strain of approximately $\epsilon_e = 10^{-3}$

and skewed toward larger values of ϵ . The analysis of this acoustic emission distribution forms the basis for a microscopic deformation model for LiF. It is hypothesized that this distribution should be identical to the distribution of dislocation source inverse loop-lengths. An expression for the probability of observing N acoustic emission bursts while the crystal is being strained from ϵ to $\epsilon + d\epsilon$ is written in terms of inverse loop-length and used to calculate average values of ϵ , ρ_M and (A_1/A_2) , the dislocation strain, mobile dislocation density and ratio of successive ultrasonic wave amplitudes, respectively. The effect of the thin films on the acoustic emission peak is discussed qualitatively and interpreted in terms of the model. Since no such peak was observed for KCl, the differences in the microscopic deformation mechanisms for that material are emphasized.

Finally, suggestions are made for further work concerned with the effects of thin films on the properties of substrate crystals and related acoustic emission phenomena.

AN INVESTIGATION OF ACOUSTIC EMISSION
FROM COATED AND UNCOATED IONIC CRYSTALS

By

Robert T. Sedgwick

A THESIS

Submitted to
Michigan State University
in partial fulfillment of the requirements
for the degree of

DOCTOR OF PHILOSOPHY

Department of Metallurgy, Mechanics
and Materials Science

1965

93824
72

ACKNOWLEDGEMENTS

I am greatly indebted to Dr. T. Triffet for his excellent guidance throughout this research project. Acting as both thesis advisor and chairman of my guidance committee, he held many discussions with me which were both helpful and encouraging

Thanks are also extended to my entire guidance committee for their constructive suggestions and interest in this work.

TABLE OF CONTENTS

	Page
ACKNOWLEDGEMENTS	ii
LIST OF FIGURES	iv
LIST OF APPENDICES	vii
I. INTRODUCTION	1
II. EXPERIMENTAL PROCEDURE	11
III. RESULTS	21
IV. DISCUSSION	44
A. Model for LiF	44
B. Skewed Acoustic Emission Distribution	48
C. Reversibility	69
D. Yield Point	70
E. Easy Glide and Work Hardening	71
F. Model for KCl	72
G. Effect of Thin Film on Dislocation Multiplication	75
H. Mobile Dislocation Density	77
I. Ultrasonic Damping	80
V. CONCLUSIONS	83
VI. SUGGESTIONS FOR FURTHER RESEARCH	86
BIBLIOGRAPHY	88
APPENDICES	92

LIST OF FIGURES

Figure	Page
1. Diagram of Experimental Arrangement	12
2. An Enlarged View of the Specimen	13
3. Schematic Diagram of Stress Transducer and its Bridge Circuit	15
4. Schematic Diagram of Strain Transducer and its Bridge Circuit	16
5. Schematic Diagram of Apparatus Used to Measure Internal Friction	17
6. Schematic Diagram of Equipment Used in Recording Acoustic Emissions	19
7. Schematic Diagram of Equipment Used in Counting Acoustic Emissions	19
8. Stress-time and Strain-time Curves	21
9. Compressive Stress-strain Curve for a LiF Single Crystal	23
10. Compressive Stress-strain Curve for an Unpolished KCl Single Crystal	24
11. Stress-strain Curves for LiF Specimens	25
12. Stress-strain Curves for KCl Specimens	26
13. Sketch of a Typical Acoustic Emission Burst	27
14. Acoustic Emission Histogram and Damping Data for Specimen 1	28
15. Acoustic Emission Histogram and Damping Data for Specimen 6	29
16. Acoustic Emission Histogram and Damping Data for Specimen 5	30
17. Acoustic Emission Histogram and Damping Data for Specimen 10	31
18. Acoustic Emission Histogram and Damping Data for Specimen 3	32

LIST OF FIGURES - continued

Figure	Page
19. Acoustic Emission Histogram and Damping Data for Specimen 8	33
20. Acoustic Emission Histogram and Damping Data for Specimen 10 Plotted Against a Contracted Strain Scale	34
21. Logarithmic Decrement Curves for LiF	36
22. Logarithmic Decrement Curves for KCl	37
23. Lattice Misfit Parameters	39
24. Sketch of Symmetrical Inverse Loop-length Distribution	46
25. Sketch of Skewed Inverse Loop-length Distribution	47
26. Skewness of Acoustic Emission Curve	52
27. Plots of Non-symmetrical Portion of Acoustic Emission Distribution	53
28. Breakdown of Total Acoustic Emission Distribution Curve	54
29. Relationship Between the Primary and Secondary Distribution	58
30. Similarity Between Acoustic Emission and Inverse Loop-length Probability Functions	59
31. Histogram of Acoustic Emissions Counted at Normal Trigger Level	73
32. Histogram of Acoustic Emissions Counted Just Above Noise Level	74
33. Stress-strain Curve for Specimen 1	94
34. Stress-strain Curve for Specimen 2	95
35. Stress-strain Curve for Specimen 3	96
36. Stress-strain Curve for Specimen 4	97

LIST OF FIGURES - continued

Figure	Page
37. Stress-strain Curve for Specimen 5	98
38. Stress-strain Curve for Specimen 9	99
39. Stress-strain Curve for Specimen 6	100
40. Stress-strain Curve for Specimen 7	101
41. Stress-strain Curve for Specimen 8	102
42. Stress-strain Curve for Specimen 10	103
43. Stress-strain Curve for Specimen 11	104
44. Logarithmic Decrement-strain Curve for Specimens 1, 3 and 4	105
45. Logarithmic Decrement-strain Curve for Specimens 6, 7 and 11	106

LIST OF APPENDICES

Appendix	Page
I. Specimen Identification Table	92
II. List of Equipment and Apparatus	93
III. Stress-strain and Logarithmic Decrement-strain Curves	94
IV. Raw Data	107

I. INTRODUCTION

A thin, solid film on the surface of a single crystal significantly affects certain of the crystal's mechanical properties. The initiation of plastic flow, the rate of work-hardening, and the shape of the entire stress-strain curve are influenced by the presence of such a film, the overall effect being a general strengthening of the crystal (1-5). This phenomenon was first noted by Roscoe (1) in 1934 and the effect bears his name. More recent work (3-27) has confirmed the existence of the Roscoe effect; but results of the later workers have not led to unanimous agreement concerning the mechanisms involved (18,24,25). Also, no mention is made in the literature of observations of the Roscoe effect on the elastic portion of stress-strain curves for linear elastic material. Nevertheless, such an effect, however small it may be, should exist and its study should be helpful in understanding the deformation mechanisms involved.

It is generally accepted that the strength of the film itself could not produce such a significant change in the mechanical properties of a macroscopic substrate crystal since, in general, a film thickness of only a few hundred angstroms is sufficient to produce the Roscoe effect. It is believed, therefore, that the thin film impedes dislocation motion and multiplication in the substrate crystal,

thus increasing its strength. Several theories have been presented which attempt to describe the nature of this interaction.

One states that a solid surface film inhibits the operation of dislocation sources which are near the crystal surface (14,18,19). Dislocation sources of this kind are known as Fisher-type sources (28). It is assumed that a random network of dislocations exists within the crystal and that when stress is applied, dislocation loops develop from segments of dislocation lines lying in favorably oriented slip planes. These loops expand and multiply according to the Frank-Read mechanism (29). Fisher pointed out that near the crystal surface many of these dislocation segments terminate at the surface and therefore are pinned only at one end. The average effective loop length of these surface sources is twice the average loop length of the interior sources and, therefore, they can operate at half the stress level necessary for the interior sources. Thus, a surface film could pin the free ends of the surface sources and in so doing raise the critical resolved shear stress necessary for dislocation multiplication.

Another theory proposed to explain the Roscoe effect assumes that dislocations emanating from interior sources are piled up by the surface film (10,11,13,16,21-24,27,30). This results in an n -fold increase in stress in the vicinity of the leading dislocation (31,32), where n is the number of dislocations in the pile-up. Although the theory predicts no effect on the critical resolved shear stress, an

increase in the rate of work-hardening can be expected as long as the film does not rupture or lose its adherence.

Of particular interest among the many observations which support the dislocation pile-up theory is the phenomenon known as the Barrett abnormal after-effect (33-36). If a single-crystal wire coated with a thin film is subjected to plastic deformation by torsion, it will tend to untwist when the applied torque is released. Barrett noted that if the film is removed immediately, the untwisting is abruptly reduced or even reversed. The phenomenon can be explained by the release of dislocations piled up against the film during the twisting process.

An additional contribution to the Roscoe effect can be attributed to the influence of the thin film upon the image force (37,38) of a dislocation near the crystal surface. This image force is caused by the reduction in strain energy of the dislocation stress field due to the absence of periodic structure beyond the crystalline surface. If no surface film is present, the image force which acts on a dislocation is always such that it attracts the dislocation toward the surface and such that the force increases as the dislocation approaches the surface. Thus, if a surface film has the effect of raising the strain energy experienced by a dislocation as it approaches the surface, its image force will be reduced. Head (39) noted that in order for dislocation motion to be inhibited by a thin film, its shear modulus must be greater than that of the substrate. Connors (40) has calculated the image force acting on an

edge dislocation approaching the coated surface of a crystal for various film thicknesses and various relative elastic properties of film and substrate material. It was found that the dislocation will pass through an equilibrium position provided c_{11} of the film is greater than c_{11} of the substrate.

Finally, Gilman (41) has stated that the Roscoe effect is observed only after substantial strain and that the effect is not primarily associated with yield phenomena; that is, the effect is mainly the result of post-yield conditions. His explanation of the Roscoe effect is that the film prevents screw dislocations from cross-gliding (42) near the surface, thereby affecting only the crystal's plastic behavior. This, of course, is in direct contradiction to the belief advanced here, that the effect of a thin film upon a linear-elastic substrate material should also be apparent in the elastic range.

As seen in the preceeding paragraphs, the attempts which have been made to explain the Roscoe effect are not in complete agreement. However, experimental results exist which support all of the theories. The present research was undertaken in order to gain further insight into the basic mechanisms underlying the Roscoe effect and to determine the extent to which the present theories are adequate. It was also felt that measurements should be extended to include the elastic range in order to determine whether or not the Roscoe effect could be observed in this region.

It is believed that the discrepancy reported in the

literature is partly due to the fact that much of the work has been performed on metallic specimens. It is well known that thin films greatly influence the mechanical properties of metals, but it is difficult to separate the effects of the film from the intrinsic mechanical properties of the substrate. This is due to the fact that metallic specimens are quite susceptible to oxide formation on their surfaces if exposed to air. Hence, it is very difficult to control film thickness and almost impossible to compare the mechanical properties of coated with uncoated crystals unless the specimens are exposed only to inert atmospheres. Even in this case little can be learned about the Roscoe effect on metallic specimens exposed to air, which is the case of interest.

In view of these difficulties, it seemed as though an understanding of the Roscoe effect might be attempted through a study of specimens whose surfaces are not readily oxidized; for example, ionic crystals. That is, an ionic crystal coated with a thin film should be used as a working model. Once the basic mechanisms involved in the process are understood, they can probably be applied to metals. In the present research, single crystal specimens of LiF and KCl coated with NaCl or CaF_2 were chosen to serve as the working models.

Some work concerning the Roscoe effect in ionic crystals has been reported. Phillips' experiments on LiF coated with various metallic films indicated that the films had no effect on the critical resolved shear stress; they did,

however, raise the strain hardening coefficient (26). He concluded from these results that Fisher-type sources (28) do not play a dominant role in the initiation of plastic flow in LiF crystals. Westwood (24) performed tests on LiF single crystals which had been coated with a coherent, reacted, alloyed layer of magnesium. He noted that the reacted coating prevented the operation of artificially introduced surface sources, thus raising the yield stress to a value sufficient to operate interior sources. The fact that such coatings had no effect on the yield stress of chemically polished LiF crystals with no artificial surface sources then led him to conclude that surface sources, although possibly important for the deformation of metal crystals, are not important for LiF. Furthermore, Westwood and Demer (23) employed etch-pit techniques in order to reveal the dislocation arrangement in reactive-coated LiF crystals after appreciable deformation. Photographs clearly indicated dislocation pile-ups beneath the surface layer.

Although the above remarks indicate that Fisher-type sources are not significant in LiF, other ionic crystals exist for which these sources possibly are of importance; for example, KCl (43). Clearly, if insight is to be gained into the mechanisms underlying the Roscoe effect through the study of coated ionic crystals, both substrate crystals for which surface sources may be important and those for which they probably are not should be used. The choice of KCl and LiF for the present work seems to be compatible with these requirements.

Furthermore, it should be of interest to study and compare specimens with and without natural macroscopic yield points; and it is known that LiF exhibits a well-defined yield point while KCl does not. In addition, the choice of these two substrate materials allows a comparison of specimens which exhibit a linear elastic region (LiF) with those which do not (KCl). The foregoing discussion also suggests that specimens having various ratios of elastic constants for the film and the substrate material should be compared. NaCl and CaF_2 were chosen for the film materials to be deposited on the LiF and KCl substrates in this case. Accepted values of c_{11} for KCl, NaCl, LiF, and CaF_2 are 3.98, 4.87, 9.90 and 16.44×10^{11} dynes/cm² (44) respectively.

Although it is known that varying the film thickness varies the mechanical properties of the substrate, it is believed that the basic dislocation mechanisms involved remain the same. Therefore, assuming that the films should be thick enough to create a marked effect in the mechanical properties of the substrate but thin enough to justify neglecting any contribution due to the compressive or tensile strength of the film itself, a nominal film thickness of 500 Å was chosen.

Many of the mechanical properties which are affected by the presence of a thin film are associated with the stress strain curve. In this work, specimens were deformed incrementally in compression and a continuous record of stress and strain was kept. Although it is desirable to compare stress-strain data obtained from coated specimens with data

obtained from uncoated specimens, a comparison of this type will not provide sufficient information to establish the dislocation mechanisms involved in the Roscoe effect. Additional measurements must be made which will help differentiate between the possible mechanisms mentioned above. Acoustic emission and ultrasonic damping measurements were selected here.

If dislocations in the substrate crystal pile up against the thin film as the specimen is being deformed, then removal of the film should allow these dislocations to escape; and if they escape in large bursts, as might be expected, it was felt that they could be detected by acoustic emission apparatus. Also, it was anticipated that an idea of the relative dislocation density within the substrate crystal could be obtained through ultrasonic damping measurements. A comparison of such measurements made on coated and uncoated specimens should indicate whether or not the presence of a thin film causes an increase in dislocation density.

In view of the facts brought out in the preceding discussion, a general plan for the present research was developed. Following is a brief outline of the research as it was carried out. Its purpose was two-fold; namely, to gain a better understanding of the basic dislocation mechanisms involved in the Roscoe effect, and to help clear up certain discrepancies which have been reported in the literature concerning this effect.

As stated above, it was decided to use single-crystal

specimens of LiF and KCl, some of which were coated with thin films (approximately 500 Å) of NaCl or CaF₂. The specimens were deformed incrementally in compression and a continuous record of stress and strain kept.

After each loading increment, ultrasonic damping measurements were recorded, using the single-transducer, pulse-echo technique. The information obtained from these measurements provided a means of estimating the relative dislocation density within the substrate crystals.

Finally, acoustic emissions emanating from the specimens during each load increment and for a short time thereafter were recorded on tape. A laminated ADP piezoelectric crystal was attached to the surface of the specimen; and during the deformation process, sound waves emanating from the specimen were transformed to electrical signals which were amplified, filtered, and recorded on tape. The tape was then played back to an electronic counter, so that what are here called acoustic emissions are actually those electrical signals which are significantly above the background noise level. It is believed that these acoustic emissions originate from elasto-plastic waves resulting from dislocation avalanches produced by the sudden release of piled up groups.

Acoustic emission measurements also provided a means of determining whether or not the thin films were responsible for these pile-ups. Certain coated specimens were held at a constant stress while their films were etched away. Thus, any dislocations piled up against the film

were allowed to escape through the surface and the acoustic emissions due to these dislocation avalanches were recorded.

The results of these observations will be presented and discussed following a more detailed description of the experimental procedure.

II. EXPERIMENTAL PROCEDURE

A diagram of the experimental arrangement is given in Figures 1 and 2. Single crystals of LiF and KCl were obtained from the Harshaw Chemical Co. (Cleveland, Ohio) in the as-cleaved condition. The dimensions of these crystals were $1/2$ in. \times $1/2$ in. \times $1-1/2$ in. with all faces having 100 orientation. Thin films (approximately 500 Å) of CaF_2 or NaCl were vacuum deposited on one or two faces of each crystal by Optics Technology, Inc. (Belmont, California) according to the specimen identification table in Appendix I. Some of the specimens were left uncoated so that a comparison could be made of data obtained from coated and uncoated crystals.

The coated specimens were deformed in compression by equal increments of stress in a specially designed testing machine. Load was measured by means of a circular load ring with four type A-5, SR-4 strain gages symmetrically attached to the two inner and outer faces of the ring along the horizontal diameter. This arrangement was similar to the ring-type tension link discussed by Perry and Lissner (45). Deformation was measured by two semi-circular thin beams constructed from spring steel with very sensitive solid state strain gages attached to their tension-side midpoints. These transducers were attached in such a manner as to measure cross-head motion and were connected in parallel in order

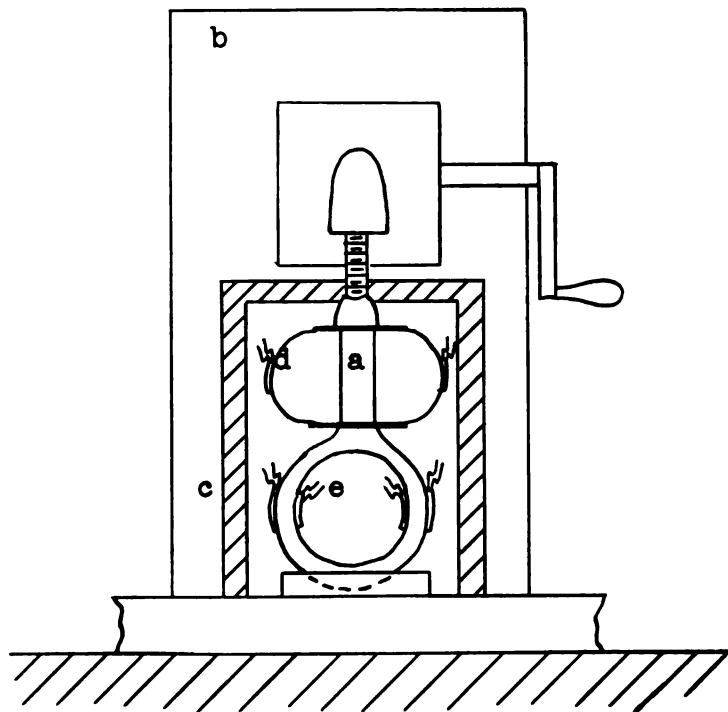


Figure 1. Diagram of Experimental Arrangement. The specimen (a) is situated in the testing machine (b). A section of the insulating box is shown at (c) while (d) and (e) are the solid state strain transducer and the stress transducer respectively. The leads shown go to the Sanborn recorder.

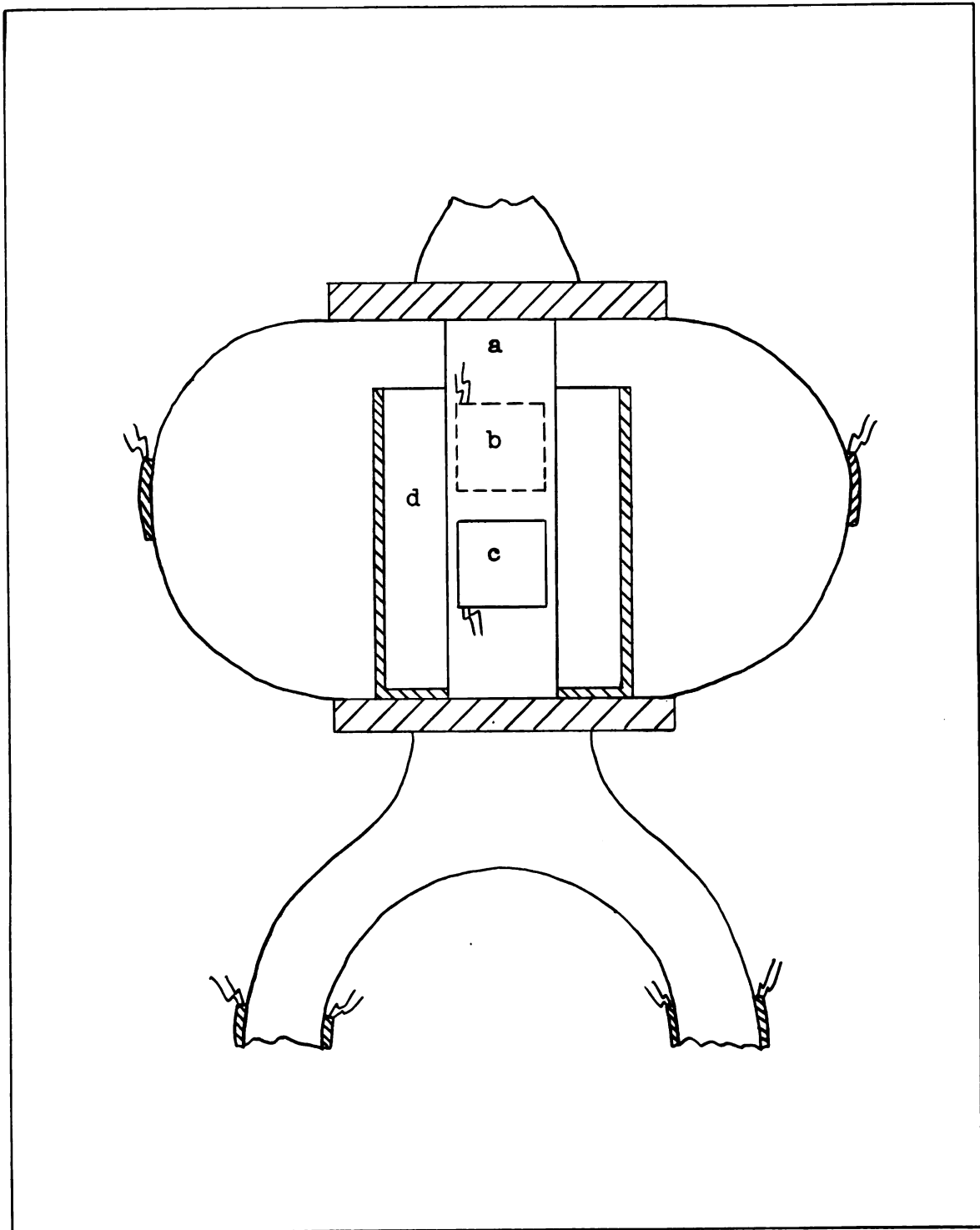


Figure 2. An Enlarged View of the Specimen. The specimen (a) is shown with the attached ADP crystal (b) and the ultrasonic quartz crystal (c). The leads go to the acoustic amplifier and the ultrasonic pre-amplifier respectively. A cross sectional view of the etchant reservoir is shown at (d).

to give a reading of average deformation. The circuitry involved in both load and deformation measurements consisted of separate bridge circuits, each containing a potentiometer in one of its arms. The bridge outputs were fed into a dual-channel Sanborn Recorder which was calibrated to read stress and strain. For a detailed analysis of the stress and strain transducer circuits, see Figures 3 and 4 and the equipment list in Appendix II.

The stress transducer was temperature-compensating but the strain transducer was not. Hence, both the specimen and the transducers were enclosed in an insulated box. All experiments were carried out at room temperature.

Ultrasonic damping measurements were made after each load increment was applied. The single transducer pulse-echo technique was employed to measure the damping along $\langle 100 \rangle$ directions parallel to the filmed surfaces. The transducer consisted of an x-cut quartz crystal (longitudinal waves) and the input pulse was supplied by an Arenberg Pulsed Oscillator. The ultrasonic circuit is shown in Figure 5 and the electronic equipment is identified in Appendix II.

Acoustic emissions from the specimens were recorded during and after each load increment on an FR 1100 Ampex tape recorder using precision tape. The acoustic emissions are believed to originate from elasto-plastic waves caused by an avalanche of dislocations as they either move through or out of the crystal. These waves are converted to electrical signals by means of a piezoelectric crystal and

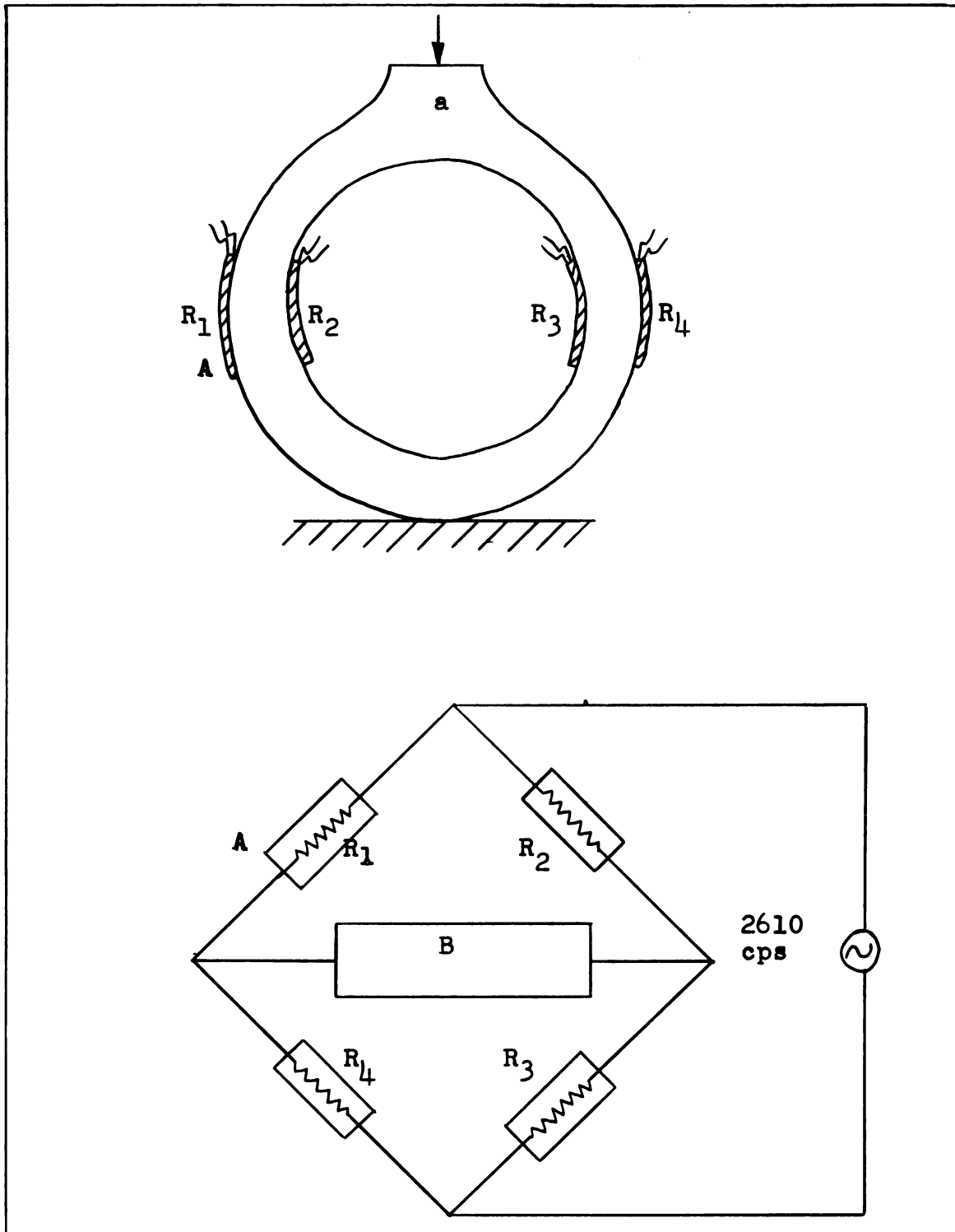


Figure 3. Schematic Diagram of Stress Transducer and its Bridge Circuit. The load ring (a) is shown with four SR-4 strain gages (A). The bridge circuit shows the arrangement of these gages together with the Sanborn recorder (B). The capital letters refer to equipment listed in Appendix II.

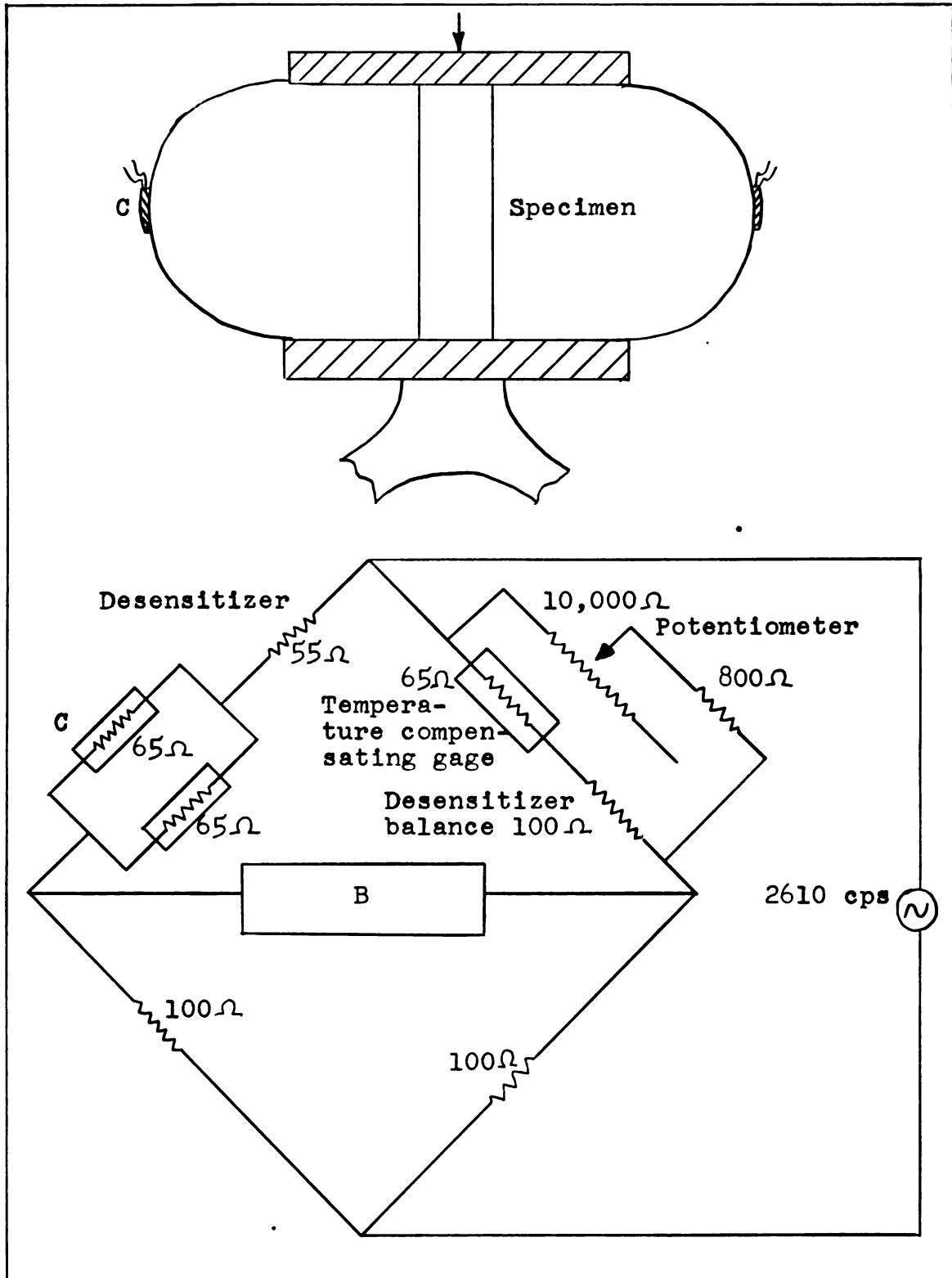


Figure 4. Schematic Diagram of Strain Transducer and its Bridge Circuit. Again the capital letters refer to equipment listed in Appendix II.

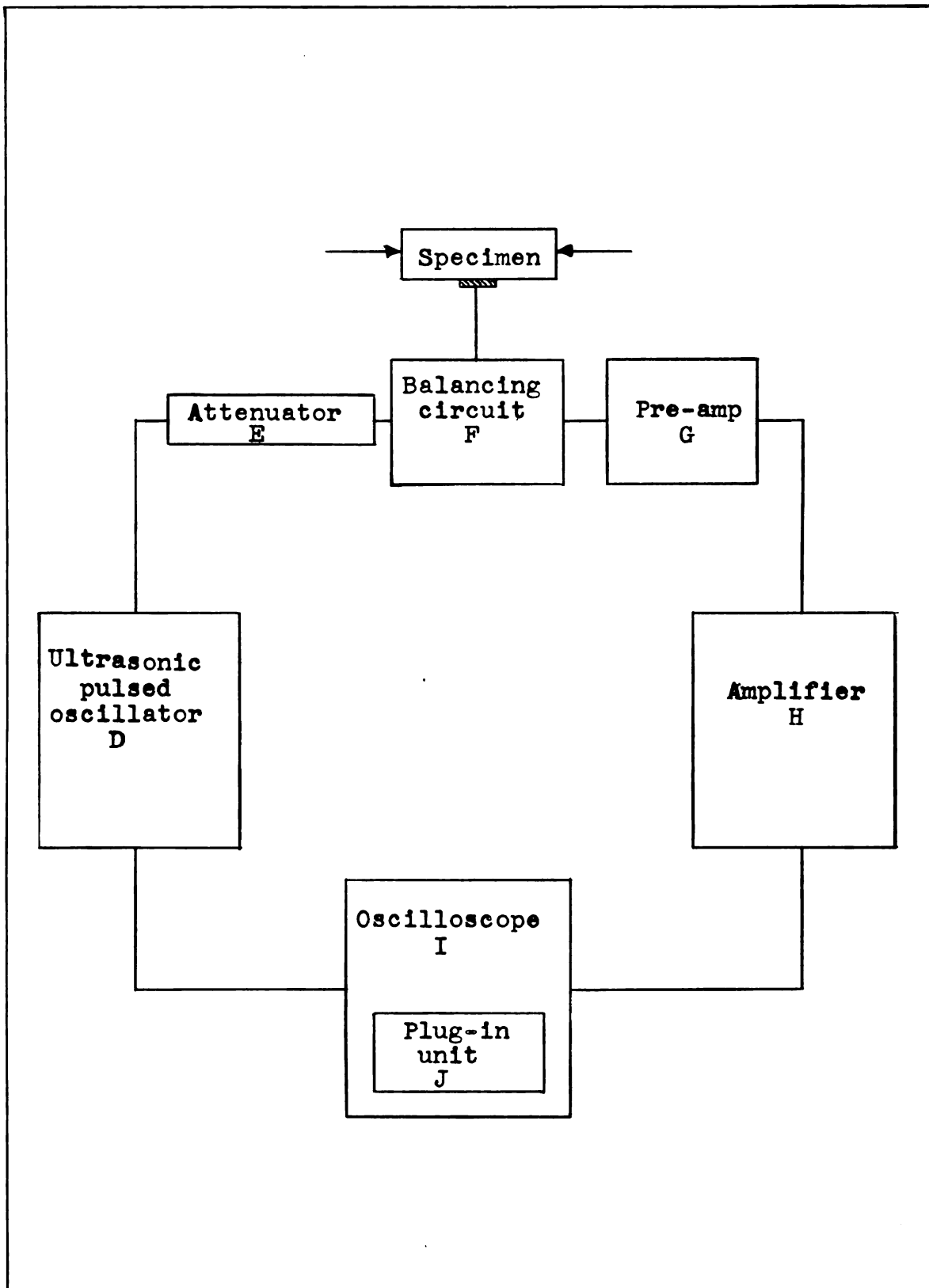


Figure 5. Schematic Diagram of Apparatus Used to Measure Internal Friction. The capital letters refer to the equipment list in Appendix II.

amplified. Only those electrical signals significantly above noise level are counted as acoustic emissions. A laminated ADP piezoelectric pick-up crystal was used for this measurement and was attached to the specimen opposite the ultrasonic transducer. This position had no observable effect on the damping measurements. The circuitry involved in both the recording of the acoustic emissions and the play-back of the tape are shown in Figures 6 and 7, respectively. Again, the equipment is identified in Appendix II. Since the signal from the ultrasonic equipment would have been picked up by the acoustical equipment, it was necessary to break the ultrasonic circuit whenever acoustical measurements were to be made, i.e. during each load increment and for a short duration thereafter, until all acoustical activity disappeared from the monitoring oscilloscope. Also, when ultrasonic measurements were being made, the tape recorder was turned off.

Care was taken to avoid the possibility of spurious noises being picked up by the acoustical system. The insulated box which enclosed the specimen isolated the ADP crystal from laboratory noises, which were held to a strict minimum. All experiments were performed between the hours of 12:01 A.M. and 5:00 A.M. when the laboratory was relatively quiet. Initial tests on non-crystalline polymer specimens indicated that the testing machine was quiet and that no spurious noise resulted from transducer slippage during straining.

The surface film was removed from certain specimens

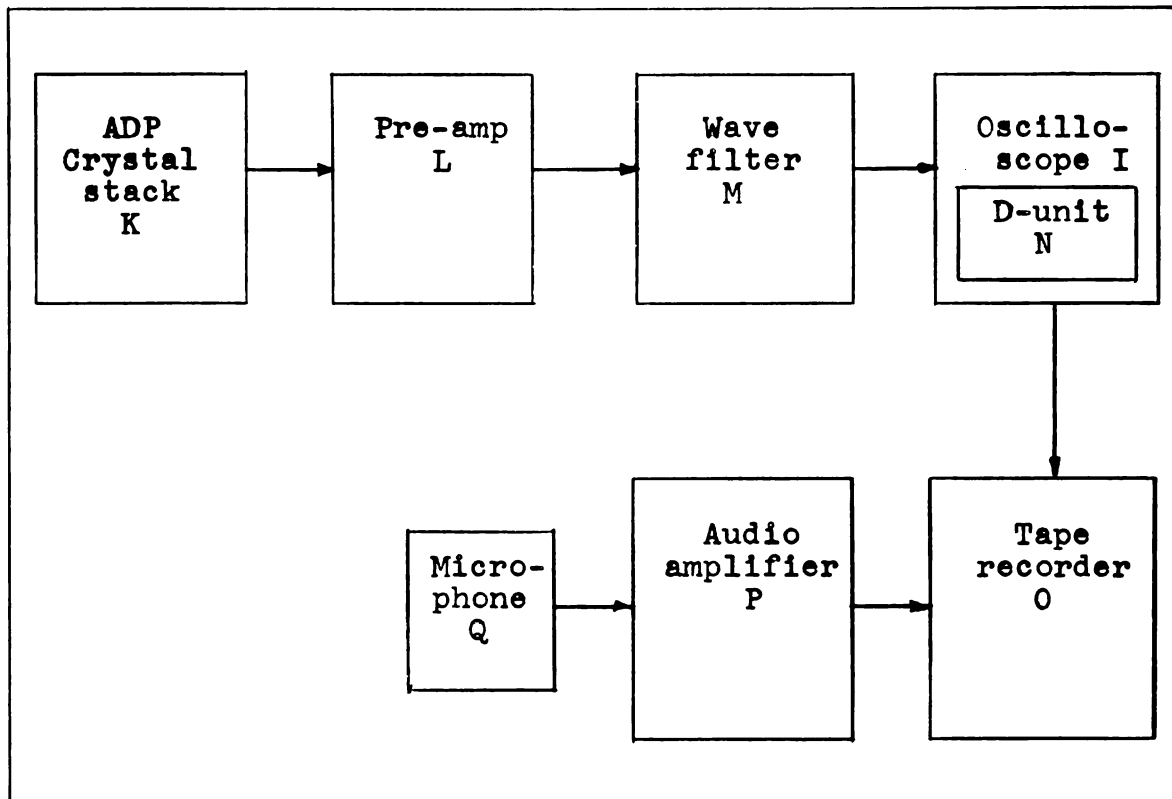


Figure 6. Schematic Diagram of Equipment Used in Recording Acoustic Emissions.

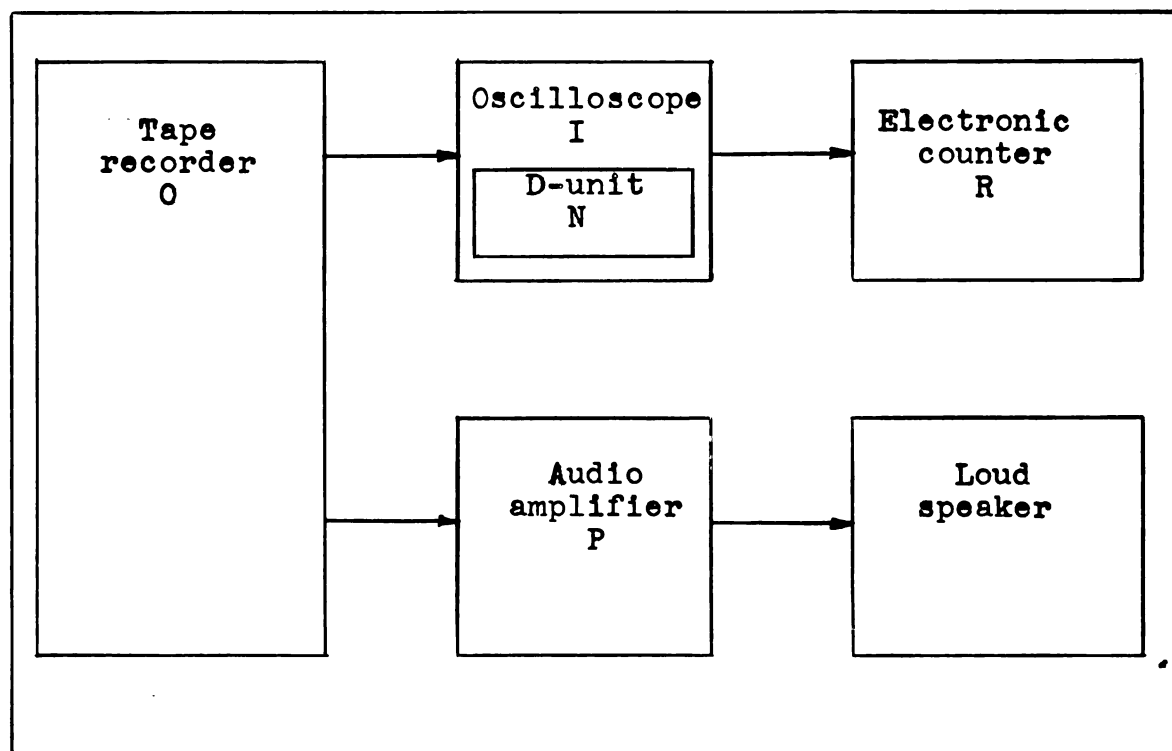


Figure 7. Schematic Diagram of Equipment Used in Counting Acoustic Emissions.

after appreciable strain had taken place. This was done by raising the level of an etchant in a semi-cylindrical glass tube attached to the filmed surface of the specimen. The specimens which were etched are indicated in Appendix I. The etchants used were distilled H_2O for the $NaCl$ films and concentrated H_2SO_4 for the CaF_2 films. Preliminary checks indicated that there was either a very low, easily identifiable noise or no noise at all introduced into the acoustical measuring system due to chemical action between the etchants and both the film and substrate material. In the case of a detectable noise, it was no higher than the general background noise level and hence did not interfere with the data-taking process.

III. RESULTS

A continuous record of stress versus time and strain versus time was kept for each specimen. However, since loading was done incrementally rather than at a constant strain rate, the stress-strain curve obtained was of a special nature. Figure 8 is a sketch of typical stress-time and strain-time curves for a single increment of loading as recorded on the Sanborn recorder. The values of σ

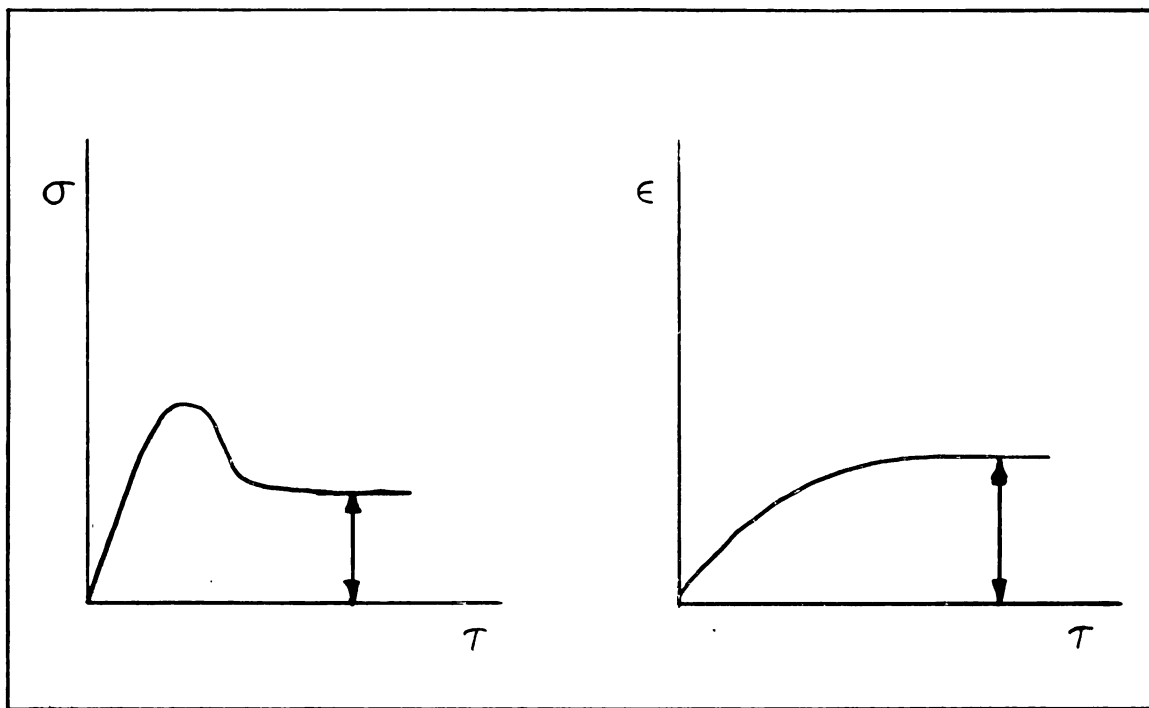


Figure 8. Stress-time and Strain-time Curves. The curves shown are for a single increment of loading.

and ϵ used to plot the stress-strain curve were those values taken from the leveled-off portion of incremental curves of the type shown in Figure 8. The stress-strain curves obtained in this manner are not expected to differ

significantly from the more conventional curves obtained when constant strain rate is used. They do, however, show more detail than standard, room-temperature curves such as those shown for LiF (46) and KCl (47) in Figures 9 and 10 respectively. The slope of the curve shown in Figure 9 is greater than that for some of the coated specimen curves of Figure 11, following. This may be due to a difference in specimen size or in strain rate. The specimen used to obtain the curve of Figure 9 was much smaller in size than those used for the plots in Figure 11 and was deformed at a greater strain rate. In fact, the strain rate used to obtain the curve of Figure 9 was $2 \times 10^{-4} \text{ sec.}^{-1}$ compared to an average value for strain rate of the order of $10^{-6} \text{ sec.}^{-1}$ used to obtain the curves of Figure 11. Figures 11 and 12 are incremental plots of stress versus strain for LiF and KCl respectively. Curves for specimens both with and without thin films are superimposed for comparison and are identified by number according to the specimen identification chart of Appendix I. The actual experimental points are plotted in Appendix III.

Acoustic emission data were also recorded for each specimen. The output from the ADP crystal was amplified and recorded on magnetic tape as shown schematically in Figure 6. The tape was then played back (see Figure 7) and an electronic counter was used to count the number of acoustic emissions of a given pulse height occurring during and shortly after each load increment. This number, N , gives a relative estimate of the actual number of acoustical

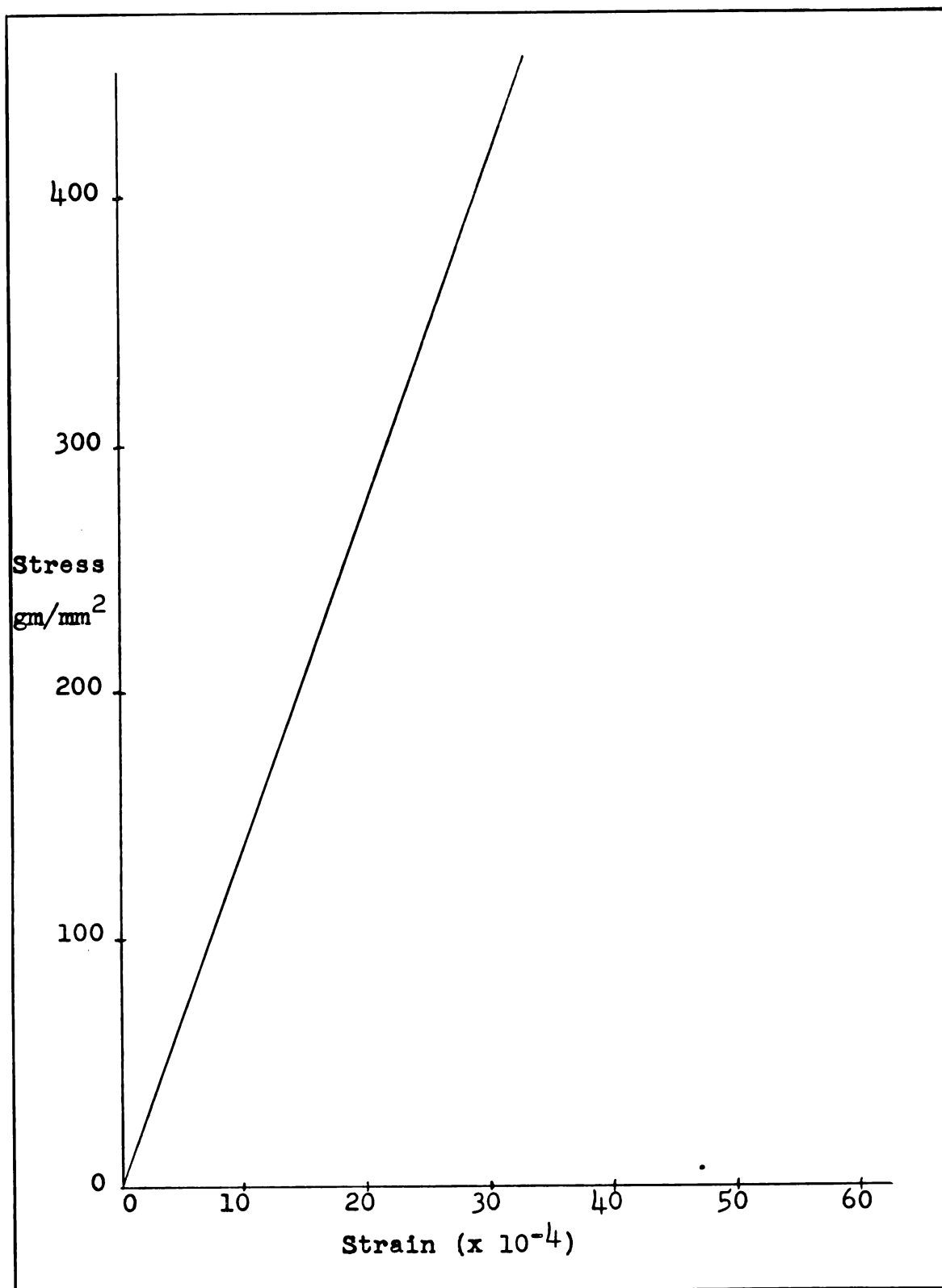


Figure 9. Compressive Stress-strain Curve for a LiF Single Crystal. This plot was taken from a stress-strain curve due to W. G. Johnston (46). The same reference shows that yield occurs at a stress of 700 gm/mm² and at a strain of 5×10^{-3} .

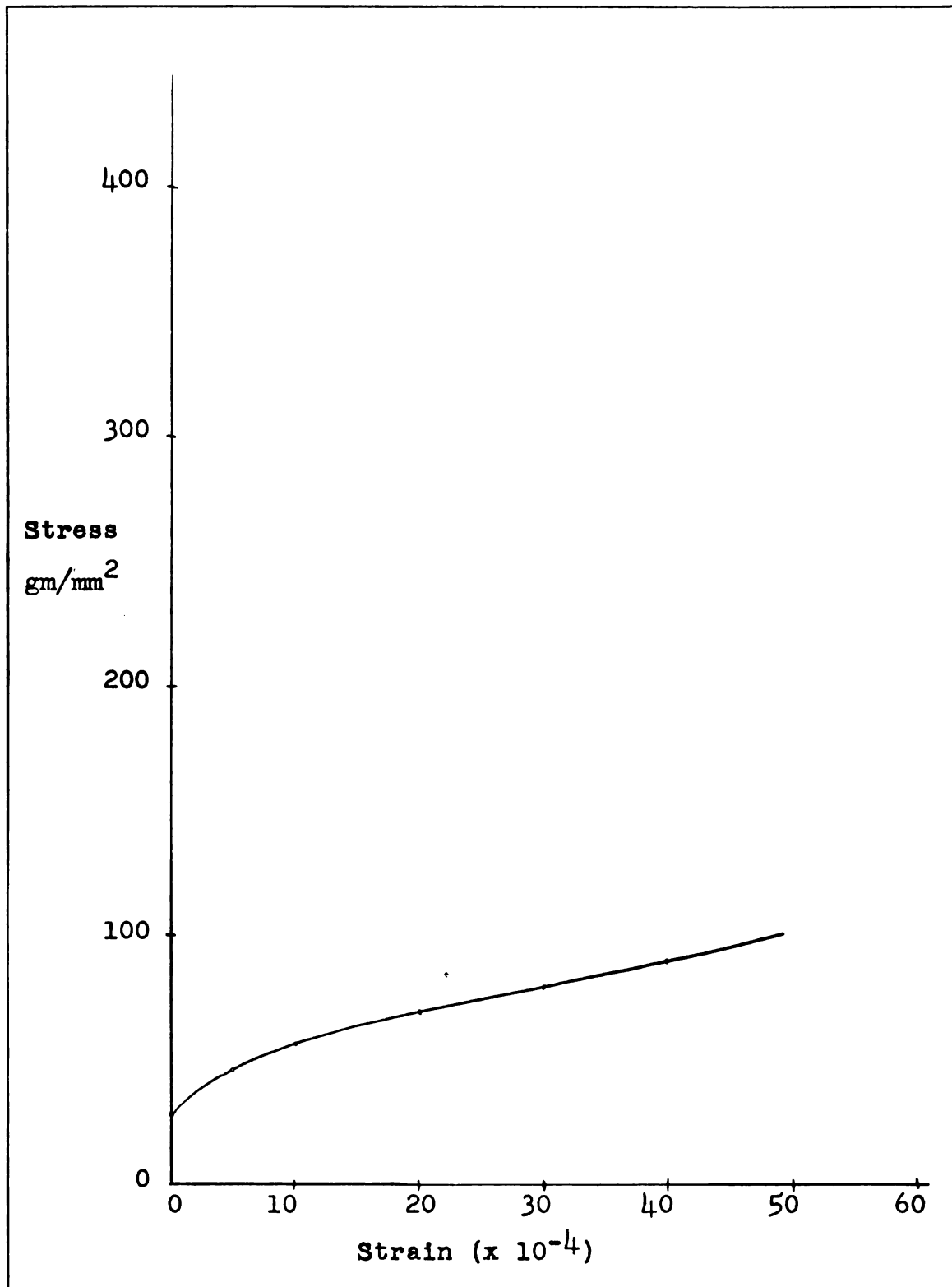


Figure 10. Compressive Stress-strain Curve for an Unpolished KCl Single Crystal. The points plotted here were read from a stress-strain curve due to T. Suzuki (47).

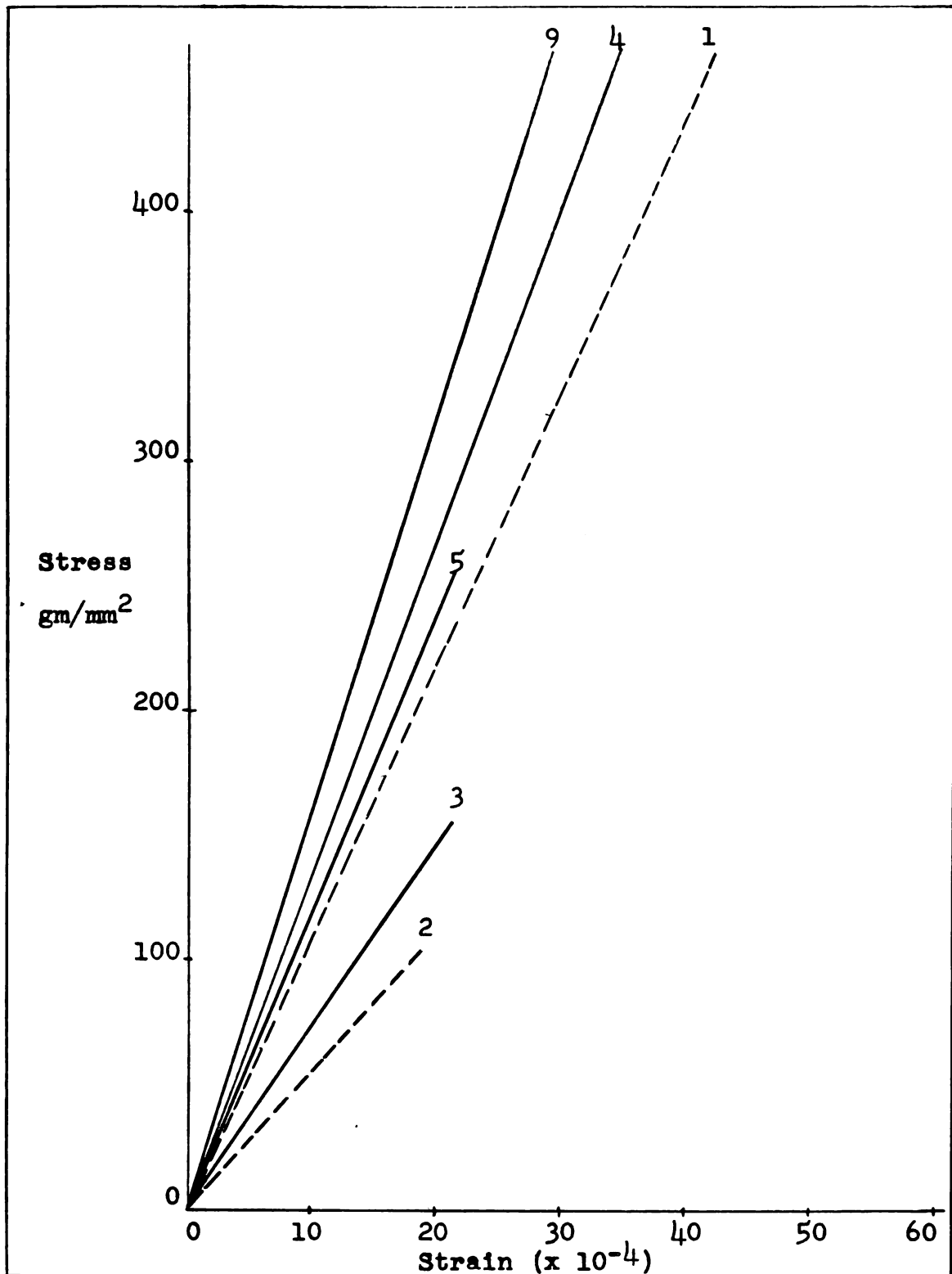


Figure 11. Stress-strain Curves for LiF Specimens. The number at the end of each curve identifies the specimen. The solid and dashed lines represent coated and uncoated specimens respectively. For actual experimental points, see Appendix III.

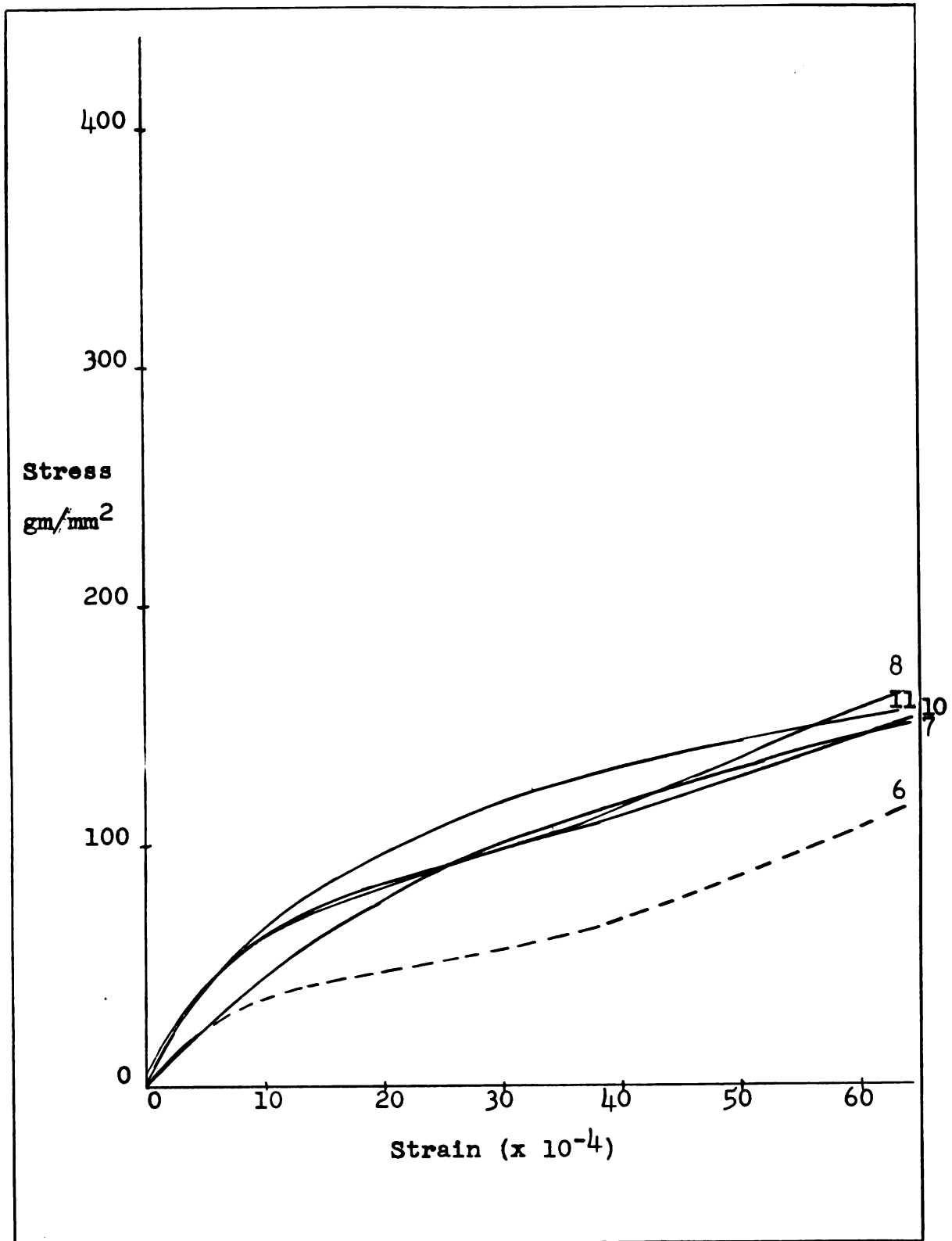


Figure 12. Stress-strain Curves for KCl Specimens. The number at the end of each curve identifies the specimen. The solid and dashed lines represent coated and uncoated specimens respectively. For actual experimental points, see Appendix III.

bursts; however, if more than one burst happened to occur at exactly the same instant they would be superimposed and therefore counted as only one. It is highly improbable that this occurrence would be regular enough to significantly change the values of N for any given load increment. A sketch of a typical acoustic burst is shown in Figure 13.

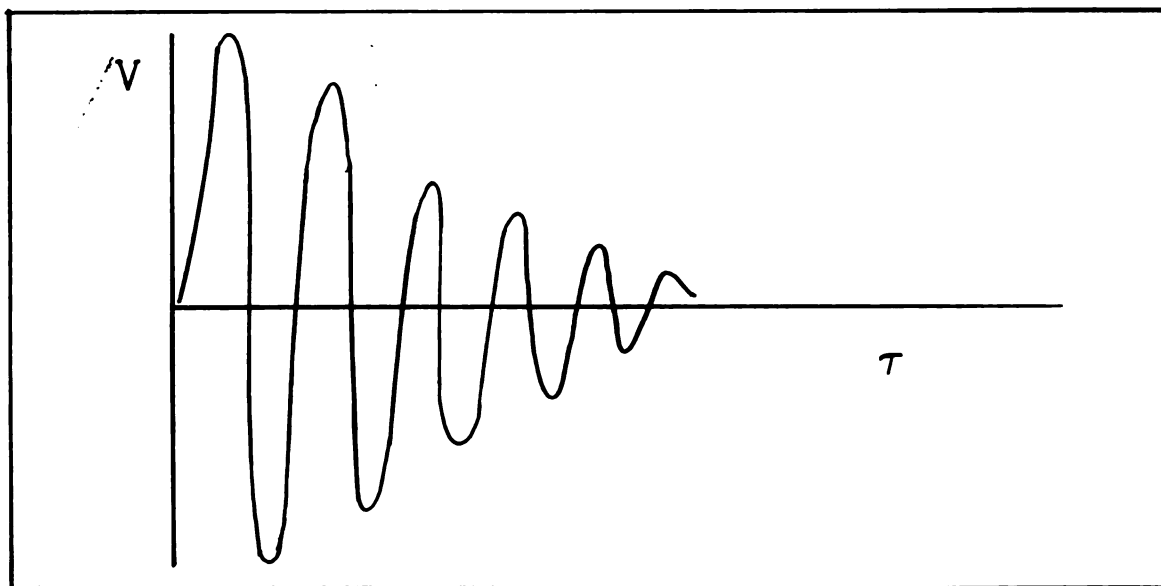


Figure 13. Sketch of a Typical Acoustic Emission Burst. Pulses of this type were seen on the monitoring oscilloscope during and after load increments and for a short time after film removal.

The symbol N represents the number of such bursts caused by a given load increment. Figures 14 and 15 are histograms of N superimposed upon stress-strain curves for uncoated LiF and KCl specimens respectively. For comparison, Figures 16 and 17 show respective plots of similar data for LiF and KCl specimens coated with NaCl. Also, Figures 18 and 19 show respective plots for LiF and KCl specimens coated with CaF_2 .

The final set of measurements recorded during these

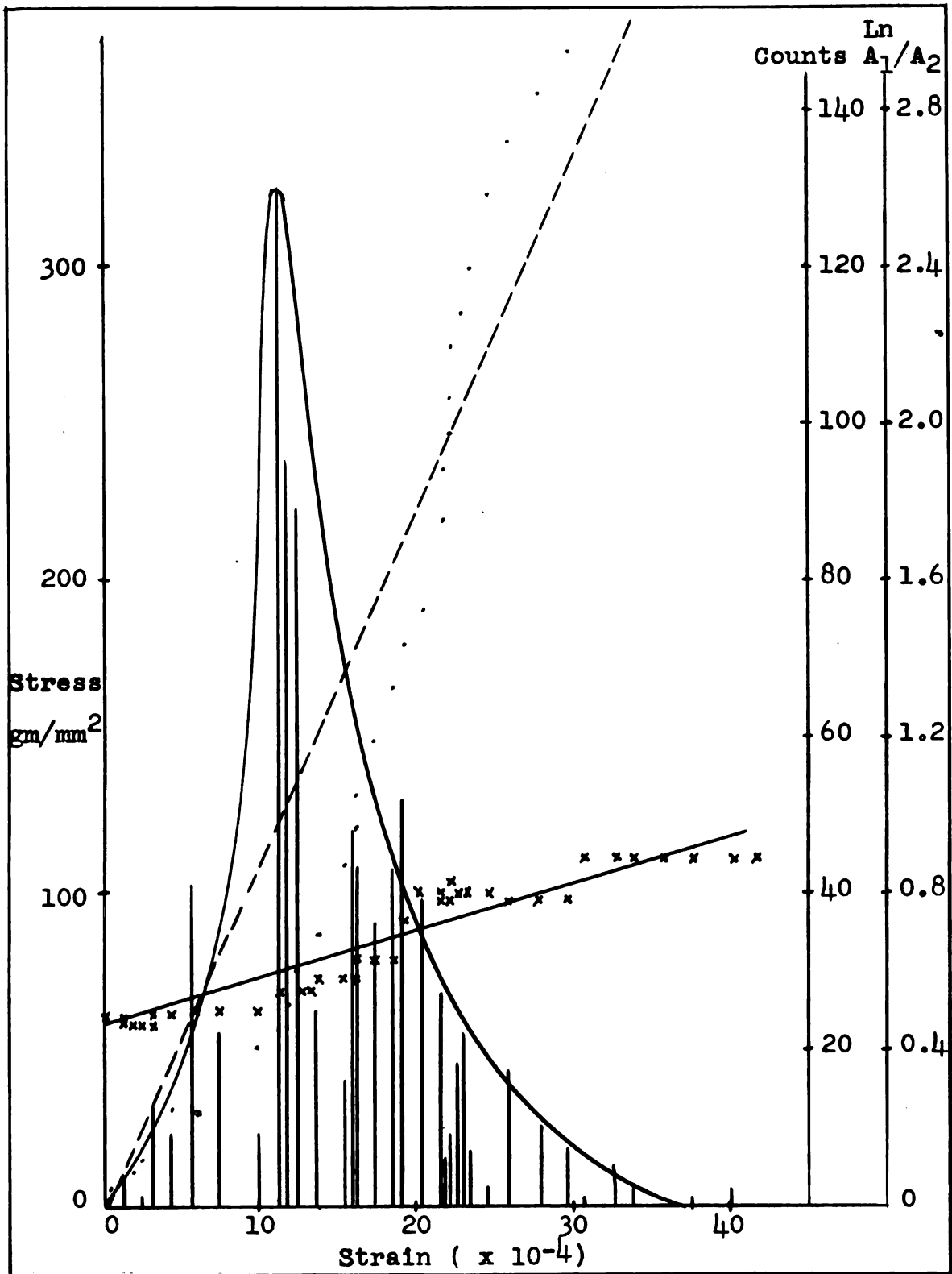


Figure 14. Acoustic Emission Histogram and Damping Data for Specimen 1. The acoustic emission histogram is superimposed upon the stress-strain curve and the log decrement curve (*) for specimen 1 (LiF, no film).

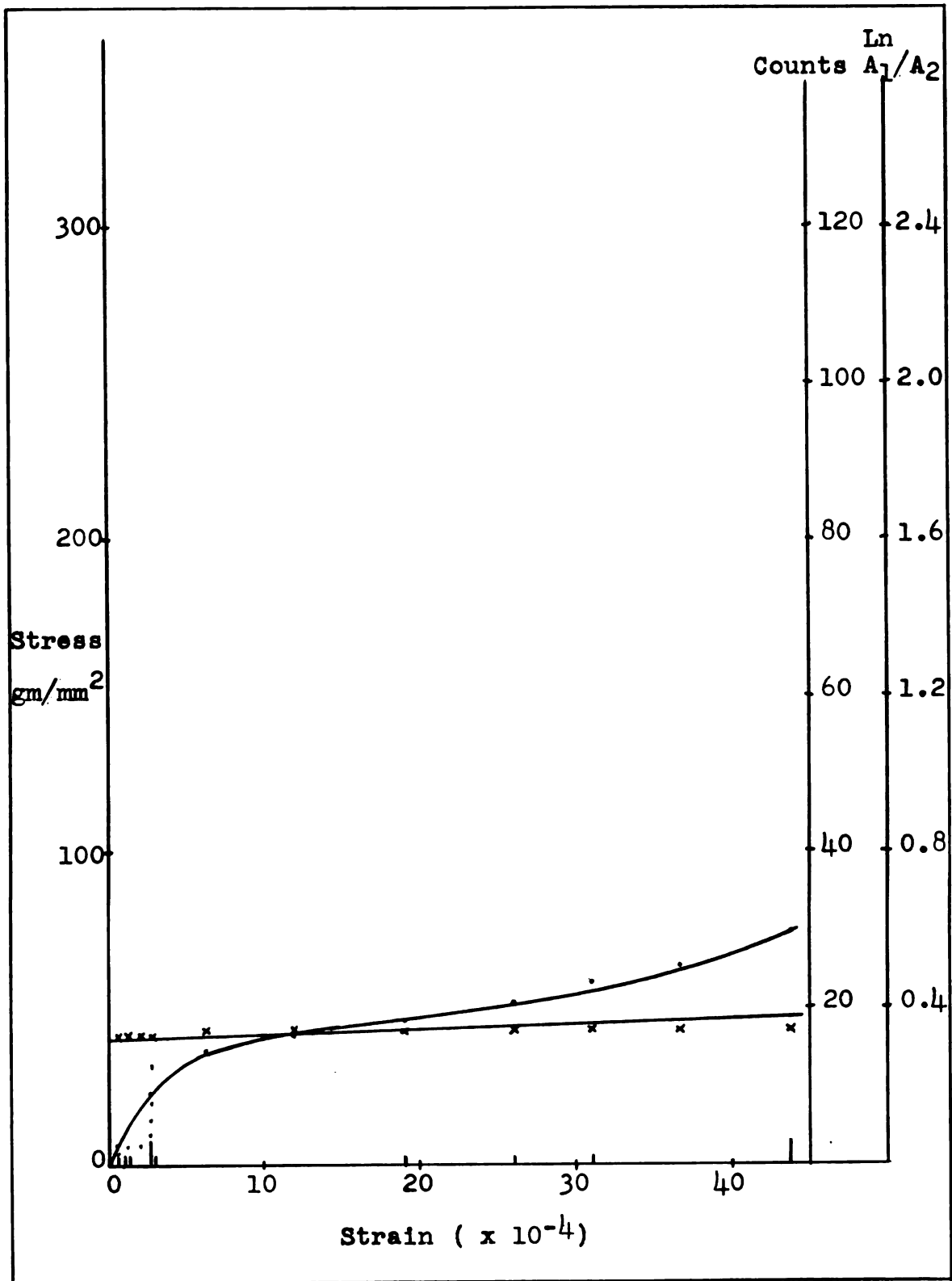


Figure 15. Acoustic Emission Histogram and Damping Data for Specimen 6. The acoustic emission histogram is superimposed upon the stress-strain curve and the logarithmic decrement curve (*) for specimen 6 (KCl, no film).

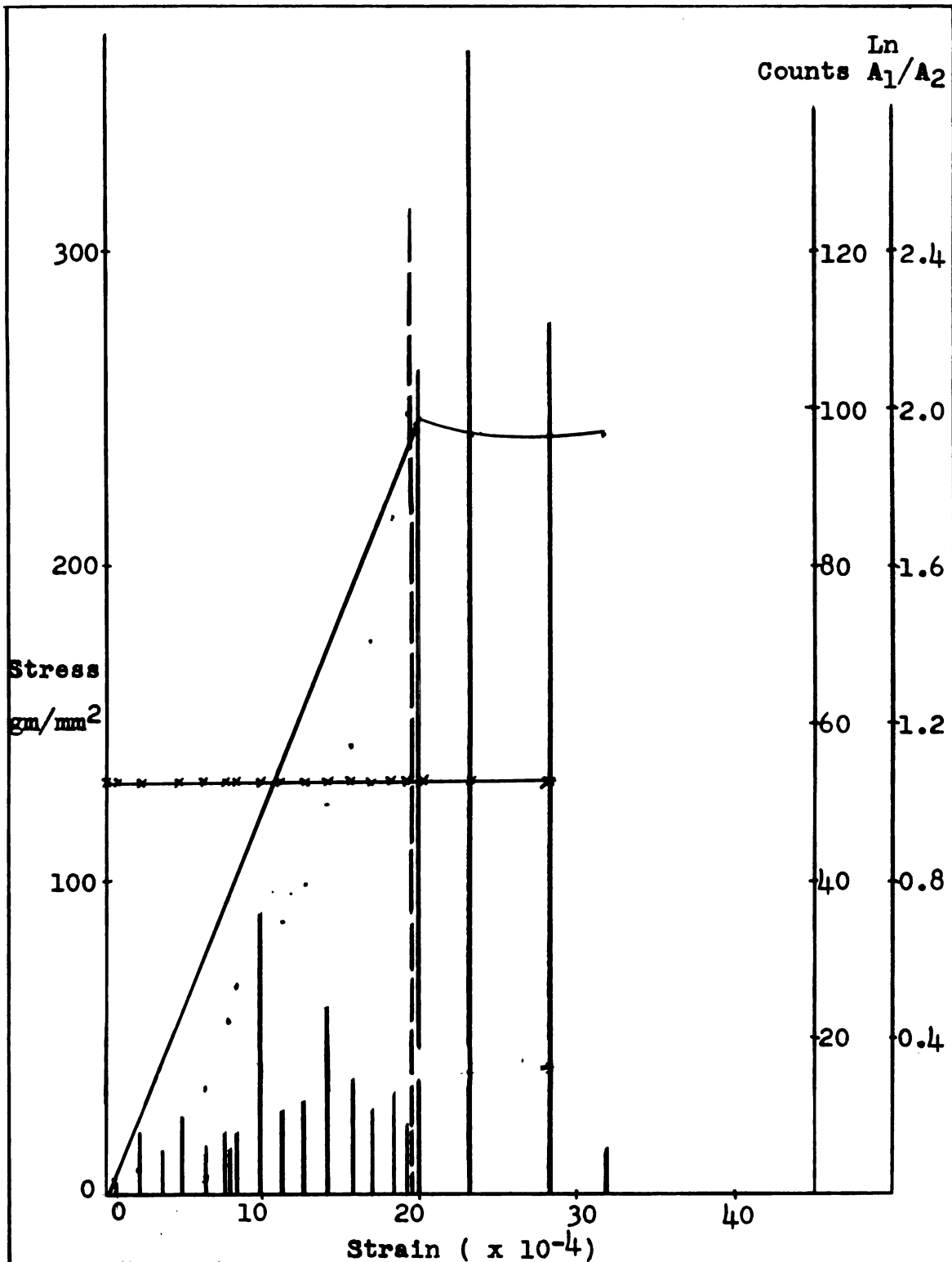


Figure 16. Acoustic Emission Histogram and Damping Data for Specimen 5. The acoustic emission histogram is superimposed upon the stress-strain curve and the logarithmic decrement curve (x) for specimen 5 (LiF, two NaCl films). The vertical dashed line indicates the value of strain at which the films were etched off.

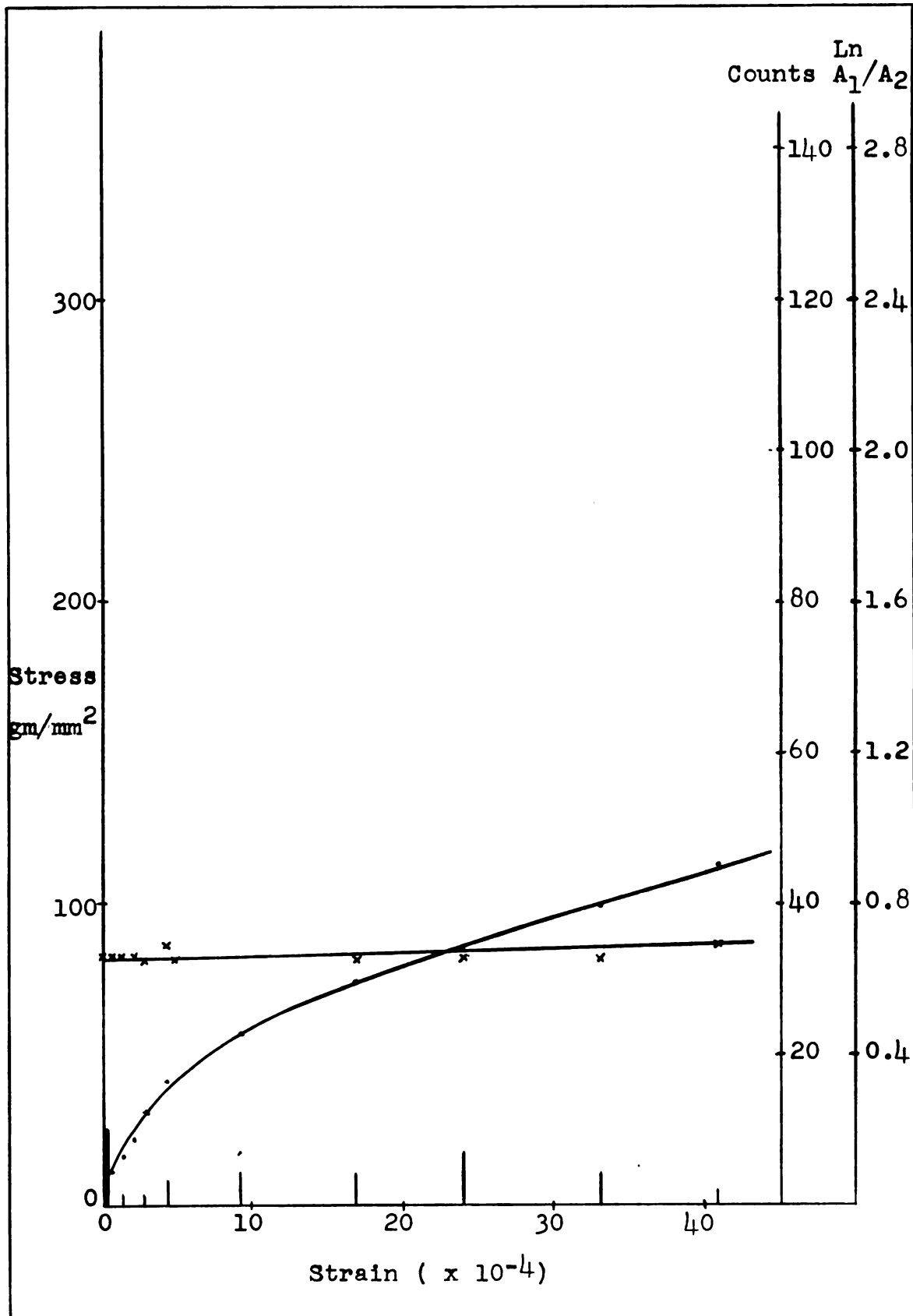


Figure 17. Acoustic Emission Histogram and Damping Data for Specimen 10. The acoustic emission histogram is superimposed upon the stress-strain curve and the logarithmic decrement curve (*) for specimen 10 (KCl, one NaCl film).

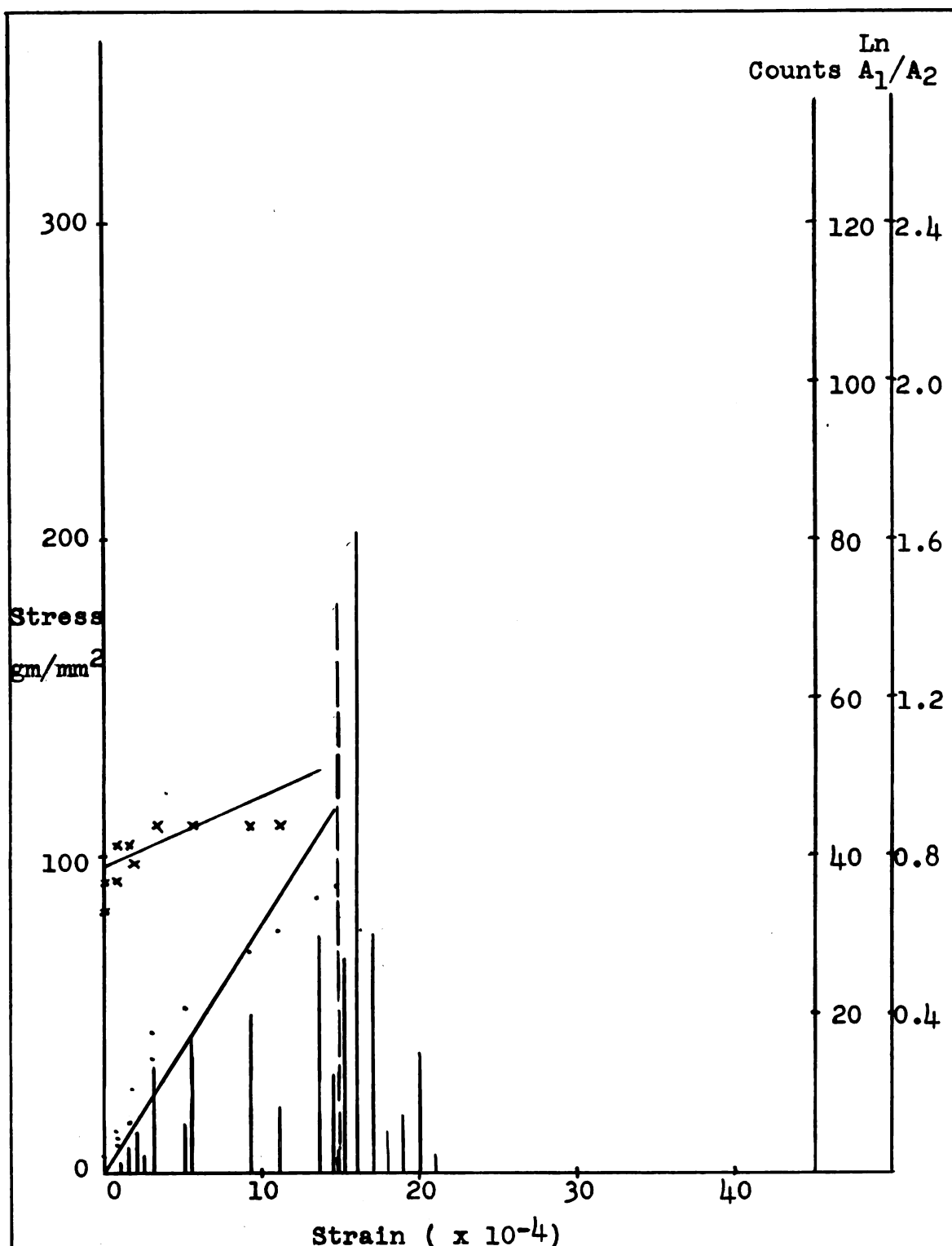


Figure 18. Acoustic Emission Histogram and Damping Data for Specimen 3. The acoustic emission histogram is superimposed upon the stress-strain curve and the logarithmic decrement curve (x) for specimen 3 (LiF, one CaF_2 film). The vertical dashed line indicates the value of strain at which the film was etched off.

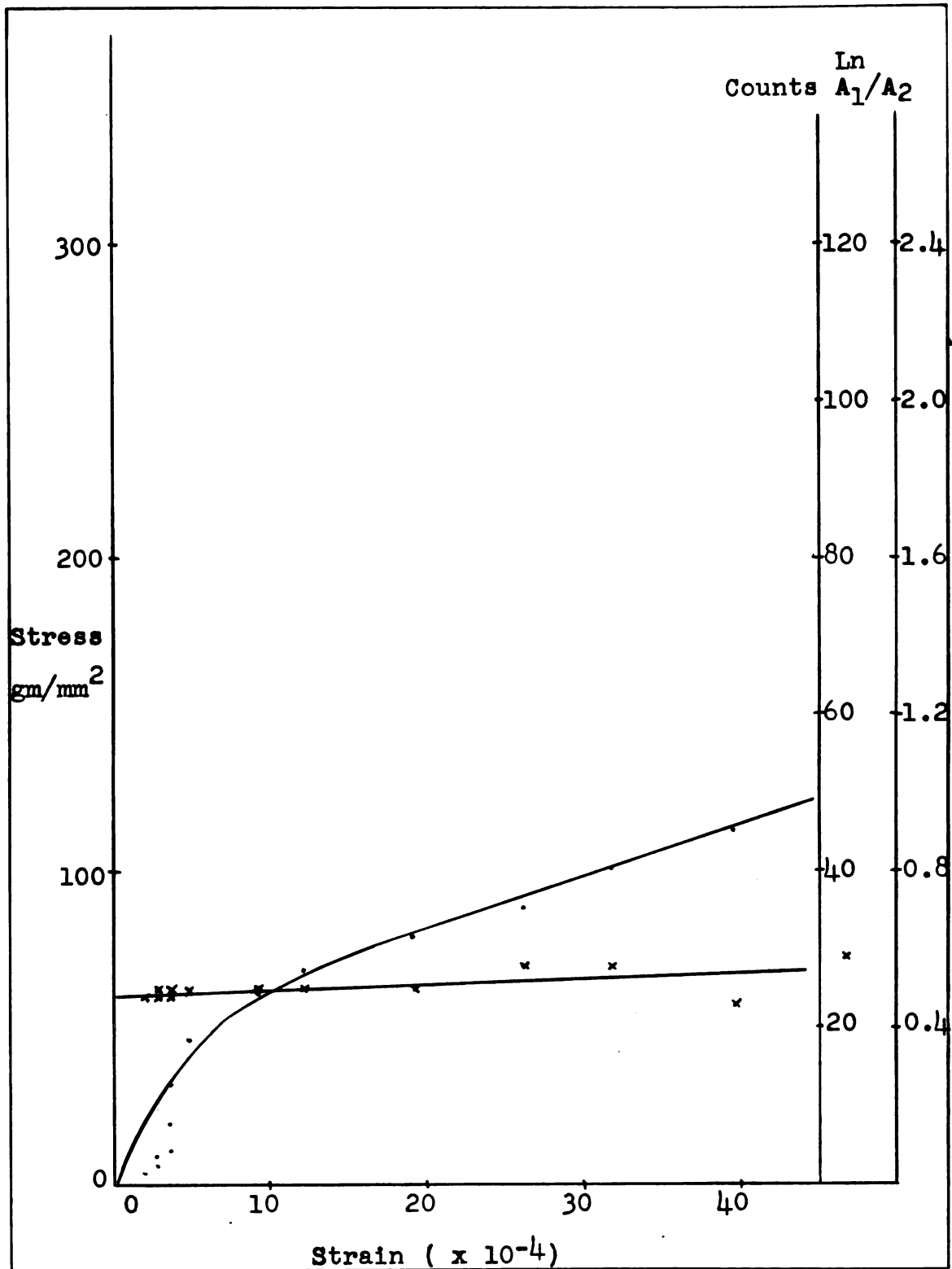


Figure 19. Acoustic Emission Histogram and Damping Data for Specimen 8. The acoustic emission histogram is superimposed upon the stress-strain curve and the logarithmic decrement curve (x) for specimen 8 (KCl, one CaF₂ film).

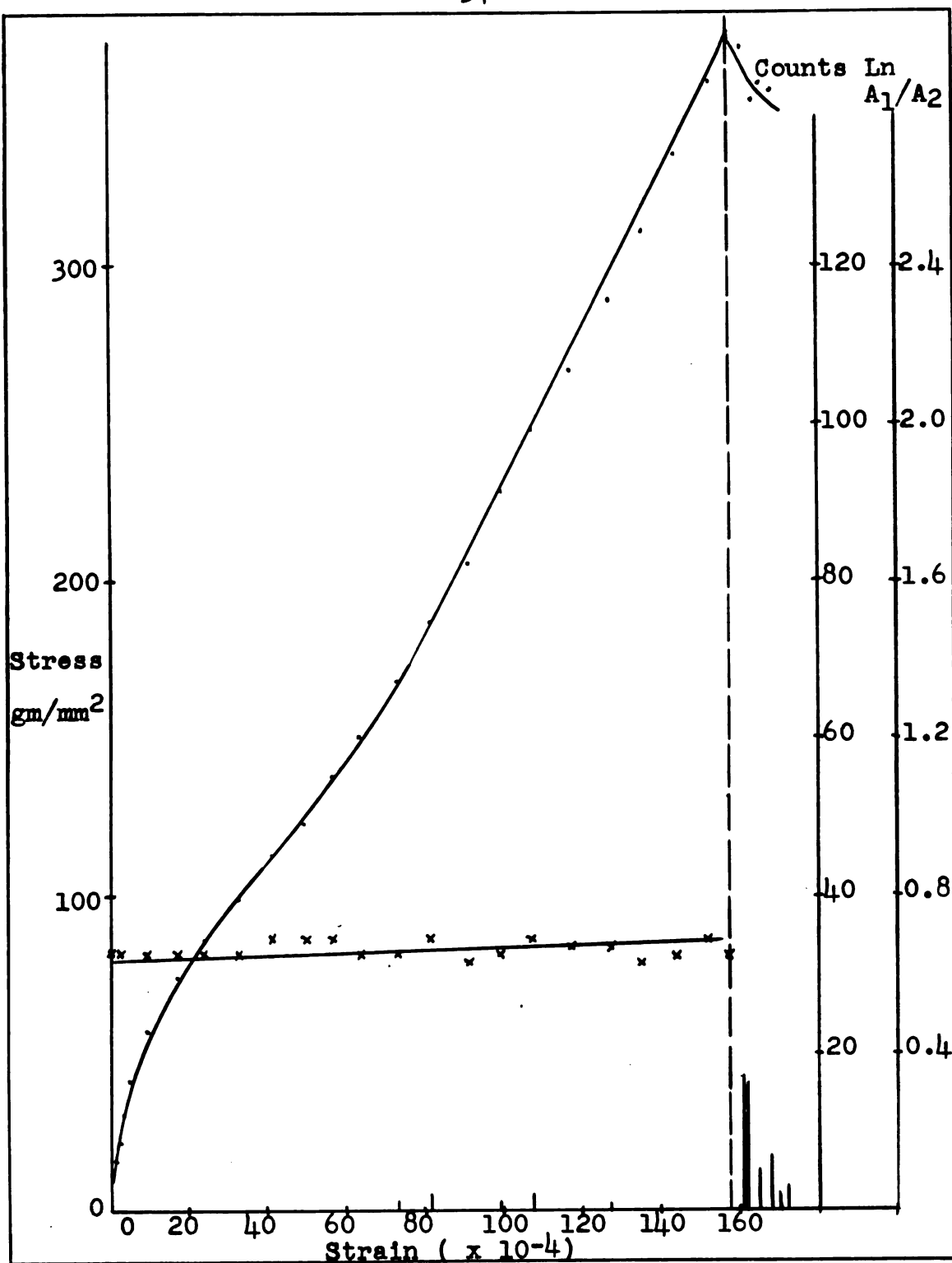


Figure 20. Acoustic Emission Histogram and Damping Data for Specimen 10 Plotted Against a Contracted Strain Scale. The acoustic emission histogram superimposed upon the stress-strain curve and the logarithmic decrement curve (x) for specimen 10 (KCl, one NaCl film). The vertical dashed line indicates the value of strain at which the film was etched off.

experiments involved ultrasonic damping data. The amplitudes of successive echos were recorded after each load increment. The logarithm of the ratio of an amplitude to its successive amplitude was used as a measure of the ultrasonic damping. Figures 21 and 22 are examples of damping curves for both coated and uncoated specimens of LiF and KCl respectively. The actual experimental points for these curves are plotted in Appendix III. Ultrasonic damping data are also plotted in Figures 14 to 20.

The vertical dashed lines in Figures 16, 18 and 20 indicate that the thin film has been etched away at that value of strain. It is particularly significant that many acoustic bursts occur immediately after the film is removed. It is also apparent from these Figures that the number of bursts occurring at this time is far greater than at any other time during the specimen's loading history.

The foregoing curves indicate several things of interest which will be discussed in the next section. However, some important points should be emphasized. First of all, Figures 11 and 12 show that the presence of a thin film on both LiF and KCl does increase the value of stress corresponding to a given value of strain above that for uncoated specimens. This fact is especially significant for the case of LiF shown in Figure 11 since the data plotted there are entirely within the elastic range. The greater slope of the coated specimens indicates that the presence of a thin surface film raises the value of E for the substrate material. Note, however, that the slope of the curve for specimen 3,

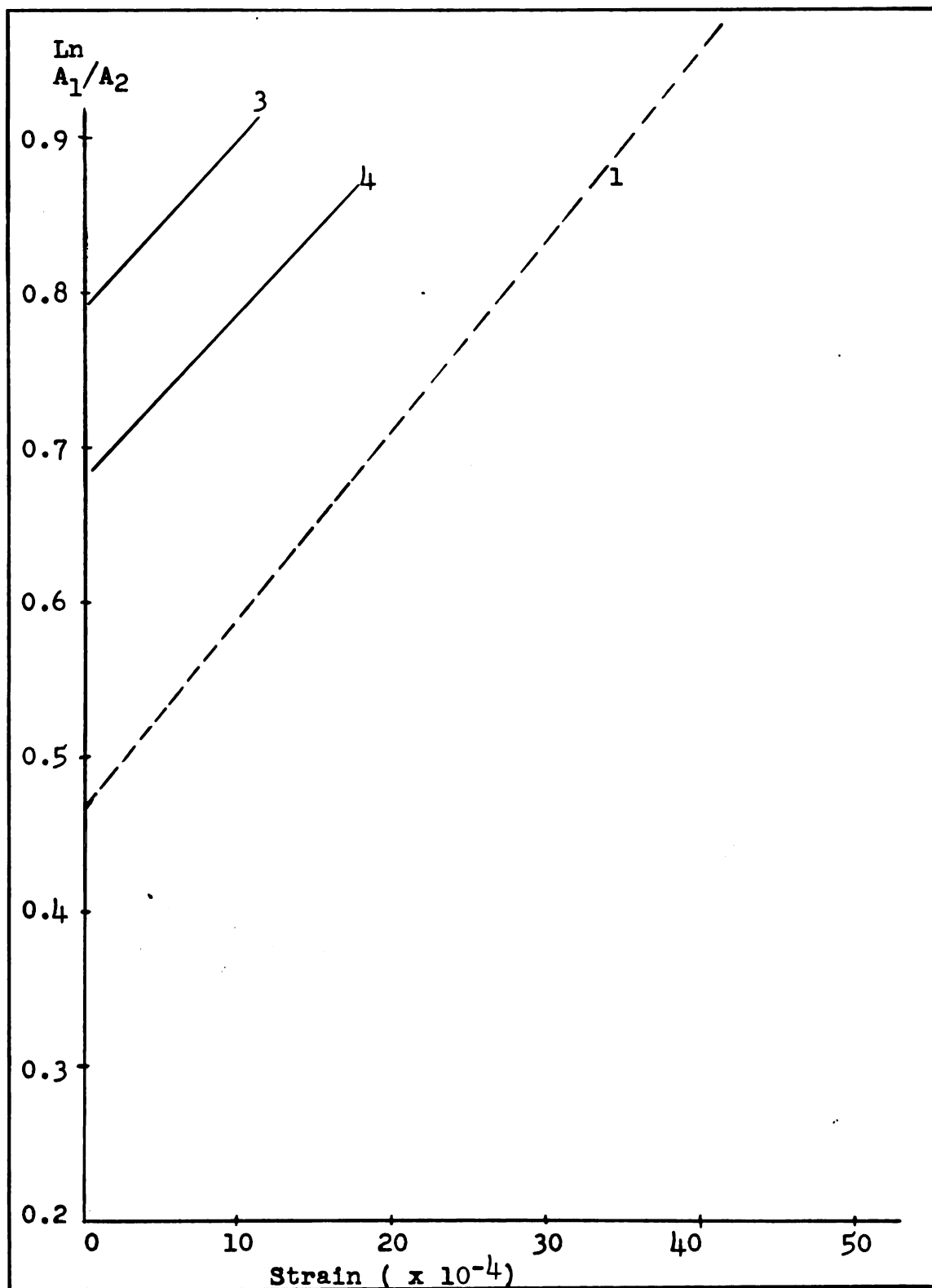


Figure 21. Logarithmic Decrement Curves for LiF. The number on each curve identifies the specimen. The actual experimental points are plotted in Appendix III.

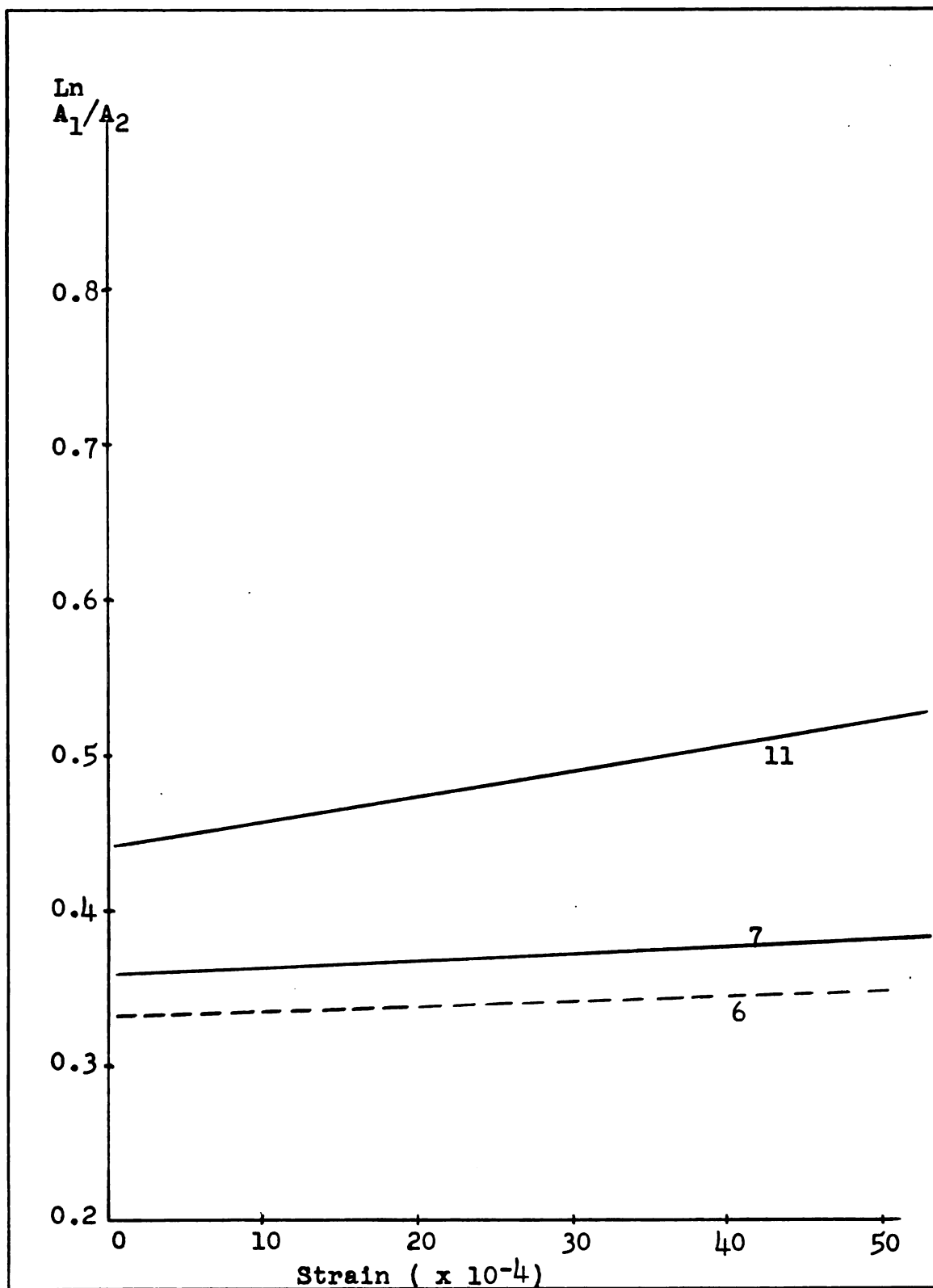


Figure 22. Logarithmic Decrement Curves for KCl. The number on each curve identifies the specimen. The actual experimental points are plotted in Appendix III.

which is coated with CaF_2 , is less than that for uncoated specimen 1. This is probably due to the fact that the test on specimen 3 was terminated at an early value of strain. Had the test been carried to larger values of strain, it is believed that the best straight line through the experimental points would have been one of greater slope. This can be seen by looking in detail at the experimental points in Appendix III corresponding to the stress-strain curves for specimens 1 and 3. For any given strain, the points associated with specimen 3 are at a higher value of stress than those associated with specimen 1. No direct correlation can be seen between E for the substrate and the ratio of elastic constants, c_{11} , of the film and substrate material. Note, in Figure 11 that the slope of the stress-strain curve for specimen 9 which had one NaCl film is greater than that for specimen 3 with one side coated with CaF_2 , and specimens 4 and 5, each with two sides coated with NaCl . This fact indicates that the interface energy due to atomic lattice misfit between the film and substrate plays a predominant role in creating the Roscoe effect.

The expression

$$\frac{a_F - a_S}{a_S}$$

can be used as a measure of the amount of lattice misfit at the film-substrate interface where a represents the atomic lattice spacing and the subscripts F and S stand for film and substrate respectively.

The lattice constants for LiF , CaF_2 , NaCl and KCl

are 4.02, 5.45, 5.63 and 6.28 Å respectively (48). The lattice misfit parameter calculated from these values are shown in the chart of Figure 23 for the four cases used here.

Substrate	Film	$\frac{a_F - a_S}{a_S}$
LiF	NaCl	0.400
LiF	CaF ₂	0.356
KCl	NaCl	-0.104
KCl	CaF ₂	-0.132

Figure 23. Lattice Misfit Parameters. The chart shows the lattice misfit parameters for various combinations of ionic crystals.

The larger the absolute value of the lattice misfit parameter, the greater is the misfit between the film and substrate material; hence the greater is the interface energy. The negative signs simply indicate that a_S is greater than a_F for that particular combination.

Note that the lattice misfit parameter is greater for LiF substrates coated with NaCl than for those coated with CaF₂. Hence, if interface energy is an important factor in creating the Roscoe effect, LiF specimens coated with NaCl should exhibit a somewhat larger stress for a given value of strain than would a similar specimen coated with CaF₂. This is found to be true and can be seen in Figure 11. The slopes of the linear portion of the stress-strain curves for specimens 4, 5 and 9, coated with NaCl, are all greater

than that for specimen 5, coated with CaF_2 .

The misfit parameters for the KCl specimens indicate that the interface energy should be greater for those coated with CaF_2 than for those coated with NaCl. This is evidenced in the stress-strain curves of Figure 12 where, in general, for a given strain, the stress is greater for specimen 8, coated with CaF_2 , than for specimens 7, 10 and 11, coated with NaCl. There is one exception, however, in the range of strain between 20 and 55×10^{-4} ; namely, the curve for specimen 11 crosses over the curve for specimen 8. This may be due to the fact that specimen 11 had two sides coated while specimen 8 was coated only on one side.

Only a portion of the stress-strain curve for specimen 2 is shown in Figure 11. For values of strain greater than 15×10^{-4} this curve varied drastically from the other curves shown. However, internal cracks were clearly visible in that specimen at a very low value of strain, 20×10^{-4} . This anomalous behavior must have been due to severe stress concentrations produced by internal imperfections within the undeformed crystal.

The stress-strain curves for coated and uncoated specimens of KCl are shown in Figure 12. Although there is no well-defined linear elastic region apparent in these curves, the effects of the thin films are seen at very low values of strain. The curves for specimens 8 and 10 which are coated with CaF_2 and NaCl respectively indicate that for a given value of strain, the corresponding stress is significantly increased above that for uncoated specimen 6.

Figure 14 shows a histogram of acoustic emission counts taken from specimen 1 (uncoated LiF) superimposed upon a portion of the elastic region of the stress-strain curve. Note that the counts attain a maximum at a strain of approximately 10^{-3} . Also it is interesting to note that the distribution of counts is not symmetrical but is skewed toward larger values of strain. This distribution is typical for LiF in the elastic range but is not observed in KCl as can be seen in Figure 15.

The maximum number of acoustic emissions in LiF occurred at strains of the order of 10^{-3} in specimens 1 and 2 which had no film and in specimens 5 and 9 which were coated with NaCl. The maximum was shifted to higher values of strain for specimens 3 and 4 which were coated with one CaF_2 film and two NaCl films respectively. Since the value of c_{11} for NaCl is less than the value of c_{11} for LiF, it must be concluded that interface energy between the film and substrate partly determines the value of ϵ_0 at which maximum acoustic emission occurs. As was mentioned previously, the interface energy is a function of the lattice misfit parameter. Hence, if the film-substrate interface energy does move the initial acoustic emission distribution peak to the right, it should be expected that specimen 4, which had two sides coated with NaCl, should exhibit the largest value of ϵ_0 , the strain at which maximum acoustic emission occurred. This is indeed the case, as a value of $\epsilon_0 = 3.8 \times 10^{-3}$ was observed for specimen 4.

It should be remembered that the lattice misfit

parameter is not the only quantity affecting the film-substrate interface energy. If epitaxial growth is attained during film deposition, the lattice misfit is probably the major contribution to the distortion at the surface and therefore the most important factor controlling the interface energy. However, if the film grows in a more random way, the effect of the lattice misfit parameter is minimized. Thus, the interface energy can be thought of more realistically as being the residual strain energy of distortion across the film-substrate interface. However, since it is difficult to obtain an exact indication of the interface energy, it must be assumed that at least the first few atomic layers of the film are deposited epitaxially and that the lattice misfit parameter indicates the relative magnitudes of the interface energy.

Figure 16 gives a good example of acoustic emission occurring after the removal of NaCl surface films from a LiF crystal. The vertical dashed line indicates the value of strain at which the film was etched. The large number of acoustic emissions occurring after etching as compared to the number before film removal is typical. Note also the drop in the stress strain curve immediately after etching. A plot of similar data for KCl is shown in Figure 20.

The logarithmic decrement taken from ultrasonic damping data for uncoated LiF (specimen 1) is also shown in Figure 14. A general increase of damping with strain is evident. A comparison of this curve with that for specimen 5 in Figure 16 indicates that the presence of a surface

film also causes an increase in damping. A similar increase in ultrasonic damping can be seen for KCl if the curves of Figures 15 and 17 are compared. Figure 15 gives the damping curve for uncoated KCl (specimen 6) while Figure 17 gives that for KCl having one side coated with NaCl (specimen 10). The effect of a surface film on the logarithmic decrement is particularly apparent in Figures 21 and 22.

Appendix IV contains the raw data for all of the specimens, some of which were not mentioned above.

IV. DISCUSSION

Typical stress-strain curves for ionic single crystals can be compared and a general distinction made between "hard" and "soft" crystals (49); if this criterion is used, crystals such as MgO and LiF must be considered hard while NaCl and KCl must be classified as soft. The evidence presented in the preceding section further indicates that LiF and KCl are governed by different deformation mechanisms. Although the nature of these differences can not be predicted from the macroscopic stress-strain curves, acoustic emission data does provide a means for comparing the microscopic deformation characteristics of the two types of crystalline materials.

A. Model for LiF

It will be assumed that a random, three-dimensional network of grown-in dislocations is present in an undeformed single crystal of LiF, and that many dislocation segments within this array lie on $\{110\}$ planes, favorably oriented for slip. It is also reasonable to assume that these segments will be distributed randomly throughout the crystal, with their lengths symmetrically distributed about some mean length. The points of their emergence from the slip plane will act as effective pinning points. When stress is applied, the favorably oriented segments will then operate as dislocation sources according to the doubly-pinned,

Frank-Read mechanism (29). For this reason the distance between two points of emergence is referred to as the loop-length for that particular dislocation source; and earlier investigators have concluded that these loop-lengths, l , will be normally distributed about a mean length, l_0 , according to the formula

$$N(l) = (L/l_0^2) l \exp(-l/l_0) \quad (1)$$

where $N(l)$ is the distribution of loop-lengths and L is the total length of dislocation within the crystal.

Two points are of special significance concerning the operation of such sources and the multiplication process involved in accommodating the macroscopic strain. First of all, it is evident that the longer loop-lengths will operate at lower values of stress than the shorter ones. This is indicated by Cottrell's equation (52)

$$l = 2r = 2\mu b/\tau \quad (2)$$

where r is the critical radius of a bowed-out dislocation loop, μ the shear modulus, b the Burgers vector and τ , the critical resolved shear stress. The critical values are reached when a straight doubly-pinned dislocation segment of length l is bowed out by the applied stress and attains a semi-circular configuration. Any slight increase in shear stress will cause the pinned segment to act as a Frank-Read source, emitting many dislocation loops without requiring additional stress. Hence, as the applied stress is increased, some of the shorter loops may bow out, but the

longer ones will be subjected to the critical value of shear stress for multiplication first. The Probability, $P(1/\ell)$, of finding a loop-length whose inverse lies between $1/\ell$ and $1/\ell + d(1/\ell)$ is defined by the equation

$$2\pi(1/\ell)P(1/\ell)d(1/\ell) = (2\pi/\ell)\ell_0^2 \exp(-\ell_0/\ell)d(1/\ell) \quad (3)$$

where $2\pi(1/\ell)d(1/\ell)$ represents an element of area in inverse loop-length space. This is represented schematically in Figure 24.

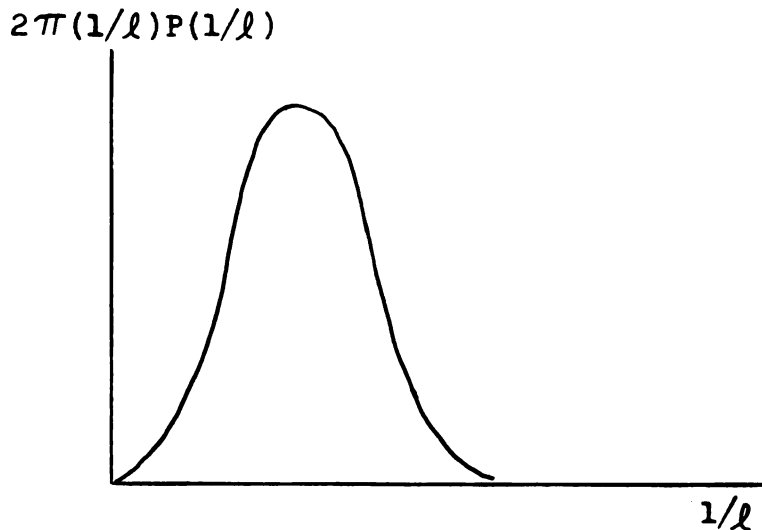


Figure 24. Sketch of Symmetrical Inverse Loop-length Distribution. The distribution shown is that which is present in the undeformed crystal.

The second point concerns the rate of dislocation multiplication once a source becomes operative. In LiF single source multiplication occurs very rapidly, creating an avalanche effect; in fact an entire slip band can be formed in as little as one tenth of a second (49). It is postulated here that an avalanche of dislocations emanating from a Frank-Read source can create an elasto-plastic wave

of sufficient energy to be picked up by the acoustic emission apparatus. Hence, in a previously undeformed crystal, the distribution of acoustic emission counts should give a relative estimate of the initial loop-length distribution, if the interaction between dislocations produced by different sources is small. However, such interaction can pin dislocation sources which have not reached the critical value of stress necessary for multiplication and, thus, effectively create more but shorter loop-lengths. That is, dislocation interaction may skew the loop-length distribution curve toward the side of shorter loops, or larger $1/\ell$, as shown in Figure 25.

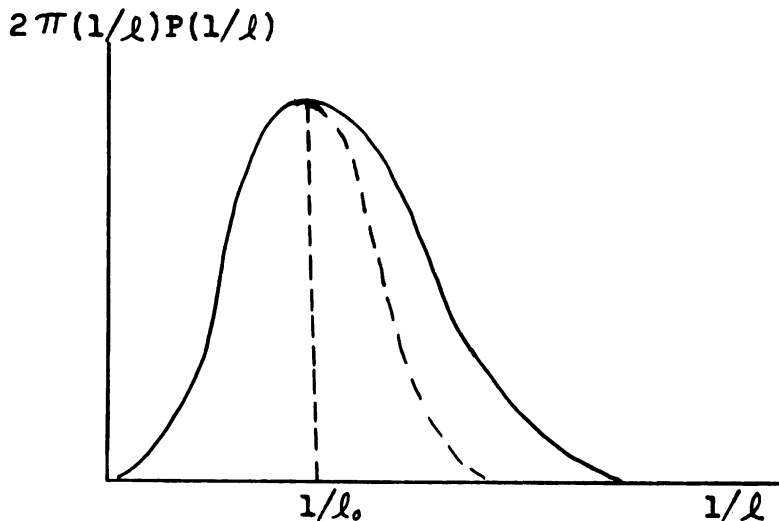


Figure 25. Sketch of Skewed Inverse Loop-length Distribution. The distribution shown is that which is present after dislocation interaction takes place.

It is evident that the release of dislocation pile-ups also gives rise to acoustic emission bursts, as will

be discussed later. There are reasons to believe, however, that the skewed distribution of acoustic bursts which occurs in the elastic range of LiF is due to the operation of dislocation sources.

First, if the distribution is attributed to the release of pile-ups, it is difficult to explain elastic recovery. Elastic strain energy can be stored in a crystal in the form of dislocation pile-ups in such a manner that the back stresses cause elastic recovery when the applied load is removed. If, however, these pile-ups are released before removal of the applied load, there will be little or no elastic recovery, from which it follows that such a process must not be dominant for linearly elastic materials such as LiF.

Also, pile-ups released when the film is etched off, even in the elastic range of LiF, produce many more acoustic emissions than are observed to take place in the initial distribution. This is also true for KCl which does not even exhibit the initial distribution of counts.

Hence, the distribution of acoustic emission counts in the elastic range must be primarily a result of the operation of dislocation sources rather than the release of pile-ups. For this reason, an analysis of the distribution provides a means for interpreting the dislocation deformation mechanism, at least for LiF.

B. Skewed Acoustic Emission Distribution

It is apparent that the curve of Figure 25, which represents the probability of finding an inverse loop-length

between $1/\ell$ and $1/\ell + d(1/\ell)$, and which is skewed to the right by dislocation interaction, resembles the acoustic emission curve for the elastic range of LiF shown in Figure 14 of the last section. However, before any direct correlation can be made between acoustic counts and inverse loop-length distribution, two important factors must be considered.

First, an expression relating dislocation source loop-length, ℓ , to the macroscopic strain, ϵ , must be developed in order to show that when $\epsilon = \epsilon_0$, the strain at which maximum acoustic emission occurs, the value of ℓ obtained is a reasonable value for the most probable loop-length.

If one dislocation loop is considered, the offset δ , which is measured along a slip plane, is given by the equation (54)

$$\delta = (A''/A')b = [A''(0.707)b] / A \quad (4)$$

where A'' is the slipped area on a slip plane of total area A' , A is the cross sectional area of the specimen, b is the Burgers vector and the factor of 0.707 enters here because in LiF the $\{110\}$ planes are favored for slip. The resolved shear strain, γ , is then found to be

$$\gamma = \delta / (A^{\frac{1}{2}} / 0.707) = A''b / [2(A^3)^{\frac{1}{2}}] \quad (5)$$

The axial strain for a given offset, δ , is found by geometry in this case to be

$$\epsilon = \Delta S / S = 0.707 \delta / S = A''b / (2AS) \quad (6)$$

where S is the undeformed length of the specimen and ΔS is the deformation. Hence, for $A = 1/4 \text{ in}^2$, $S = 3/2 \text{ in}$, and $b = a/0.707$, where a is the lattice spacing for LiF and is equal to 4.02 \AA (53), the above formula gives

$$A'' = 0.337\epsilon \times 10^8 \text{ in}^2 . \quad (7)$$

It is known from simple elastic theory that the resolved shear stress, τ , for this case can be written as

$$\tau = \sigma/2 = E\Delta S/(2S) = EA''b/(4AS) . \quad (8)$$

Hence, when the shear stress reaches the critical value for the operation of a dislocation source of length ℓ , the expression for τ in Equation (8) can be set equal to Cottrell's expression, Equation (2), for critical resolved shear stress as a function of loop-length. This yields

$$EA''b/(4AS) = 2\mu b/\ell \quad (9)$$

and it is found that

$$\ell = 8\mu AS/(EA'') = 23.7\mu V \times 10^{-8}/(E\epsilon) ,$$

where V is the volume of the specimen, μ is the shear modulus, and use has been made of the expression (7) for A'' . Let

$$23.7\mu V \times 10^{-8}/E = C_1 , \quad (10)$$

a constant with the dimensions of inches; then

$$\ell = C_1/\epsilon , \quad (11)$$

which is the desired relation. It is assumed here that

the strain is a result of dislocation motion only; i.e., any strain due to a change in the lattice parameter has been neglected in the calculation.

Since ϵ_o , the value of strain in the elastic region of LiF for which maximum acoustic emission occurs, was observed to be of the order of 10^{-3} , this should give a reasonable value for the most probable loop-length when substituted into the above equation. To evaluate C_1 in Equation (10), a ratio of $\mu/E = 6.28/15$ can be calculated from the equation (54)

$$\mu/E = (c_{12} + c_{44})/(2c_{44} + 3c_{12}) \quad (12)$$

where the accepted values of c_{12} and c_{44} for LiF are 4.2×10^{11} and 6.28×10^{11} dynes/cm², respectively. If this ratio and the specimen dimensions are used, the most probable dislocation loop-length is found to be

$$\ell_o = 0.945 \times 10^4 \text{ \AA} \quad (13)$$

This is within one order of magnitude of the critical loop-length of about 10^4 b suggested by Cottrell (55) for a "typical" applied stress.

Granato and Lucke (50) assumed a symmetrical distribution of loop-lengths about a mean length ℓ_o . Therefore, the second factor which must be considered before a direct correlation can be made between acoustic counts and inverse loop-length distribution is the cause and character of the skewed acoustical curve; and, of course, this must be accompanied by a satisfactory physical explanation of the

corresponding inverse loop-length distribution curve.

The skewness of the acoustic emission curve can be defined by subtracting the symmetrical part of the curve, as illustrated in Figure 26. This symmetrical portion will

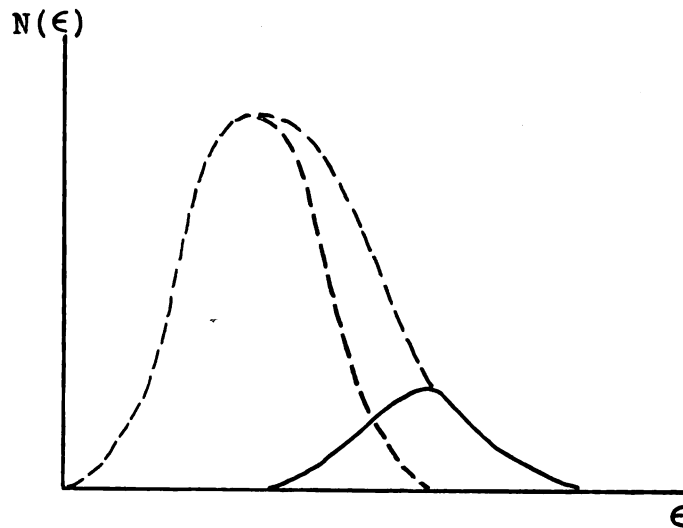


Figure 26. Skewness of Acoustic Emission Curve. The curve shown is the remaining portion after the symmetric curve has been subtracted.

be referred to as the 'primary' distribution, since it is assumed that the initial distribution of loop-lengths is random and therefore symmetrically distributed about some mean length. The curve obtained by subtracting the primary distribution curve from the total curve will be called the 'secondary' distribution. It is assumed due to the operation of shorter dislocation sources created during deformation. Plots constructed from actual experimental data follow.

It can be seen from Figure 27 that the secondary distribution is also skewed towards shorter loop-lengths. It is reasonable to imagine that the secondary curve too is

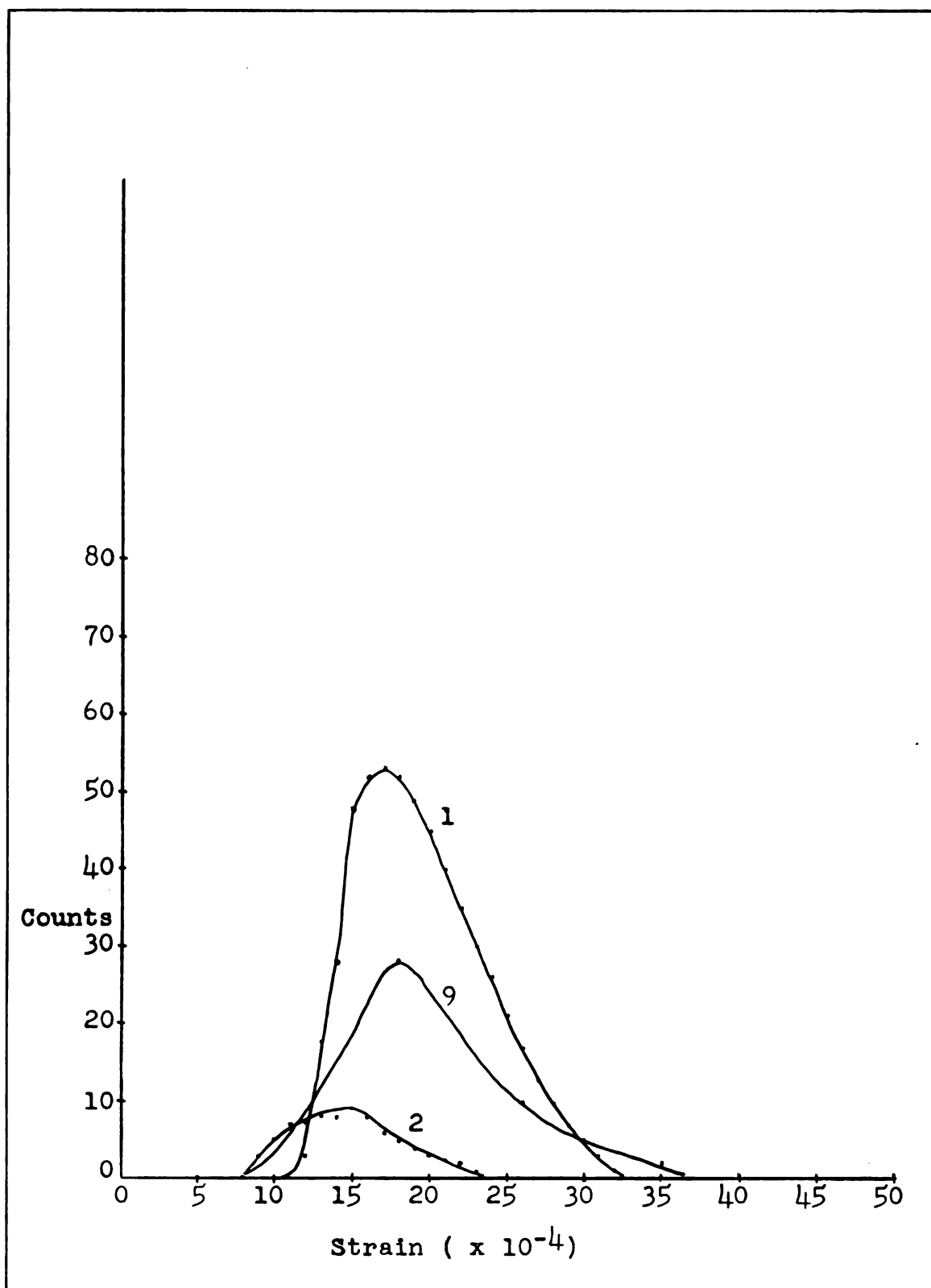


Figure 27. Plots of Non-symmetrical Portion of Acoustic Emission Distribution. The plots shown are for the elastic range of LiF.

composed of a symmetrical part and a portion which is skewed toward shorter loop-lengths. Here, however, only second order effects will be considered. The entire acoustic emission distribution curve will be assumed to consist of a symmetric portion centered about ϵ_0 and a symmetric secondary portion, as shown in Figure 28.

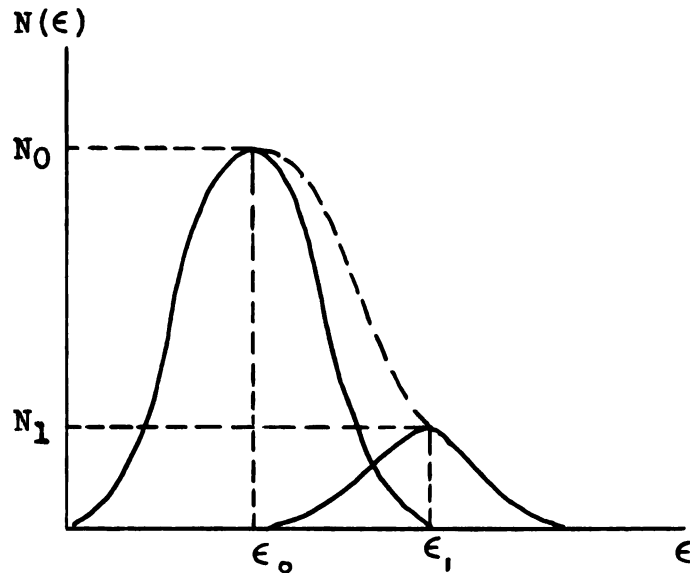


Figure 28. Breakdown of Total Acoustic Emission Distribution Curve. It is assumed that the total curve is the sum of two symmetric curves.

The ratio of amplitudes of the secondary and primary acoustic emission distribution curves can be used as a measure of the amount of skewness due to dislocation interaction, i.e. N_1/N_0 in Figure 28. It is found from the experimental data that Specimens 1 and 2, which are uncoated LiF, have values for N_1/N_0 of 0.400 and 0.384 respectively. Specimen 9, which has one side coated with NaCl, has a value of 0.357 while Specimens 4 and 5, both of which have two sides coated

with NaCl, have values of 0.142 and 0.211 respectively.

These results indicate that the presence of a surface film reduces the value of N_1/N_0 , i.e. reduces the amount of skewness in the acoustic emission distribution. The reduction can only be due to one of the following:

- (1) The number of acoustic emission counts may be increased in the region $\epsilon < \epsilon_0$.
- (2) The number of acoustic emission counts may be reduced in the region $\epsilon > \epsilon_0$.
- (3) The maximum in the acoustic emission distribution, N_0 , may occur at a larger value of strain.

It is not likely that the presence of a film could create any dislocation sources with loop-lengths longer than ℓ_0 . In fact, if anything, it would have a tendency to shorten the effective loop-lengths near the surface. However, it was mentioned before that surface sources are not important for the deformation of LiF. Nor is it probable that a thin film could cause less dislocation interaction and thus lower the amplitude of the secondary portion of the curve. For these reasons, (1) and (2) above are probably not important; and it can be concluded that the presence of a surface film has a tendency to shift N_0 toward larger values of strain. It will be shown later (page 77) that this is due to the combination of a real and an apparent shift in the loop-length distribution toward shorter loop-lengths.

It is quite reasonable that the plot of $2\pi(1/\ell)P(1/\ell)d(1/\ell)$ versus $1/\ell$ of Figure 25 should be similar to the plot of

N versus ϵ shown in Figure 28. As emphasized earlier, the dislocation sources with the longest loop-lengths will be activated at the lowest stress increments; and these sources will continue to operate until the stress is somehow reduced below the critical value for dislocation multiplication. For example, if a leading dislocation becomes pinned by internal imperfections, other dislocations or a surface film, and if the barrier is of sufficient strength, the following dislocations will become piled up. The back stress from the pile-up will then reduce the stress at the source below the critical value for operation.

As additional stress increments are applied, further straining must be accommodated by one of the following mechanisms:

- (a) Release of the pile-ups, thus allowing an inoperative source to become operative again.
- (b) Operation of a shorter source created during deformation and, therefore, one lying on a slip plane very near a plane on which a source has previously operated.
- (c) Operation of a source which has not previously operated, hence, one with a shorter loop-length.

It should be noted that (a) and (b) are closely related to previously operative sources while (c) is concerned with previously inoperative sources. Hence, it is logical that mechanism (c) should be more prevalent at lower strains.

Since the longer sources attain their critical operating stress at smaller values of strain, it follows that mechanism (c) is more likely to occur when $\ell > \ell_0$, that is, in the first

part of the curve shown in Figure 25.

When $\ell > \ell_0$, i.e. $1/\ell < 1/\ell_0$, the number of previously inoperative sources which are available to operate at a given critical value of stress increases as the critical stress value increases. This can be seen by letting τ_1 be the critical stress required to operate a source of loop-length $\ell_1 > \ell_0$, and letting N_1 be the number of these loops. Then as τ_1 increases, N_1 increases. Note, however, that for $\ell_1 < \ell_0$, N_1 decreases as τ_1 increases. Since the number of previously inoperative loops is now decreasing, the strain can not be accommodated simply by the operation of these loops. Hence, when $\ell < \ell_0$ all of the available, previously inoperative loops of the proper length will operate and the remaining strain must be accommodated by the reactivation of a blocked source or by the operation of a new source created during the deformation process. As the stress continues to increase, fewer of the primary sources and more of the secondary sources will operate. This is shown schematically in Figure 29 (a) and again in Figure 29 (b), where the probability of finding the inverse of a loop-length between $1/\ell$ and $1/\ell + d(1/\ell)$ is plotted against $1/\ell$.

Figure 29 reflects the fact that a finite number of primary dislocation sources whose loop-lengths are symmetrically distributed about a mean length ℓ_0 are initially present within the crystal. The secondary sources, i.e. the reactivated or newly-created sources, begin to operate at $\ell = \ell_0$, when the number of primary sources attaining their critical stress for multiplication is at a maximum;

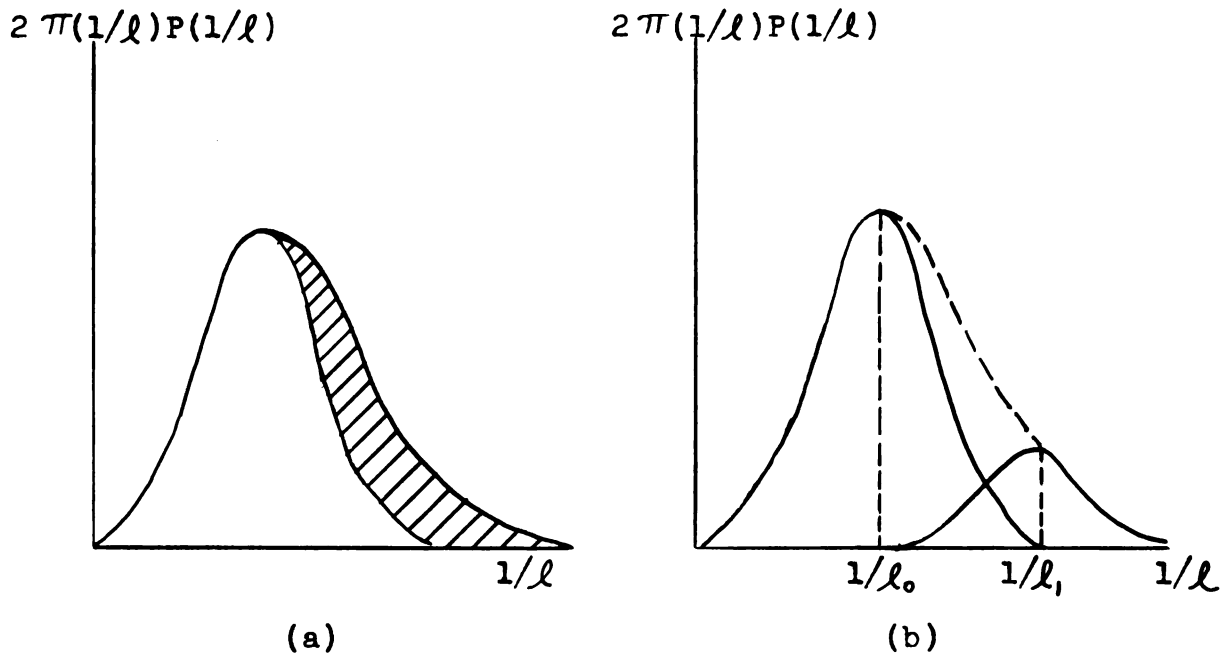


Figure 29. Relationship Between the Primary and Secondary Distribution. The portion subtracted from the total distribution can be represented by a displaced symmetric curve as in Figure 28.

and at the point where the primary sources are exhausted, the number of secondary sources reaches a maximum.

The foregoing discussion indicates that it is feasible to make a direct correlation between the acoustic emission distribution of Figure 28 and the probability distribution of inverse loop-lengths shown in Figure 29. However, a correlation of this type is more meaningful if both distributions are expressed in terms of probability. The observed acoustic emission distribution function, $N(\epsilon)$, divided by the total number of acoustic emissions in the distribution, N_t , gives the probability density; which, when multiplied by $d\epsilon$, becomes the desired total probability function. It should be noted that the factor, $d\epsilon$,

does not alter the form of the distribution. Hence the probability of finding N acoustic emissions between ϵ and $\epsilon + d\epsilon$ can be expressed as

$$P(\epsilon)d\epsilon = N(\epsilon)d\epsilon / \left[\int N(\epsilon)d\epsilon \right] \quad (14)$$

or simply as

$$P(\epsilon) = N/N_t \quad (15)$$

where it is understood that N is a function of ϵ and N_t represents the total number of emissions. Figure 30 indicates the similarity between the two probability functions.

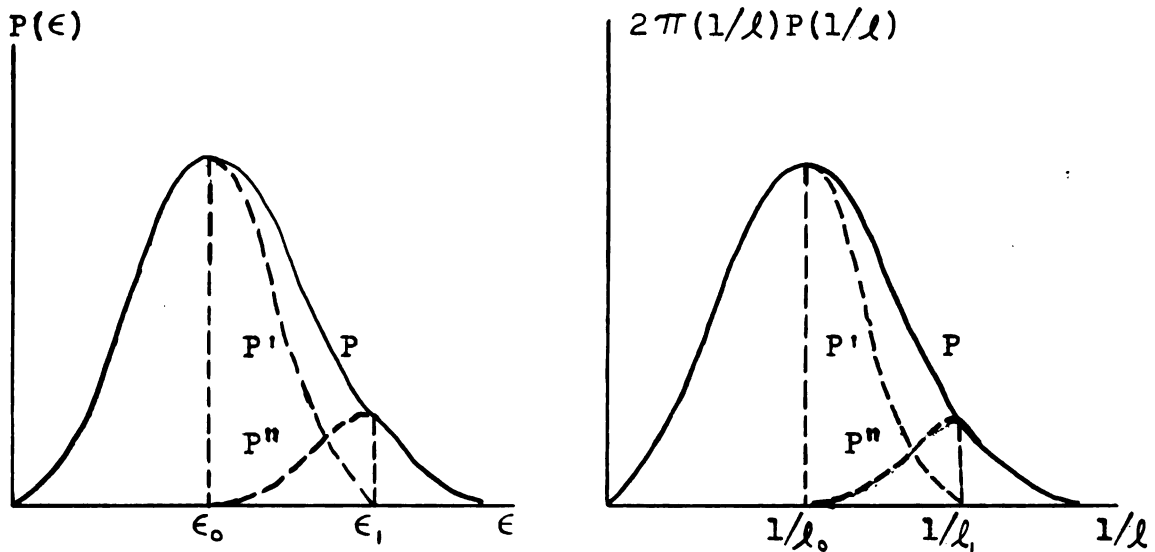


Figure 30. Similarity Between Acoustic Emission and Inverse Loop-length Probability Functions.

The primed numbers refer to the primary curves and the double-primed numbers to the secondary curves.

The probability of observing N acoustic emissions while the specimen is being strained from ϵ to $\epsilon + d\epsilon$ is the sum of two probabilities;

$$P(\epsilon)d\epsilon = [P'(\epsilon) + P''(\epsilon)] d\epsilon \quad (16)$$

where

$$P'(\epsilon)d\epsilon = (A/N_0) \exp(-\epsilon/\epsilon_0) d\epsilon \quad (17)$$

and

$$P''(\epsilon)d\epsilon = (B/N_1)(\epsilon - \epsilon_0) \exp[-(\epsilon - \epsilon_0)/\epsilon_1] d\epsilon \quad (18)$$

Equation (17) is taken from elementary statistical theory and expresses the contribution of the symmetrical part of the acoustic emission count distribution to the probability of observing a given number of acoustic emissions between ϵ and $\epsilon + d\epsilon$. This is a normal distribution, symmetrical about ϵ_0 , the strain at which the maximum number of acoustic emissions, N_0 , occurs. Equation (18) is similar except for the fact that the distribution it represents is transferred along the ϵ axis an amount ϵ_0 , and it expresses the contribution of the skewed part of the acoustic emission count distribution to the total probability curve.

In the same way, the probability of finding an inverse loop-length between $1/\ell$ and $1/\ell + d(1/\ell)$ can be expressed as

$$2\pi(1/\ell) [P'(1/\ell) + P''(1/\ell)] d(1/\ell) \quad (19)$$

where

$$\begin{aligned} 2\pi(1/\ell)P'(1/\ell)d(1/\ell) = \\ 2\pi(1/\ell) \ell_0^2 \exp(-\ell_0/\ell)d(1/\ell) \end{aligned} \quad (20)$$

and

$$2\pi(1/l)P''(1/l)d(1/l) = 2\pi(1/l - 1/l_0) \exp[-l_1(1/l - 1/l_0)]d(1/l) \quad (21)$$

Equation (20) is the same as Equation (3) and represents the symmetrical portion of the total probability curve while Equation (21) represents the skewed part. A direct correlation between the two probabilities gives

$$\begin{aligned} (A/N_0) \exp(-\epsilon/\epsilon_0)d + [B(\epsilon - \epsilon_0)/N_1] \exp[-(\epsilon - \epsilon_0)/\epsilon_1]d\epsilon \\ = 2\pi(1/l)l_0^2 \exp(-l_0/l)d(1/l) \\ + 2\pi(1/l - 1/l_0) \exp[-l_1(1/l - 1/l_0)]d(1/l). \end{aligned} \quad (22)$$

But since it was assumed that the primary distribution is due to the original distribution of loop-lengths and that the secondary distribution is caused by dislocation interaction, the primary and secondary probabilities can be considered independent and therefore equated separately to obtain

$$\begin{aligned} (A/N_0)\epsilon \exp(-\epsilon/\epsilon_0)d\epsilon = \\ 2\pi(1/l)l_0^2 \exp(-l_0/l)d(1/l) \end{aligned} \quad (23)$$

and

$$\begin{aligned} [B(\epsilon - \epsilon_0)/N_1] \exp[-(\epsilon - \epsilon_0)/\epsilon_1]d\epsilon = \\ 2\pi(1/l - 1/l_0)l_1^2 \exp[-l_1(1/l - 1/l_0)]d(1/l) \end{aligned} \quad (24)$$

It should be noted that the independence of the primary and secondary distributions is of a special type. Clearly it is possible that the change in the distribution of inverse

loop-lengths due to dislocation interaction may depend upon the distribution initially present in the undeformed crystal. However, for any given crystal, the primary distribution is fixed and can not be changed by deformation. This implies that, although the primary distribution can influence the secondary distribution, the inverse is not true. Hence for any given primary curve, the primary and secondary curves should be independent.

$P(\epsilon)d\epsilon$ can now be expressed as a function of $(1/l)$:

$$P(\epsilon)d\epsilon = 2\pi l_0^2(1/l) \exp(-l_0/l)d(1/l) + 2\pi(1/l - 1/l_0)l_1^2 \exp[-l_1(1/l - 1/l_0)]d(1/l) \quad (25)$$

And equating the arguments and the coefficients of the exponents in Equation (23) gives

$$\epsilon = (\epsilon_0 l_0)/l \quad (26)$$

which agrees with Equation (11), and

$$A = 2\pi N_0/\epsilon_0^2 \quad (27)$$

while from Equation (24) it follows that

$$B = 2\pi l_1^2 N_1/\epsilon_0^2 l_0^2 \quad (28)$$

It is worth emphasizing that, since $N(\epsilon)$ can be measured in the manner described above (e.g. Figure 14), the probability distribution of inverse loop-lengths can in effect be determined experimentally. The first term on the right in Equation (25) is, of course, the original distribution of inverse loop-lengths in the undeformed crystal. The

second term causes the skewness in the distribution and is itself caused by the deformation.

The expression for $P(\epsilon)d\epsilon$ as a function of $1/\ell$ should be useful in calculating average values of variables which depend primarily on dislocation source loop-length. For any variable, $A(1/\ell)$, the average value, \bar{A} , can be expressed as (56)

$$\bar{A} = \int A(1/\ell) P(\epsilon) d\epsilon / \left[\int P(\epsilon) d\epsilon \right]. \quad (29)$$

As an example, the average elastic strain due to dislocation motion can be calculated by substituting the expression

$$\epsilon = C_1 (1/\ell) \quad ,$$

obtained from Equation (11), into this equation:

$$\bar{\epsilon} = C_1 \int (1/\ell) P(\epsilon) d\epsilon / \left[\int P(\epsilon) d\epsilon \right] \quad (30)$$

where the limits of integration should extend from zero to the value of $1/\ell$ at the yield point.

For simplicity, Equation (30) can be written as

$$\bar{\epsilon} = C_1 I_1 / I_2 \quad (31)$$

and a substitution of $y = 1/\ell$ made. The value of I_1 can then be calculated by making use of Equation (25):

$$\begin{aligned} I_1 = & 2\pi \ell_0^2 \int_0^{\frac{\epsilon_y}{C_1}} y^2 \exp(-\ell_0 y) dy \\ & + 2\pi \ell_1^2 \int_0^{\frac{\epsilon_y}{C_1}} y^2 \exp[-\ell_1(y - 1/\ell_0)] dy \\ & - (2\pi \ell_1^2 / \ell_0) \int_0^{\frac{\epsilon_y}{C_1}} y \exp[-\ell_1(y - 1/\ell_0)] dy \end{aligned} \quad (32)$$

where the upper limit of integration, ϵ_y/C_1 , is the value of $1/\ell$ at the yield point and is obtained from Equation (11). Integrating from zero to ϵ_y/C_1 gives

$$\begin{aligned} I_1 = & [-2\pi/\ell_0^2] [(\ell_0^2 \epsilon_y^2/C_1^2 + 2\ell_0\epsilon_y/C_1 + 2) \exp(-\ell_0\epsilon_y/C_1) - 2] \\ & - [2\pi/\ell_1] \exp(\ell_1/\ell_0) [(\ell_1^2 \epsilon_y^2/C_1^2 + 2\ell_1\epsilon_y/C_1 + 2) \exp(-\ell_1\epsilon_y/C_1) - 2] \\ & + [2\pi/\ell_0] \exp(\ell_1/\ell_0) [(\ell_1\epsilon_y/C_1 + 1) \exp(-\ell_1\epsilon_y/C_1) - 1] \end{aligned} \quad (33)$$

Similarly,

$$\begin{aligned} I_2 = & 2\pi\ell_0^2 \int_0^{\epsilon_y/C_1} y \exp(-\ell_0 y) dy \\ & + 2\pi\ell_1^2 \int_0^{\epsilon_y/C_1} y \exp[-\ell_1(y - 1/\ell_0)] dy \\ & - [2\pi\ell_1^2/\ell_0] \int_0^{\epsilon_y/C_1} \exp[-\ell_1(y - 1/\ell_0)] dy \end{aligned} \quad (34)$$

or

$$\begin{aligned} I_2 = & -2\pi [(\ell_0\epsilon_y/C_1 + 1) \exp(-\ell_0\epsilon_y/C_1) - 1] \\ & - 2\pi \exp(\ell_1/\ell_0) [(\ell_1\epsilon_y/C_1 + 1) \exp(-\ell_1\epsilon_y/C_1) - 1] \\ & + (2\pi\ell_1/\ell_0) \exp(\ell_1/\ell_0) [\exp(-\ell_1\epsilon_y/C_1) - 1] \end{aligned} \quad (35)$$

The substitutions $C_1 = \epsilon_0 \ell_0$, $\epsilon_y = m\epsilon_0$ and $\ell_1 = \ell_0/2$ can now be carried out in Equations (33) and (35). It is found that

$$\begin{aligned} I_1 C_1 = & 2\pi\epsilon_0 [2 - (m^2 + 2m + 2) \exp(-m) \\ & + 3 \exp(1/2) - (1/2) \exp(1/2 - m/2) (m^2 + 3m + 6)] \end{aligned}$$

and for $m = 3$,

$$I_1 C_1 = 2\pi \epsilon_0 (1.69) \quad (36)$$

The value $m = 3$ effectively assumes that the secondary acoustic emission curve is symmetric, with yield occurring after all secondary sources cease to operate. For the non-symmetrical case a larger value of m should be used. Also,

$$I_2 = 2\pi \left[1 - (m + 1) \exp(-m) + (1/2) \exp(1/2) - (m/2 + 1/2) \exp(1/2 - m/2) \right]$$

or

$$I_2 = 2\pi (0.895) \quad (37)$$

when the substitution, $m = 3$, is made. Equation (31) now gives

$$\bar{\epsilon} = 1.84 \epsilon_0 \quad (38)$$

The expression for C_1 above comes from Equation (11) evaluated at $\epsilon = \epsilon_0$ and ϵ_y , the strain at the yield point, is taken to be equal to some numerical factor, m (here set equal to 3), times ϵ_0 . The relationship between ℓ_1 and ℓ_0 can be obtained from Figure 30.

The value of $\bar{\epsilon}$ denotes the macroscopic strain at which the dislocation sources of average length, $\bar{\ell}$, become operative, provided the strain due to changes in the lattice parameter is neglected. Hence, $\bar{\epsilon}$ is and should be greater than ϵ_0 , the critical strain for the most probable loop-length, since the distribution is skewed.

In order to estimate the error involved in neglecting the portion of the elastic strain due to changes in lattice parameter, it is possible to compare the energy needed to strain the specimen an amount corresponding to a strain ϵ as calculated by continuum mechanics with that obtained from dislocation theory. It is assumed here that if no dislocation motion occurs, the entire strain is due to changes in the lattice parameter. This gives rise to homogeneous deformation, and for small strains, the strain energy can be approximated by continuum theory. The energy necessary to cause an axial deformation equivalent to a strain ϵ can be expressed as $w = (1/2)E\epsilon^2$ and $w = (1/2)\tau^2/\mu$ for pure axial compressive stress and pure shear, respectively (57).

It is assumed that the strain energy associated with a change in lattice parameter, w_c , can be calculated from the axial stress formula,

$$w_c = (1/2)E\epsilon^2 \quad (39)$$

while that associated with dislocation motion, from the pure shear formula,

$$w_d = (1/2)\tau^2/\mu \quad (40)$$

Equation (40) can be re-written as

$$w_d = 2\mu b^2/\ell^2 \quad (41)$$

by using equation (2) and the ratio of the strain energy due to change in lattice parameter to that due to dislocation strain becomes

$$\begin{aligned}
 w_c/w_d &= (1/4)(E/\mu)(\epsilon_o^2 \ell_o^2/b^2) \\
 &= (1/4)(E/\mu)(\epsilon_o^2 \ell_o^2/b^2)
 \end{aligned}
 \tag{42}$$

Equation (12) gives $E/\mu = 15/6.28$ and it is known that $b = 5.6 \text{ \AA}$ (see page 50); also, since ϵ_o is of the order of 10^{-3} and $\ell_o \approx 10^4 \text{ \AA}$ (Equation 13), Equation (42) can be rewritten as

$$w_c/w_d \approx 2 \tag{43}$$

This states that the energy needed to strain a crystal an amount ϵ by reducing the lattice parameter, is twice that needed to obtain the same strain by dislocation motion. It is therefore concluded that as long as there are mobile dislocations of sufficient number to accommodate the strain, very little or no change in lattice parameter should be observed. This implies that the contribution to the total strain by lattice parameter changes probably is not important for $\epsilon < \epsilon_o$, but becomes increasingly important as the active dislocation sources become exhausted.

It was found that the average dislocation strain, $\bar{\epsilon}$, is equal to $1.84\epsilon_o$ for the case when the crystal is strained from zero to $3\epsilon_o$. If the entire strain were a result of lattice parameter changes, it would be expected that the average strain for this case would be $1.5\epsilon_o$. This seems to indicate that at least on the average, the mobile dislocations are more than able to accommodate the total strain in the region up to $3\epsilon_o$. Consequently, neglecting lattice

parameter changes in the above calculations seems justified.

Of course, in the elastic range of LiF, the average stress needed to operate a dislocation source of length ℓ can now be written as $\bar{\sigma} = E\epsilon = 1.84E\epsilon$ for the case when $m = 3$. Furthermore, since $(1/\ell)$ is linearly related to ϵ , an average dislocation loop-length of $\bar{\ell} = (1/1.84)\ell$ can be obtained.

It is interesting to compare the average values $\bar{\epsilon}$, $\bar{\sigma}$ and $\bar{\ell}$ obtained here to the corresponding average values for the case of no dislocation interaction, that is when the average values are ϵ_0 , $E\epsilon_0$ and C_1/ϵ_0 respectively. This indicates that dislocation interaction raises the average values of stress and strain at which a dislocation source of length ℓ becomes operative by a factor of 1.84 while simultaneously reducing the average loop-length by the same factor. Thus, the factor 1.84 constitutes a measure of the dislocation interaction effect in the elastic range of LiF.

It is also possible to compare the number 1.84 with the calculated ratio, R , of the amplitudes of the primary and secondary distribution curves. Equations (17) and (18) evaluated at ϵ_0 and ϵ_1 respectively give

$$P'(\epsilon_0) = A\epsilon_0/N_0\epsilon \quad (44)$$

and

$$P''(\epsilon_1) = B(\epsilon_1 - \epsilon_0) / [N_1 \exp(1 - \epsilon_0/\epsilon_1)] \quad (45)$$

Hence

$$R = AN_1\epsilon_0 \exp(-\epsilon_0/\epsilon_1) / [N_0B(\epsilon_1 - \epsilon_0)]$$

and, since $\epsilon_1 = 2\epsilon_0$,

$$R = AN_1 / [BN_0 \exp(1/2)] \quad (46)$$

If the expressions for A and B from Equations (27) and (28) are used,

$$R = (\ell_0/\ell_1)^2 \exp(-1/2) \quad (47)$$

or by applying Equation (11)

$$R = (\epsilon_1/\epsilon_0)^2 \exp(-1/2) = 4 \exp(-1/2) = 2.42 . \quad (48)$$

The ratio of amplitudes, R, is also a dimensionless measure of the dislocation interaction and compares favorably with the factor 1.84.

The amplitudes of the primary and secondary acoustic emission distributions for Specimen 1 are given in Figures 14 and 27 respectively. The ratio of these amplitudes is 2.45 which is in excellent agreement with R and comparable in magnitude to the factor 1.84.

C. Reversibility

Since the distribution $N(\epsilon)$ is observed entirely within the elastic range of LiF, the model must also explain reversibility in this material. But it is reasonable to believe that the sources can also act as sinks when the applied stress is removed and the internal stress distribution is mainly due to the back stress created by dislocation pile-ups. Probably many dislocations will never return to their source because of interactions, while some dislocations will

have completely left the crystal. However, such irreversibility must be too sensitive to be measured by the instruments used here. No stress concentrations could be detected in the relaxed specimens by ordinary polarized light techniques.

D. Yield Point

The yield point of LiF should also be explained by the model presented here. In the elastic range, the model is governed by an exhaustion phenomenon in which all of the original dislocation sources and those created during elastic deformation are eventually used up. It was postulated, however, that these sources ceased to operate when the back stress from dislocation pile-ups attained a critical value. Thus, the macroscopic yield stress should be due to one or a combination of the following mechanisms;

- (1) The stress reaches a critical value which is great enough to cause the dislocation pile-ups to overcome their barriers and hence create a dynamic avalanche effect.
- (2) The stress reaches a critical value which is sufficient to cause cross-slip from the existing slip planes. This mechanism produces 'band-broadening'.
- (3) Many new sources, which are not associated with the original dislocation sources or those created in the early stages of elastic deformation, are created at the yield stress.

Since cross-slip is difficult in LiF at room temperature (58-60), and since the applied stress would be insufficient to create many new sources, it is believed that (2) and (3) are not probable under the present conditions. Hence, the yield point in LiF is most likely due to a dynamic

avalanche effect created when many dislocation pile-ups overcome their barriers.

It can be seen in Figure 14, and this will be discussed later, that removal of the film does cause a sudden drop in the stress-strain curve. This must be due to the release of dislocation pile-ups directly beneath the surface film, or those which were created because of the stress concentrations associated with the surface pile-ups. In the natural yield of a clean LiF crystal, however, it is probable that many interior pile-ups also break away.

E. Easy Glide and Work Hardening

The present model for LiF is not concerned specifically with the easy glide and work hardening regions of the stress strain curve. However, a brief summary of the present understanding of these regions will be sufficient to complete the model and show that no direct conflict arises. A recent review article by Nabarro et al (61) gives a good account of the current state of knowledge for hard ionic crystals.

In a typical stress-strain curve for LiF, the rounded yield point is followed by a reduction in stress and a flat portion called the easy glide region, or Stage I. In this region the glide bands which have already been formed are spreading through the virgin crystal. In the light of the model presented here, this would be due to a dynamic multiplication effect occurring when the blocked sources become unblocked at the macroscopic yield point; and it might be expected to continue until dislocation interaction once

again causes the process to slow down or stop. The stress-strain curve then enters a linear work-hardening region called Stage II hardening. In this region the entire crystal becomes filled with glide bands; these bands widen and eventually, cracks form and failure occurs.

F. Model for KCl

There is no definite distribution of acoustic emissions in the early stages of deformation of KCl crystals comparable to that observed in the elastic range of LiF. However, if the tape is scanned just above noise level, acoustic emissions are observed. Figures 31 and 32 show acoustic data plotted from counts taken at two different levels, but the level used in Figure 31 is the one comparable to that used for the LiF specimen shown in Figure 14. The meaning may be that in KCl, dislocations are not created in the avalanche-type bursts characteristic of LiF. Figure 32 indicates that the bursts created in KCl are of relatively low magnitude; thus, they may be caused either by many slowly moving dislocations or very few rapidly moving dislocations.

In view of these observations, an exhaustion-type theory can not explain the early stages of deformation in KCl. It is believed that the lack of high-magnitude acoustic data is due to the fact that dislocations move at a much slower rate in KCl than in LiF (49). Sources in KCl will, therefore, be blocked much easier than those in LiF, due to the smaller dynamic forces associated with the moving dislocations. However, there is no indication that either

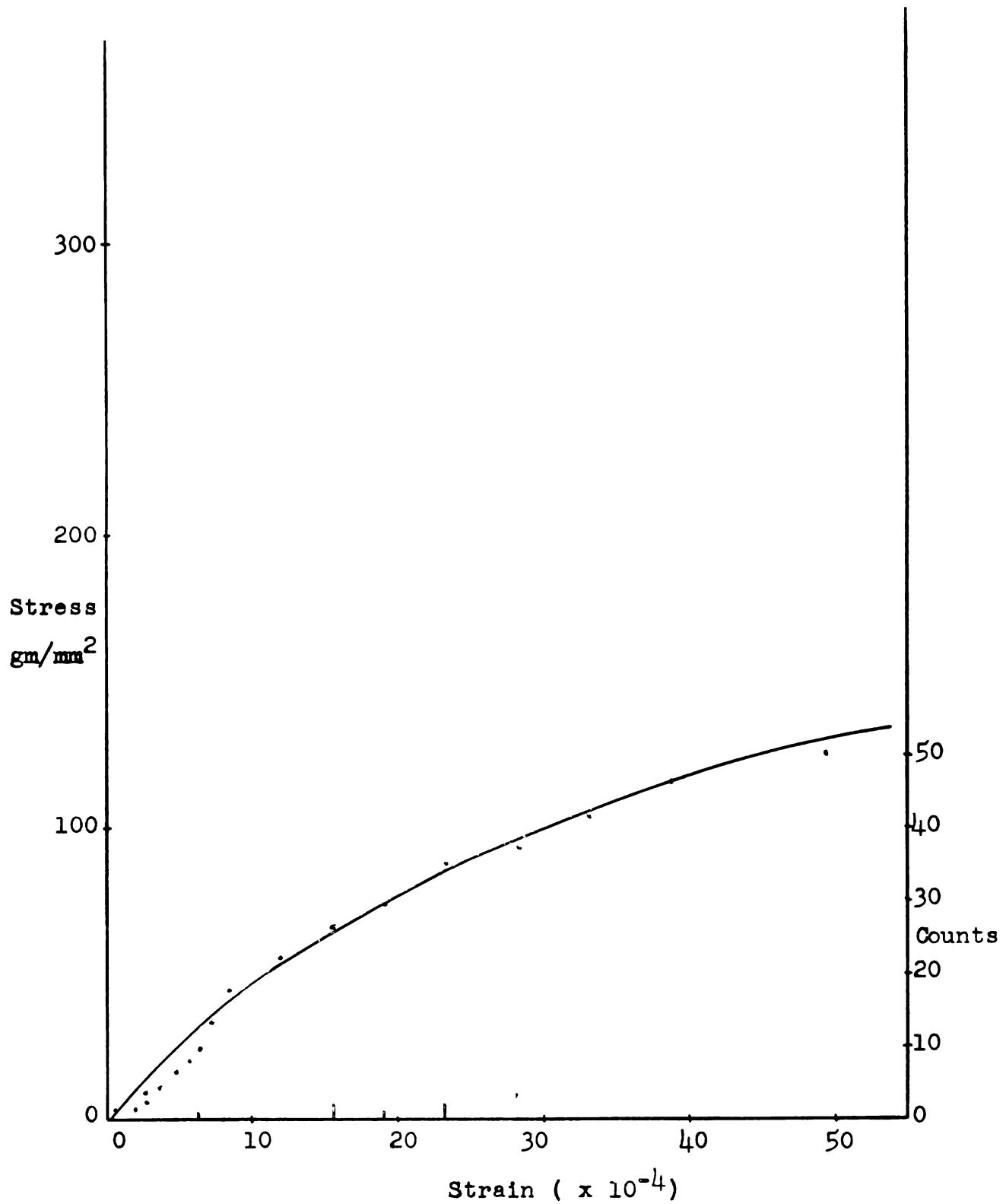


Figure 31. Histogram of Acoustic Emissions Counted at Normal Trigger Level. The data are plotted from Specimen 7 (KCl, two NaCl films).

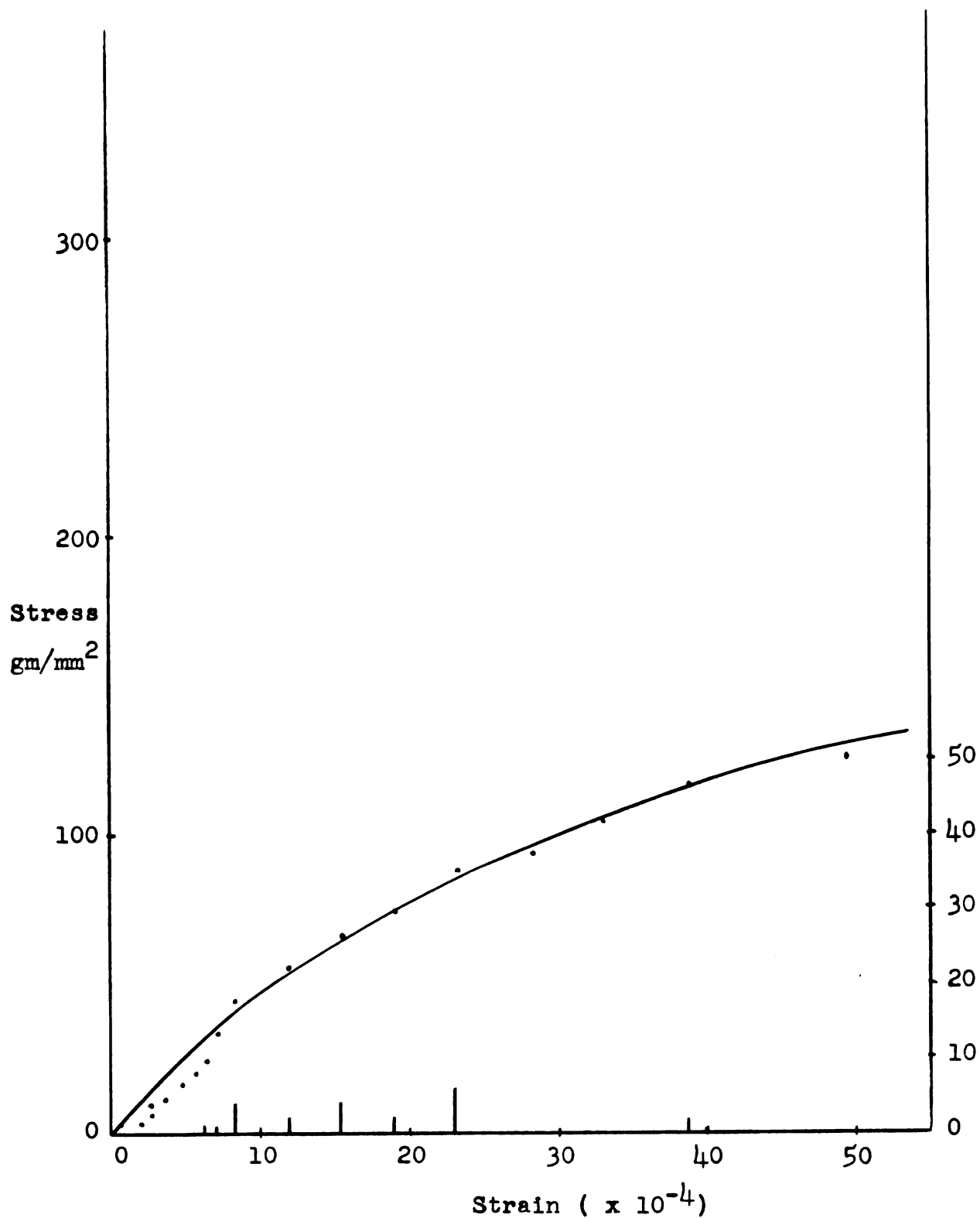


Figure 32. Histogram of Acoustic Emissions Counted Just Above Noise Level. The data are plotted from Specimen 7 (KCl, two NaCl films).

dislocation multiplication or the release of pile-ups gives rise to appreciable acoustic emission, except in the case when surface films are removed, as shown in Figure 20. Even then the number of acoustic emissions, when compared to that for LiF, is relatively low.

The difference in dislocation velocity in LiF and KCl is undoubtedly due to the differences in the chemical composition and structure of the two materials. In general it might be speculated that materials in which dislocation velocity is high are more likely to exhibit a macroscopic yield point than are those in which dislocation velocity is low. The case when energy barriers capable of supporting large dislocation pile-ups exist within or on the surface of such a material may constitute an exception; but even then the barriers must be overcome in order for an abrupt drop in the stress-strain curve to occur, as happened when the surface films were etched from the deformed KCl specimens tested here.

G. Effect of Thin Film on Dislocation Multiplication

It was brought out previously that four mechanisms of substrate hardening due to the presence of a solid surface film have been mentioned in the literature; these are:

- (1) Dislocation pile-ups beneath the surface film due to a difference in elastic moduli of the film and substrate material.
- (2) A change in the image force acting on dislocations very near the surface.
- (3) Inhibiting of cross-glide at the crystal-line surface.

(4) Inhibiting of surface sources.

Although all of these mechanisms are possible, it is believed that the effects of greatest magnitude are due to dislocation pile-ups beneath the surface film. This is substantiated by the fact that a large number of acoustic emissions are always observed when the surface films are etched away. Furthermore, general cross-glide is unlikely in LiF at room temperature (58-60) and surface cross-glide arising from the removal of the thin film could not account for the large number of acoustic emissions observed. It has already been observed that surface sources are not important for the deformation of LiF (28).

In the work-hardening region of both LiF and KCl, the presence of a thin film is known to cause an increase in the rate of work-hardening. This effect is, without doubt, due to the fact that the film prevents dislocations from leaving the crystal through the surface. Of much greater interest is the effect of the thin film during the early stages of straining, i.e., in the elastic range. The following discussion pertains only to LiF, since it has a well-defined, linear elastic region, while KCl does not.

The stress-strain curves of Figure 11 prove that the slope in the elastic region is affected by the presence of a thin film. Furthermore, a greater increase in slope is observed for film materials with larger values of c_{11} . A change in the slope of the elastic portion of the stress-strain curve means that the thin films have an effect on Young's modulus, E , of the substrate. The relationship

$$l_0 \epsilon_0 = 23.7 \times 10^{-8} \nu \mu / E \quad (49)$$

can be obtained from Equations (10) and (11) evaluated at $\epsilon = \epsilon_0$; and for the specimens used in this work, the expression becomes

$$l_0 \epsilon_0 = 8.89 \times 10^{-8} \mu / E \quad (50)$$

It was observed experimentally that the presence of a surface film caused an increase in both E and ϵ_0 . Hence if Equation (50) is to be true, the presence of the film must cause a corresponding increase in the ratio μ/l_0 ; and it is reasonable to assume that l_0 decreases while at the same time μ increases.

The shift in the loop-length distribution is probably due to two separate factors. First, the back stresses from dislocation pile-ups would tend to strengthen the crystal in the same manner as would a shortening of the mean dislocation loop-length of the original dislocation sources. This would cause only an apparent reduction in l_0 . Secondly, the surface film would reduce the effective loop-lengths of dislocation sources near the surface of the crystal, causing a real reduction in l_0 . Finally, μ must increase if E increases since they are related by the equation (62)

$$E = \mu(2\mu + 3\lambda)/(\mu + \lambda) \quad (51)$$

H. Mobile Dislocation Density

In the model presented for LiF, the mobile dislocation density should be highest when the greatest number of initial

sources are at their critical stress for multiplication. This occurs at a strain of ϵ_0 when the most probable loop-length, l_0 , has attained its critical stress. Gilman (63) and Johnston (64) have developed an expression for mobile dislocation density as a function of strain. This expression is

$$\rho_M = (\rho_0 + \beta \epsilon) \exp(-\phi \epsilon) \quad (52)$$

where ρ_M is the mobile dislocation density, ρ_0 is the initial dislocation density, β is a constant and ϕ is called the attrition coefficient. By the above reasoning the mobile dislocation density will attain a maximum at a value of strain which satisfies the equation

$$(d \rho_M / d \epsilon)_{\epsilon_0} = 0 \quad (53)$$

which gives

$$-\phi (\rho_0 + \beta \epsilon_0) \exp(-\phi \epsilon_0) + \beta \exp(-\phi \epsilon_0) = 0$$

or

$$\phi = \beta / (\beta \epsilon_0 + \rho_0) \quad (54)$$

For LiF, $\beta \approx 10^9$ dislocations/cm² (64) and $\epsilon_0 \approx 10^{-3}$ from page 51. If these values are used in the expression for ϕ , it follows that $\beta \epsilon_0 \gg \rho_0$, hence $\phi \approx 1/\epsilon_0 \approx 10^3$. Thus the expression for mobile dislocation density becomes

$$\rho_M = (\rho_0 + \beta \epsilon) \exp(-\epsilon/\epsilon_0) \quad (55)$$

which is an equation of the same form as Equation (17) for

$P'(\epsilon)d\epsilon$ provided ρ_0 is small. This fact agrees with the model presented here, since it is to be expected that the greatest number of acoustic emissions due to dislocation multiplication in LiF should occur at the strain for which the mobile dislocation density is a maximum.

If the relationship $\ell = C_1/\epsilon$ of Equation (11) and the substitution of $y = 1/\ell$ are applied to Equation (55) it becomes

$$\rho_M = (\rho_0 + \beta C_1 y) \exp(-\ell_0 y) \quad (56)$$

and the average value can be written as

$$\bar{\rho}_M = \int \rho_M (1/\ell) P(\epsilon) d\epsilon / \left[\int P(\epsilon) d\epsilon \right] \quad (57)$$

or simply

$$\bar{\rho}_M = I_3/I_2 \quad (58)$$

where I_2 is given by equation (35) and was found equal to $2\pi(0.895)$ for $m = 3$, and

$$I_3 = \int (\rho_0 + \beta C_1 y) \exp(-\ell_0 y) P(\epsilon) d\epsilon \quad (59)$$

When the proper substitutions are made and the integration carried out, it is found that $\bar{\rho}_M$ is of the order of 10^6 mobile dislocations/cm². This is certainly a reasonable average value for mobile dislocation density in the elastic range of LiF. The value of 10^{10} to 10^{12} dislocations/cm² estimated by Van Beuren (65) for "moderately deformed" polar crystals is several orders of magnitude higher than the value obtained here. The difference lies in the fact that

etch-pit techniques give estimates of total dislocation density whereas the value of 10^6 dislocations/cm² calculated above is for mobile dislocation density only.

I. Ultrasonic Damping

The ultrasonic damping data can perhaps best be used to obtain a qualitative estimate of the relative density of stationary dislocations. The piezoelectric crystal was of the same dimension as the cross section of the specimen; hence the damping effect is an integrated one in that it averages the total damping across the entire specimen cross section. It is to be expected, however, that most of the dislocation pile-ups due to the thin films would be near the crystal surface. Additionally, the large size of the piezoelectric crystal probably introduced reflections from the sides of the specimen; but this should not affect the relative magnitudes appreciably, since the effect should be approximately the same for all specimens. It will be remembered that the ultrasonic generator had to be disconnected during the application of each load increment and for a short time thereafter, until the acoustic emission ceased, because of interference between the acoustic emission and ultrasonic damping signals.

Two important observations can be made on the basis of damping data plotted in Figures 14-22. Damping in general increases with strain, and is greater in the coated specimens. Both facts support the models developed here for LiF and KCl. The increase in damping with strain indicates that dislocation

density increases in this case, which must be true. Furthermore, the fact that damping is greater in the coated crystals, as seen in Figures 21 and 22, indicates that dislocation density is greater due to pile-ups beneath the film.

Since the effect is averaged over the specimen cross section, however, it is surprising that the difference in damping in the coated and uncoated specimens is so distinct. Either the density of dislocations beneath the film is much greater than the internal dislocation density, or the stress field created by the surface pile-ups helps to create other pile-ups further away from the surface. Although the second possibility seems preferable, both are compatible with the models presented.

It was seen in Figure 21 that the logarithmic decrement is a linear function of strain. This can be represented by the equation

$$\ln (A_1/A_2) = \alpha \epsilon + b_0 \quad (60)$$

where α is the slope of the line and b_0 is the y-intercept. If the substitution $b_0 = \ln B_0$ is made, Equation (60) can be put in the form

$$A_1/A_2 = B_0 \exp(\alpha \epsilon) \quad (61)$$

and by using the relationship (11) it becomes

$$A_1/A_2 = B_0 \exp[\alpha \epsilon_0 (l_0/l)] \quad (62)$$

This expresses the ratio of successive amplitudes in terms of $(1/l)$; hence, an average value, $\overline{(A_1/A_2)}$, can be obtained

in the way as before.

For Specimen 1 the values of $\alpha \epsilon_0 = 0.128$ and $B_0 = 1.57$ can be taken from Figure 21; and Equation (62), for this particular case, becomes

$$A_1/A_2 = 1.57 \exp[0.128(\ell_0/\ell)] \quad (63)$$

Using Equation (29) the average value can be expressed as

$$\overline{(A_1/A_2)} = [1/2\pi(0.895)] \int (A_1/A_2) P(\epsilon) d\epsilon \quad (64)$$

since it was shown in Equation (37) that

$$I_2 = \int P(\epsilon) d\epsilon = 2\pi(0.895)$$

If the usual substitution $y = \ell/\ell_0$ is made, Equation (64) becomes

$$\overline{(A_1/A_2)} = (1.57/0.895) \int_0^{\epsilon_y/C_1} \exp(0.128 \ell_0 y) P(\epsilon) d\epsilon \quad (65)$$

or

$$\begin{aligned} \overline{(A_1/A_2)} = (1.57/0.895) & \left\{ \ell_0^2 \int y \exp(-0.872 y) dy \right. \\ & + (\ell_0^2/4) \exp(1/2) \int y \exp(-0.372 \ell_0 y) dy \\ & \left. - (\ell_0/4) \exp(1/2) \int \exp(-0.372 \ell_0 y) dy \right\} \quad (66) \end{aligned}$$

where the limits, $\epsilon_y/C_1 = m/\ell_0$, are obtained by the substitutions $\epsilon_y = m\epsilon_0$ and $C_1 = \epsilon_0 \ell_0$. For $m = 3$, it is found that

$$\overline{(A_1/A_2)} = 2.04 \quad (67)$$

which states that, on the average, the amplitude of an ultrasonic pulse in LiF should be about twice that of its reflected pulse; and this is verified by the data in Appendix IV.

V. CONCLUSIONS

The two principal causes of acoustic emission from ionic single crystals during the early stages of straining appear to be the release of dislocation pile-ups and the operation of fast dislocation sources; the latter occurring only in 'hard' crystals, such as LiF, where dislocation velocity is high. When 'soft' ionic crystals, such as KCl, are strained, acoustic emission is observed only when pile-ups are released and these are of a much lower level; presumably because dislocation velocity is lower and therefore the elasto-plastic waves created are of smaller amplitude.

The removal of a surface film from a strained crystal, whether LiF or KCl, always gives rise to high level acoustic emission, implying that dislocations piled up beneath the film during straining are released. In addition the presence of a thin, solid, surface film is observed to raise the value of stress corresponding to a given strain above that for an uncoated crystal, thus providing further evidence for the presence of dislocation pile-ups. This is particularly evident in the elastic range of LiF where the presence of a film is seen to raise the value of young's Modulus, E .

The energy barriers which prevent dislocations from escaping through the surface, and thus create the pile-ups, are attributed partly to a film-substrate ratio of the elastic constant c_{11} which is greater than one, but mainly to the residual strain energy due to lattice distortion

at the film-substrate interface.

In both coated and uncoated crystals of LiF, a definite acoustic emission distribution is observed in the elastic range and seems to be a result of the operation of dislocation sources. When the number of emissions, N , observed at a given strain, ϵ , is plotted versus ϵ , a bell-shaped curve, with maximum at $\epsilon_0 = 10^{-3}$ and skewed toward larger values of ϵ , is obtained. The skewness is attributed to dislocation interactions. From the curve, a total probability function expressing the probability of observing N acoustic emissions while the specimen is being strained from ϵ to $\epsilon + d\epsilon$ is developed. This probability is then correlated with a similar probability function for the distribution of dislocation source inverse loop-lengths, and an expression for the acoustic emission probability function in terms of inverse loop-length is obtained.

The expression can be used to calculate the average value of any variable which depends upon $(1/\ell)$ by means of the formula

$$\bar{A} = \int A(1/\ell) P(\epsilon) d\epsilon / \left[\int P(\epsilon) d\epsilon \right] .$$

Average values calculated here for dislocation strain, mobile dislocation density and ratio of successive ultrasonic wave amplitudes are $\bar{\epsilon} = 1.84\epsilon_0$, $\bar{\rho}_M \approx 10^6 \text{ cm}^{-2}$ and $\overline{A_1/A_2} = 2.04$ which agree very well with accepted values and experimental data.

The dimensionless factor, 1.84, mentioned above can be used as a measure of the influence of dislocation

interaction on the original inverse loop-length distribution since it is also the ratio of the actual average dislocation strain to that average value which would be obtained provided no interaction takes place.

A comparison of strain energies indicates that dislocation strain in the elastic range predominates over strain due to lattice parameter changes; and a comparison of the calculated average value of strain for the two extreme cases, $\bar{\epsilon} = 1.84\epsilon_0$ and $\bar{\epsilon}_L = 1.5\epsilon_0$ respectively, indicates that on the average the total strain can be accommodated by dislocation motion only.

Finally, it is observed that ultrasonic damping in both LiF and KCl increases with strain and is generally greater for a coated rather than an uncoated specimen.

VI. SUGGESTIONS FOR FURTHER RESEARCH

This work has lead to several other avenues of research which seem worth exploring.

It is felt that the electron-microscope would be a valuable tool to use in conjunction with the acoustic emission apparatus in determining the exact nature of the initial distribution and operation of dislocation sources in hard ionic crystals. Unfortunately, however, LiF melts when subjected to the electron beam. Hence, a hard ionic material such as MgO, which can be studied by the electron microscope, should be subjected to tests similar to those performed here on LiF to determine whether this material exhibits a similar acoustic emission distribution in the elastic range. If this is found to be true, tests performed on MgO single crystals under the electron microscope should be quite profitable.

An attempt to correlate yield phenomena and dislocation velocity with acoustic emission distribution in the macroscopic elastic range for various materials might prove to be of interest. It was found here that for LiF, in which dislocation velocity is high, the acoustic emission distribution in the macroscopic elastic range follows a skewed curve and the material yields only after the dislocation sources associated with this distribution are exhausted. For KCl, in which dislocation velocity is low, no initial acoustic emission distribution is observed and there is no macroscopic

yield point. If a study of different materials indicated that a macroscopic yield point is a function of dislocation velocity and pre-yield acoustic emission distribution, then much could be learned concerning yield phenomena.

Finally, other investigations using coated LiF and KCl single crystals could easily be devised. Specimen size effect would be of considerable interest as well as variation in film thicknesses. Also, different types of loading conditions such as tension or simple bending might be used. Research featuring coated bi-crystals or large-grained polycrystalline materials should prove to be especially interesting.

BIBLIOGRAPHY

1. Roscoe, R.; Nature, Lond. 133, 912 (1934).
2. Roscoe, R.; Phil. Mag. 21, 399 (1936).
3. Kramer, I. R., and Demer, L. J.; Prog. in Mat. Sci. 9, No. 3, 1 (1961).
4. Cottrell, A. H., and Gibbons, D. F.; Nature, Lond. 162, 488 (1948).
5. Harper, S., and Cottrell, A. H.; Proc. Phys. Soc. B 63, 331 (1950).
6. Andrade, E. N. DaC., and Henderson, C.; Phil. Trans. Royal Soc. A 244, 177 (1951).
7. Brown, A. F., and Honeycombe, R. W. K.; Phil. Mag. 42, 1146 (1951).
8. Gilman, J. J., and Read, T. A.; Trans. AIME (Met.) 194, 875 (1952).
9. Andrade, E. M. DaC.; Inst. of Metals Monograph and Report Series No. 13, 133 (1953).
10. Paxton, H. W., and Cottrell, A. H.; Acta Met. 2, 3 (1954).
11. Gilman, J. J.; ASTM Spec. Tech. Rep. No. 171, 3 (1955).
12. Suzuki, H., Ikeda, S., and Takeuchi, S.; J. Phys. Soc. Japan 11, 382 (1956).
13. Takamura, J.; Mem. Fac. Eng. Kyoto Univ. 18, 255 (1956).
14. Greenough, G. B., and Ryder, D. A.; Inst. of Metals Journal 84, 467 (1956).
15. Garstone, J., Honeycomb, R. W. K., and Greetham, G.; Acta Met. 5, 485 (1956).
16. Weiner, L. C., and Gensamer, M.; J. of Inst. Metals 85, 441 (1957).
17. Lipsett, F. R., and King, R.; Proc. Phys. Soc. B 70, 608 (1957).
18. Rosi, F. D.; Acta Met. 5, 348 (1957).
19. Adams, M. A.; Acta Met. 6, 327 (1958).

20. Fleischer, R. L., and Chalmers, B.; Trans. AIME (Met.) 212, 265 (1958).
21. Brame, D. R., and Evans, T.; Phil. Mag. 3, 971 (1958).
22. Evans, T., and Schwarzenberger, D. R.; Phil. Mag. 4, 889 (1959).
23. Westwood, A. R. C., and Demer, L. J.; Nature 186, 146 (1960).
24. Westwood, A. R. C.; Phil. Mag. 5, 981 (1960).
25. Gilman, J. J.; Phil. Mag. 6, 159 (1961).
26. Phillips, W. L., Jr.; J. Am. Ceramic Soc. 44, 395 (1961).
27. Class, W. H., Machlin, E. S., and Murray, G. T.; Trans. AIME (Met.) 221, 769 (1961).
28. Fisher, J. C.; Trans. AIME (Met.) 194, 531 (1954).
29. Read, W. T., Jr.; "Dislocations in Crystals", McGraw-Hill Book Co., New York, p 76 (1953).
30. Aerts, E., and Dekeyser, W.; Acta Met. 4, 557 (1956).
31. Cottrell, A. H.; "Dislocations and Plastic Flow in Crystals", Oxford University Press, p 105 (1953).
32. Eshelby, J. D., Frank, F. C., and Nabarro, F. R. N.; Phil. Mag. 42, 351 (1951).
33. Barrett, C. S.; Acta Met. 1, 2 (1953).
34. Barrett, C. S.; Trans. AIME (Met.) 197, 1652 (1953).
35. Barrett, C. S., Aziz, P. M., and Markon, I.; Trans. AIME (Met.) 197, 1655 (1953).
36. Edelson, B. I., and Robertson, W. D.; Acta Met. 2, 583 (1954).
37. Cottrell, A. H.; "Dislocations and Plastic Flow in Crystals", Oxford University Press, pp 55, 103 (1953).
38. Read, W. T., Jr.; "Dislocations in Crystals", McGraw-Hill Book Co., New York, p 132 (1953).
39. Head, A. K.; Phil. Mag. 44, 92 (1953).
40. Conners, G. H.; PhD Thesis, Michigan State University (1962).
41. Gilman, J. J.; Phil. Mag. 6, 159 (1961).

42. Johnston, W. G., and Gilman, J. J.; J. Appl. Phys. 31, 632 (1960).
43. Suzuki, T.; "Dislocations and Mechanical Properties of Crystals", Ed. by Fisher et al, John Wiley and Sons, Inc., New York, p 215 (1957).
44. Hearmon, R. F. S.; Phil. Mag. 5, 323 (1956).
45. Perry, C. C., and Lissner, H. R.; "The Strain Gage Primer", McGraw-Hill Book Co., Inc., New York, p 201 (1955).
46. Johnston, W. G.; J. Appl. Phys. 33, 2719 (1962).
47. Suzuki, T.; "Dislocations and Mechanical Properties of Crystals" Ed. by Fisher et al, John Wiley and Sons, Inc., New York, p 224 (1957).
48. Kittel, C.; "Introduction to Solid State Physics", John Wiley and Sons, Inc., New York, pp 41, 80 (1953).
49. Mendelson, S.; Phil. Mag. 8, 1633 (1963).
50. Granato, A., and Lucke, K.; J. Appl. Phys. 27, 583 (1956).
51. Koehler, J. S.; "Imperfections in Nearly Perfect Crystals", John Wiley and Sons, Inc., New York, p 197 (1952).
52. Cottrell, A. H.; "Dislocations and Plastic Flow in Crystals", Oxford University Press, p 84 (1953).
53. Kittel, C; "Introduction to Solid State Physics", John Wiley and Sons, Inc., New York, p 80 (1953).
54. Triffet, T.; "Introduction to the Mechanics of Discontinuous Media", Unpublished Manuscript, pp 3-23 - 3-27.
55. Cottrell, A. H.; "Dislocations and Plastic Flow in Crystals", Oxford University Press, p 84 (1953).
56. Menzel, D. H.; "Fundamental Formulas of Physics", Dover Publications, Inc., New York, p 113 (1960).
57. Ford, H.; "Advanced Mechanics of Materials", John Wiley and Sons, Inc., pp 346, 347 (1963).
58. Gilman, J. J.; Acta Met. 7, 608 (1959).
59. Hulse, C. O., Copley, S. M. and Pask, J. A.; J. Am. Ceramic Soc. 46, 317 (1963).

60. McEvily, A. J., Jr., and Machlin, E. S.; "Fracture", John Wiley and Sons, Inc., New York, p 450 (1959).
61. Nabarro, F. R. N., Basinski, Z. S., and Holt, D. B.; Adv. in Phys. 13, 193 (1964).
62. Triffet, T.; "Introduction to the Mechanics of Discontinuous Media", Unpublished Manuscript, p 3-27.
63. Gilman, J. J.; Private Communication.
64. Johnston, W. G.; J. Appl. Phys. 33, 2716 (1962).
65. Van Bueren, H. G.; "Imperfections in Crystals", North-Holland Publishing Co., p 74 (1960).

APPENDICES

Appendix I: Specimen Identification Table

<u>Specimen Number</u>	<u>Substrate Material</u>	<u>Film Material</u>	<u>No. of Sides Coated</u>	<u>Etched</u> (Yes or No)
1	LiF	None	-	-
2	LiF	None	-	-
3	LiF	CaF ₂	1	Yes H ₂ SO ₄
4	LiF	NaCl	2	No
5	LiF	NaCl	2	Yes H ₂ O
6	KCl	None	-	-
7	KCl	NaCl	2	No
8	KCl	CaF ₂	1	No
9	LiF	NaCl	1	Yes H ₂ O
10	KCl	NaCl	1	yes H ₂ O
11	KCl	NaCl	2	Yes H ₂ O

Appendix II: List of Equipment and Apparatus

<u>Reference Code</u>	<u>Description of Equipment</u>
A	Four SR-4 Strain Gages, Type A-5 Res. 119.6 ± 2 ohms; gage factor $2.01 \pm 1 \%$.
B	Twin-viso Sanborn Recorder, Model 60-1300.
C	Two Precision Solid State strain gages.
D	Arenberg Ultrasonic Pulsed Oscil- lator PG-650-C.
E	Arenberg Attenuator ATT-693.
F	Balancing Network, Arulab WB 100 S. N.
G	Arenberg Pre-amplifier PA-620.
H	Arenberg Wide Band Amplifier WA-600.
I	Tektronix Oscilloscope, Type 532.
J	Tektronix Plug-in Unit, Type 53/54C.
K	Laminated ADP Crystal Stack.
L	Tektronix Type 122 Low-level Pre-amplifier.
M	Spencer-Kenedy Variable Electron- ic Filter, Model 302.
N	Tektronix Plug-in Unit, Type 53/54D.
O	Ampex Series FR-1100 Recorder/Re- producer.
P	Knight Audio Amplifier KN 3010.
Q	Bell and Howell Microphone 302.
R	Hewlett-Packard Electronic Counter, Model 523B.

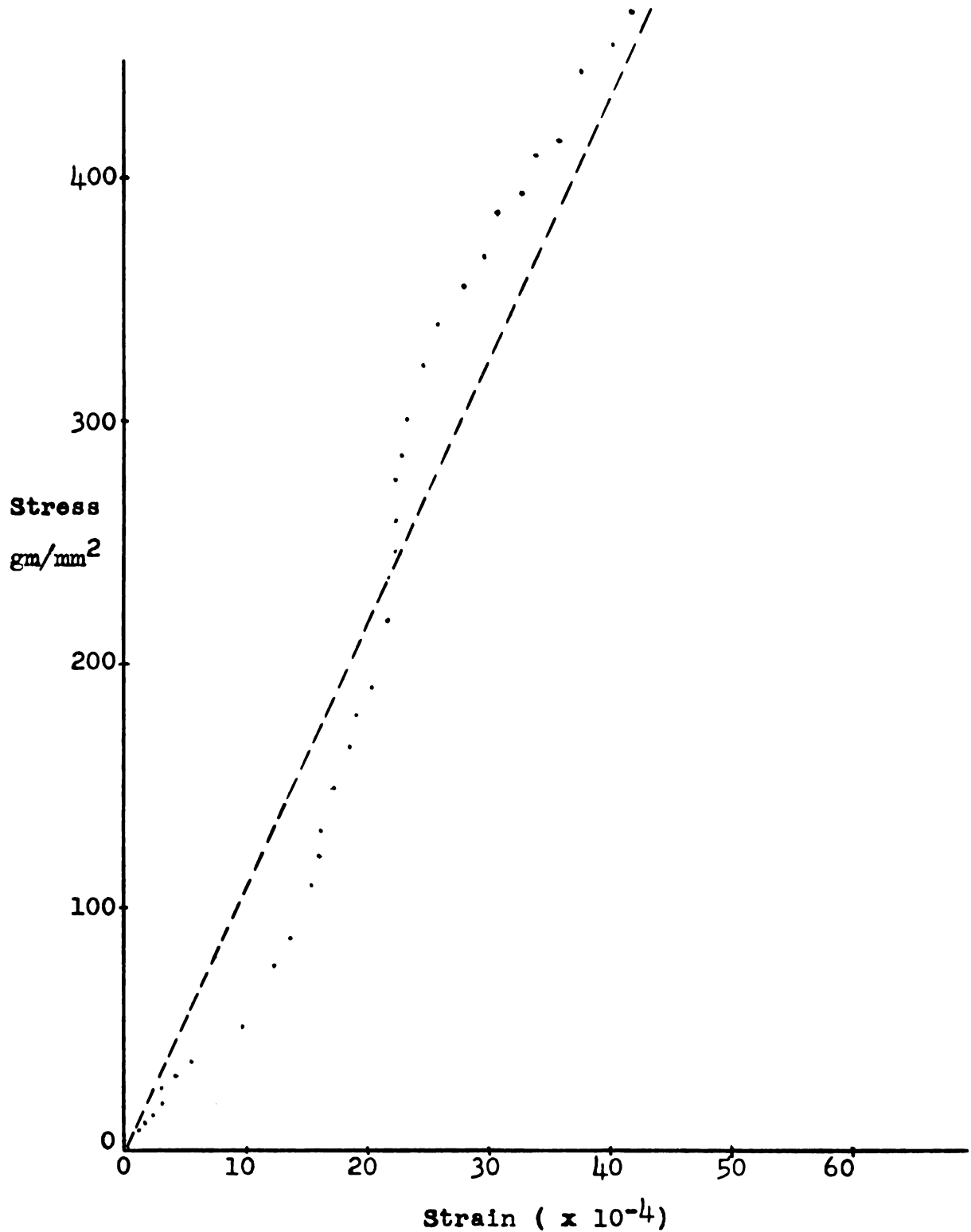
Appendix III:Stress-Strain and Logarithmic Decrement-Strain Curves

Figure 33. Stress-strain Curve for Specimen 1. (LiF, No Film.)

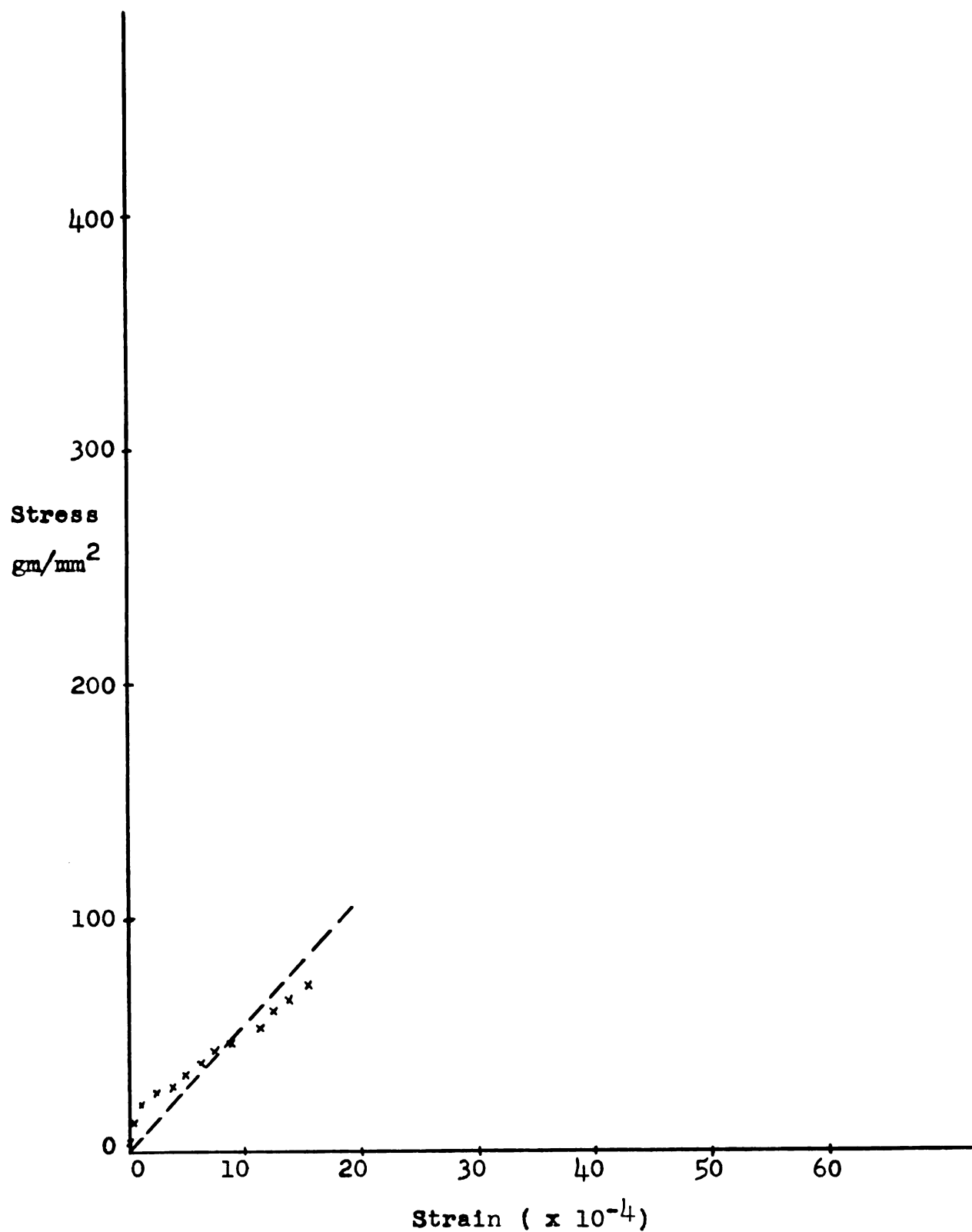


Figure 34. Stress-strain Curve for Specimen 2. (LiF, No Film.)

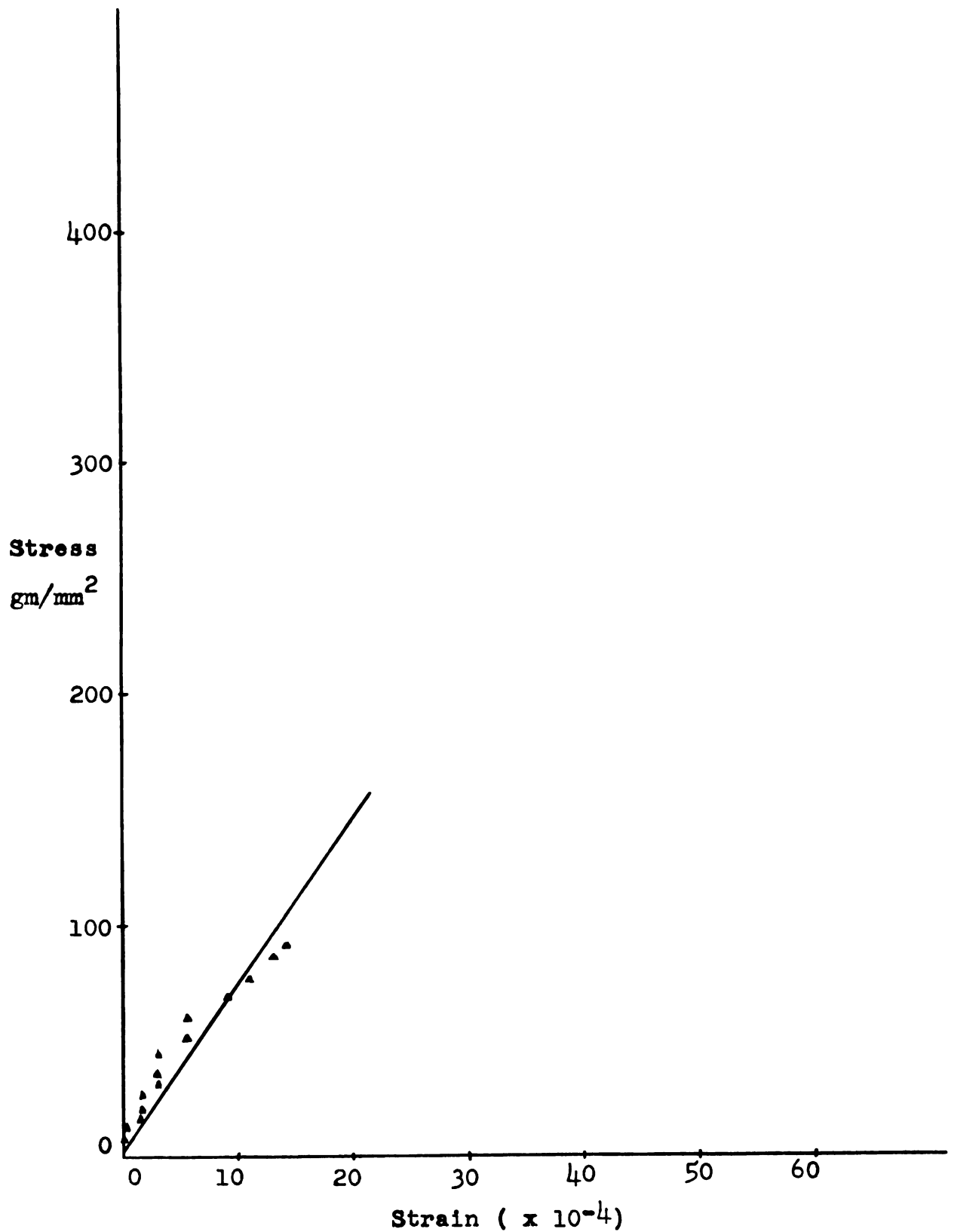


Figure 35. Stress-strain Curve for Specimen 3. (LiF, One CaF₂ Film.)

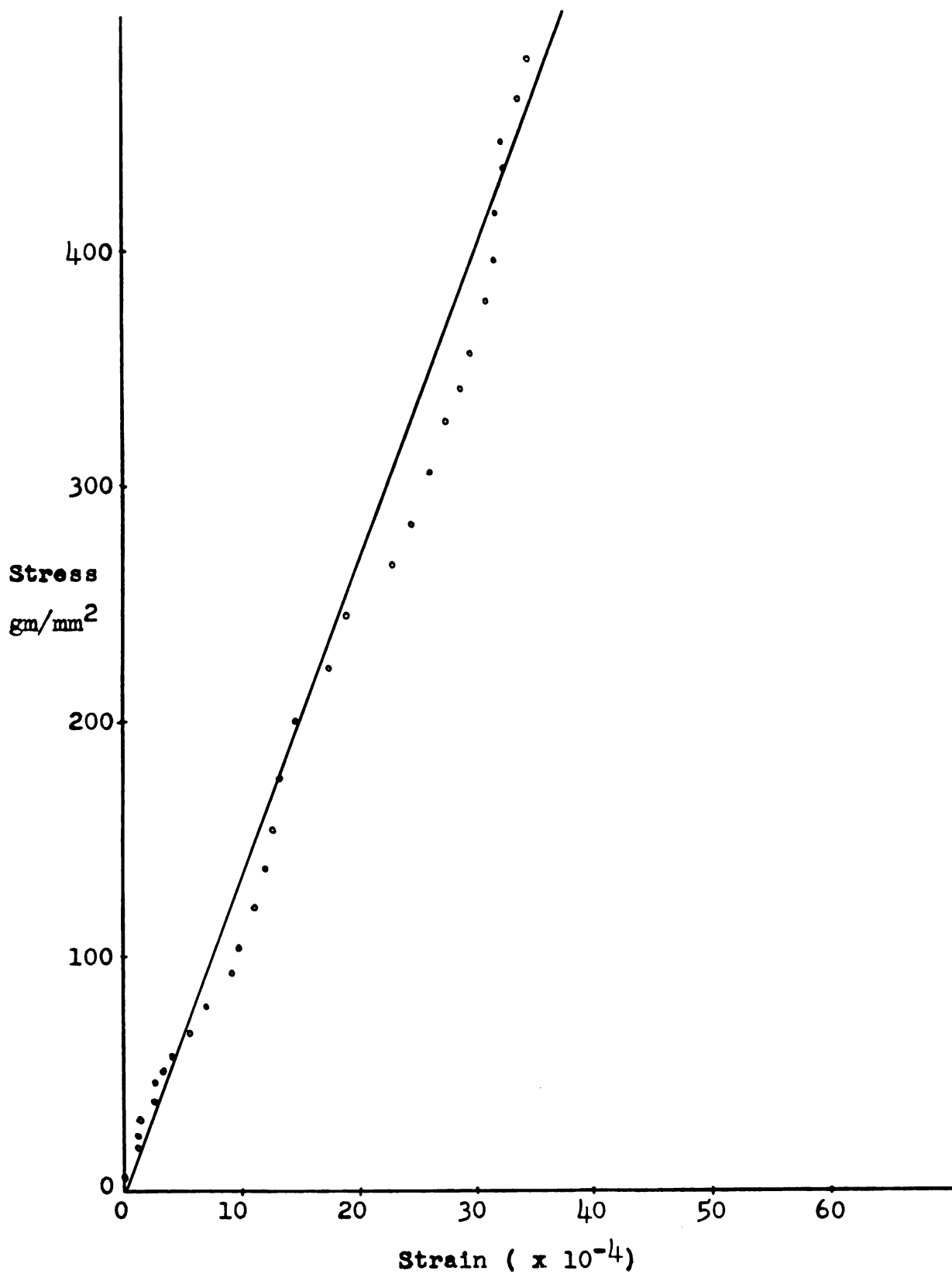


Figure 36. Stress-strain Curve for Specimen 4. (LiF, Two NaCl Films.)

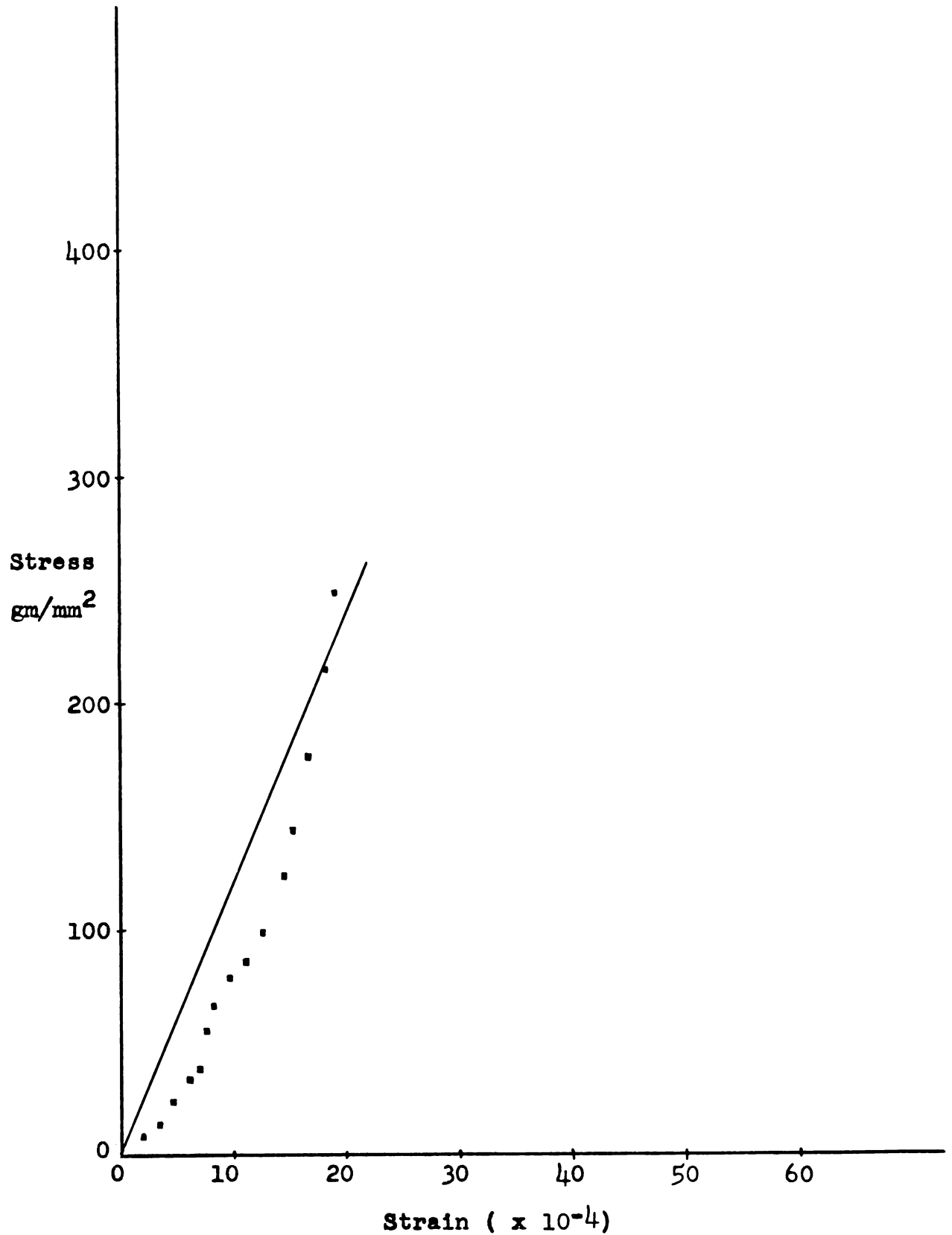


Figure 37. Stress-strain Curve for Specimen 5. (LiF, Two NaCl Films.)

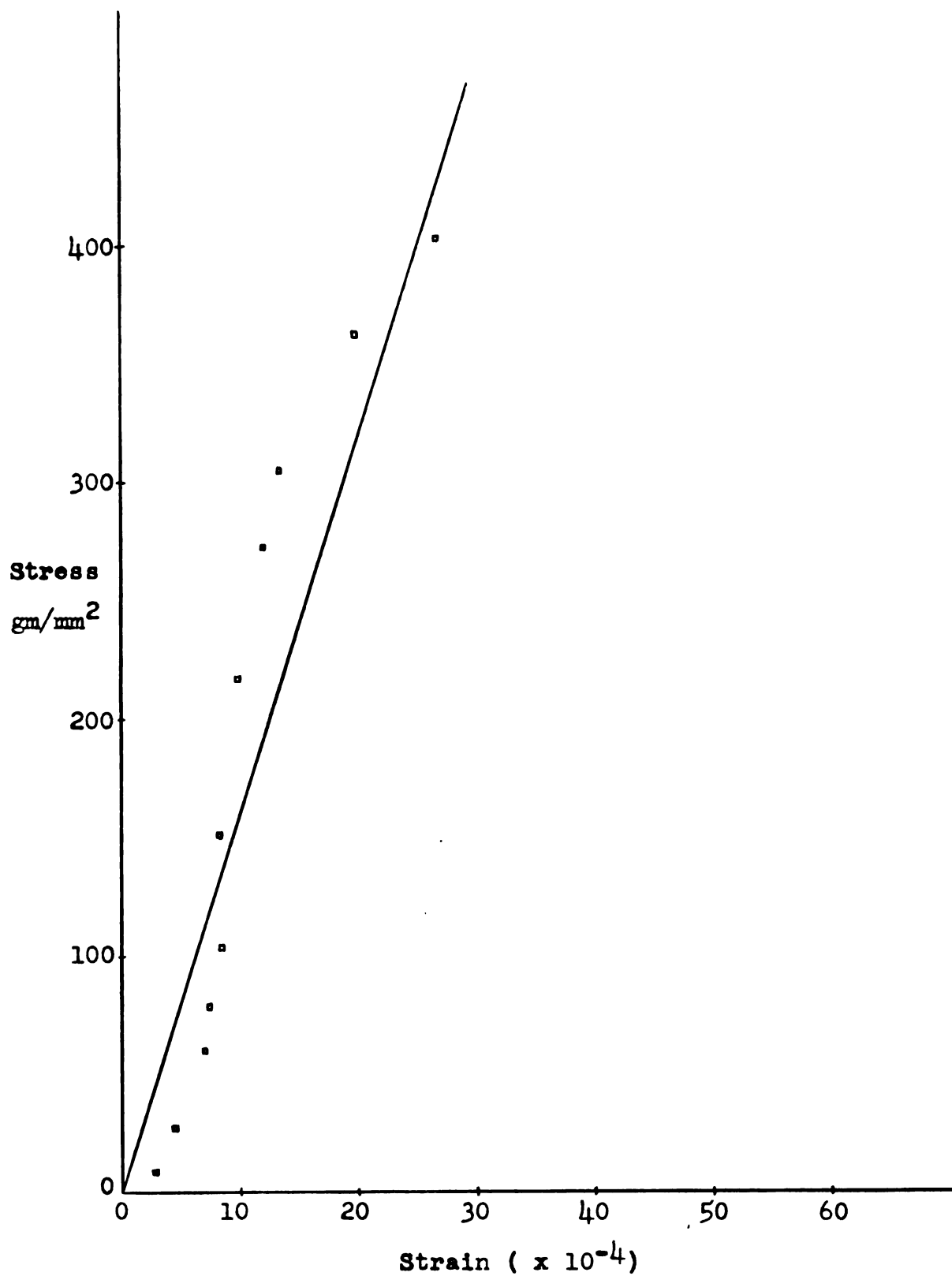


Figure 38. Stress-strain Curve for Specimen 9. (LiF, One NaCl Film.)

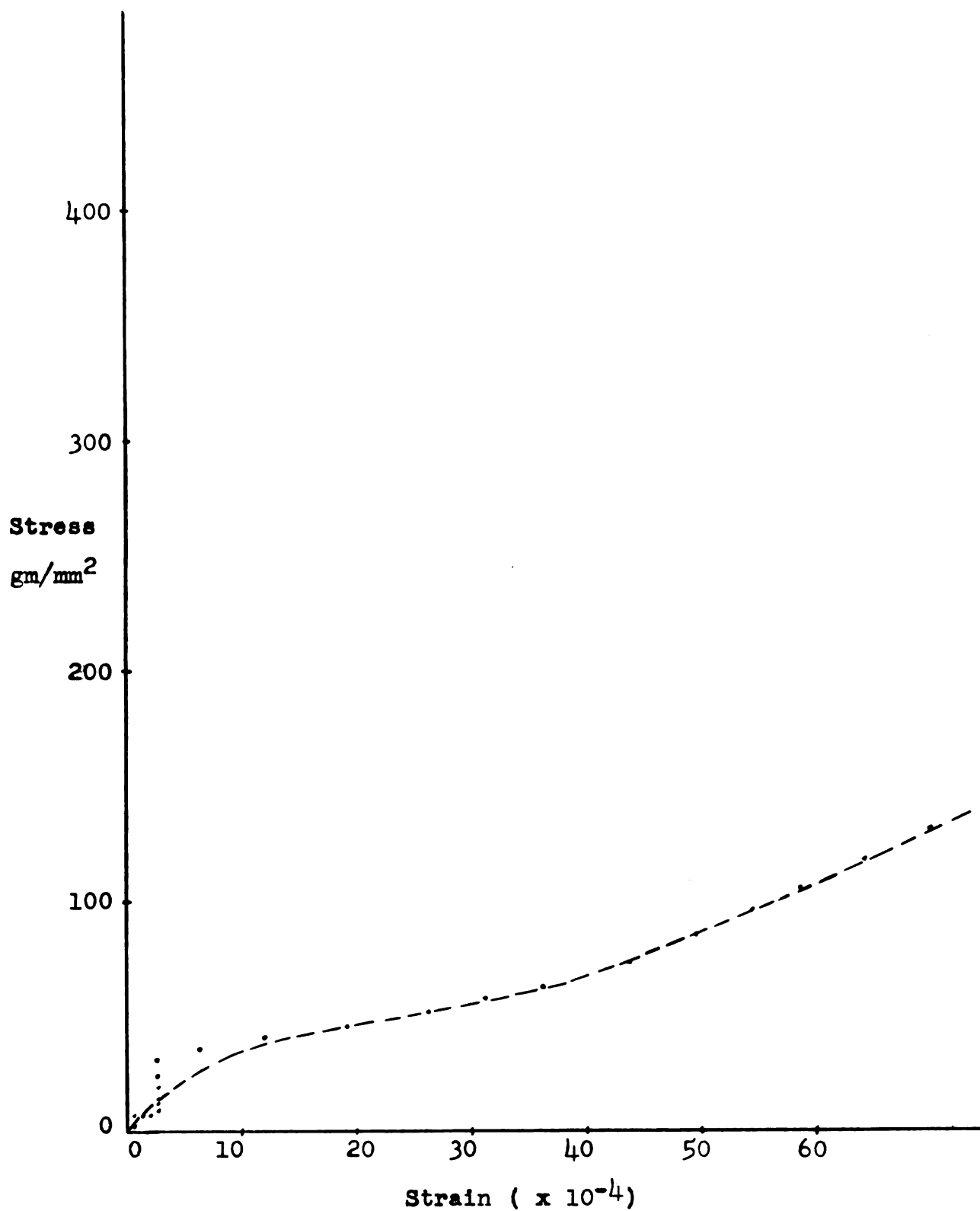


Figure 39. Stress-strain Curve for Specimen 6. (KCl, No Film.)

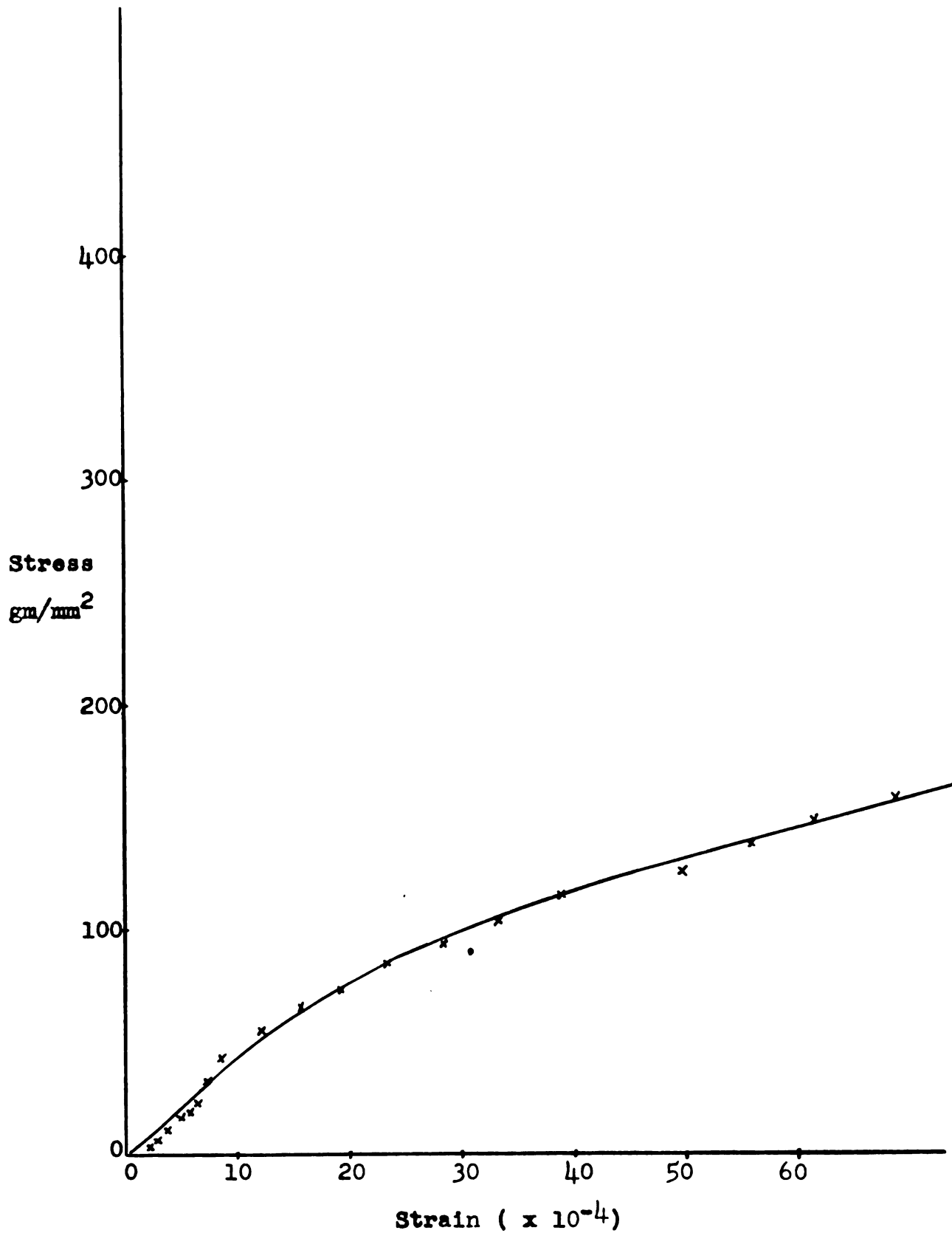


Figure 40. Stress-strain Curve for Specimen 7. (KCl, Two NaCl Films.)

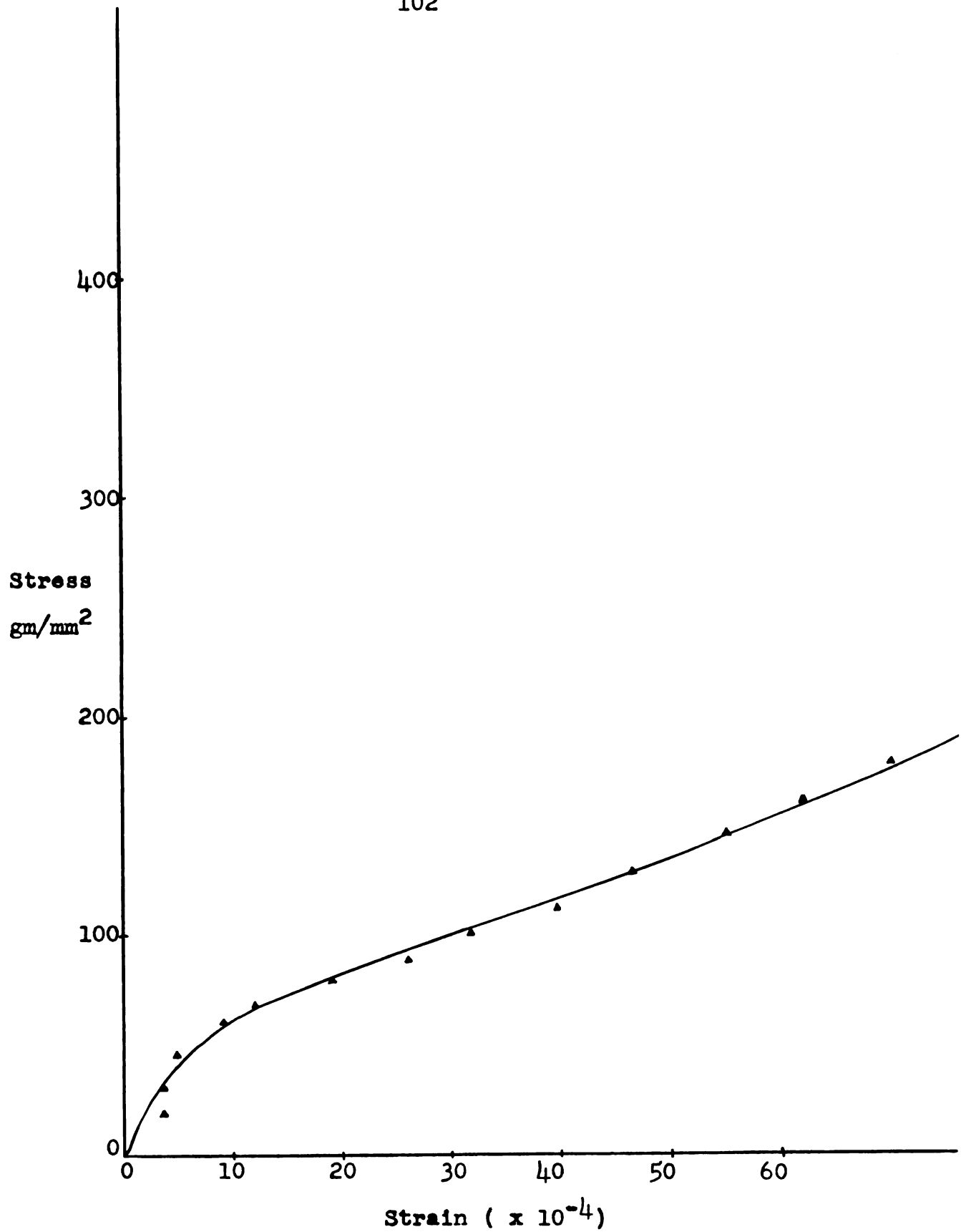


Figure 41. Stress-strain Curve for Specimen 8. (KCl, One CaF₂ Film.)

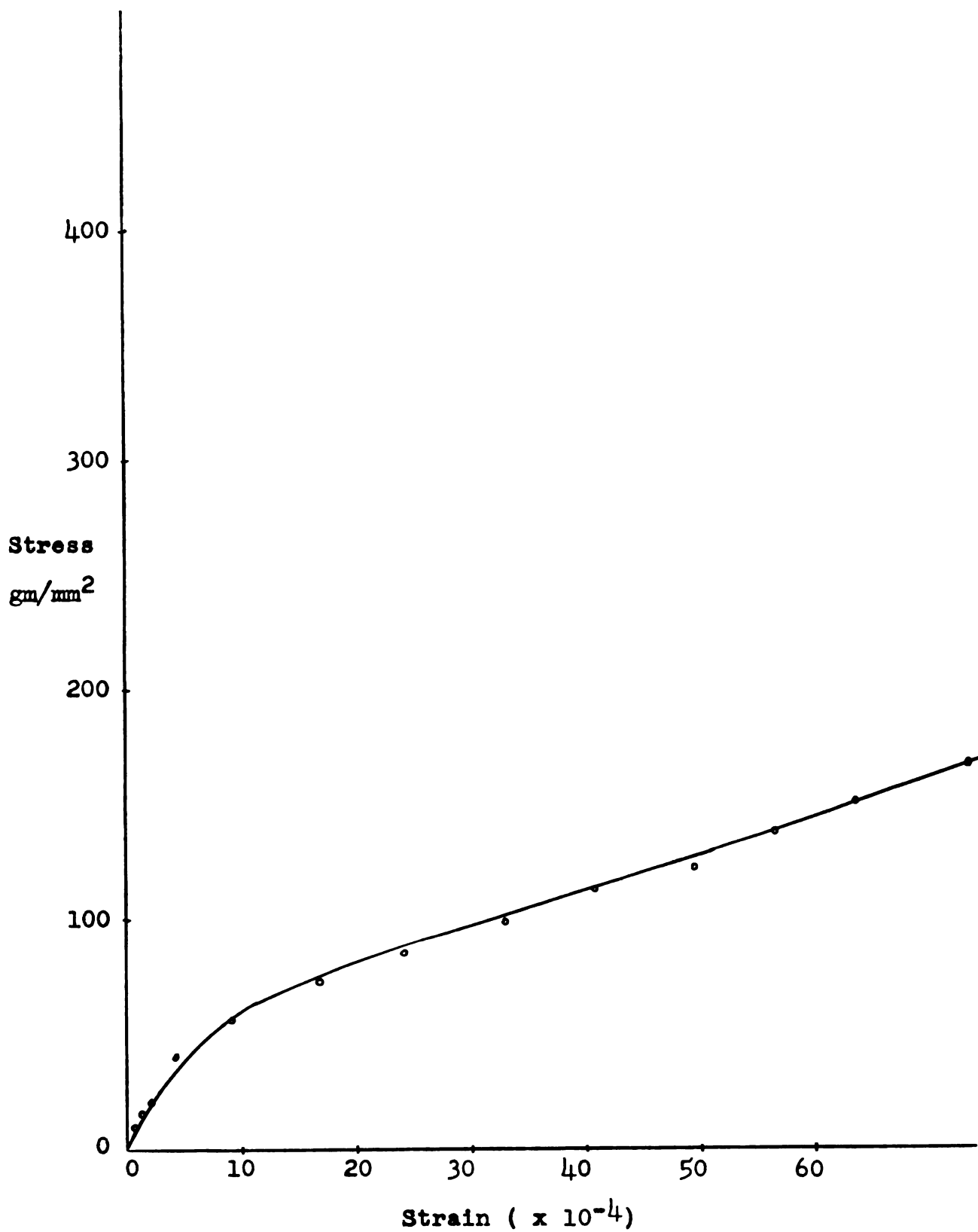


Figure 42. Stress-strain Curve for Specimen 10. (KCl, One NaCl Film.)

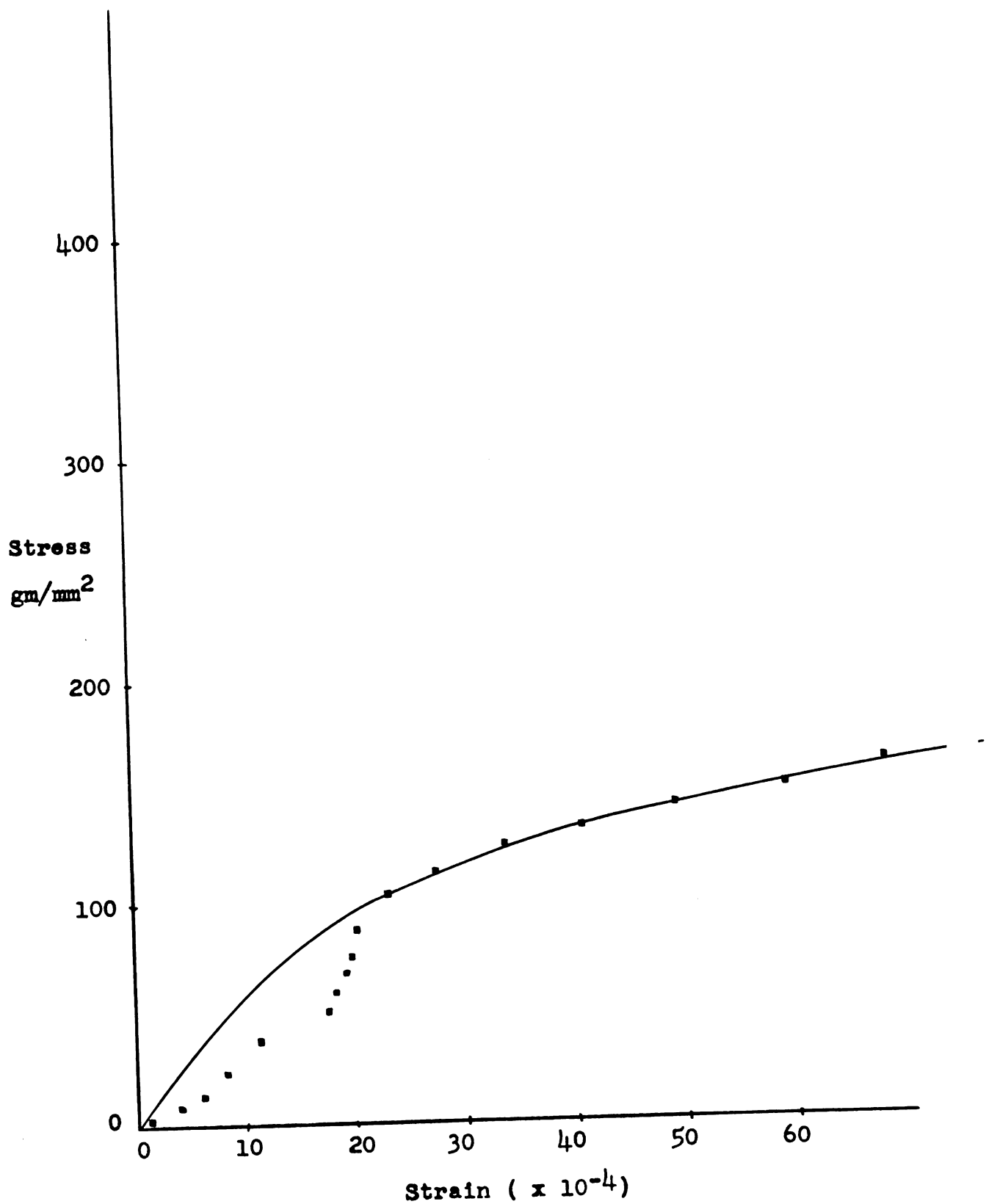


Figure 43. Stress-strain Curve for Specimen 11. (KCl, Two NaCl Films.)

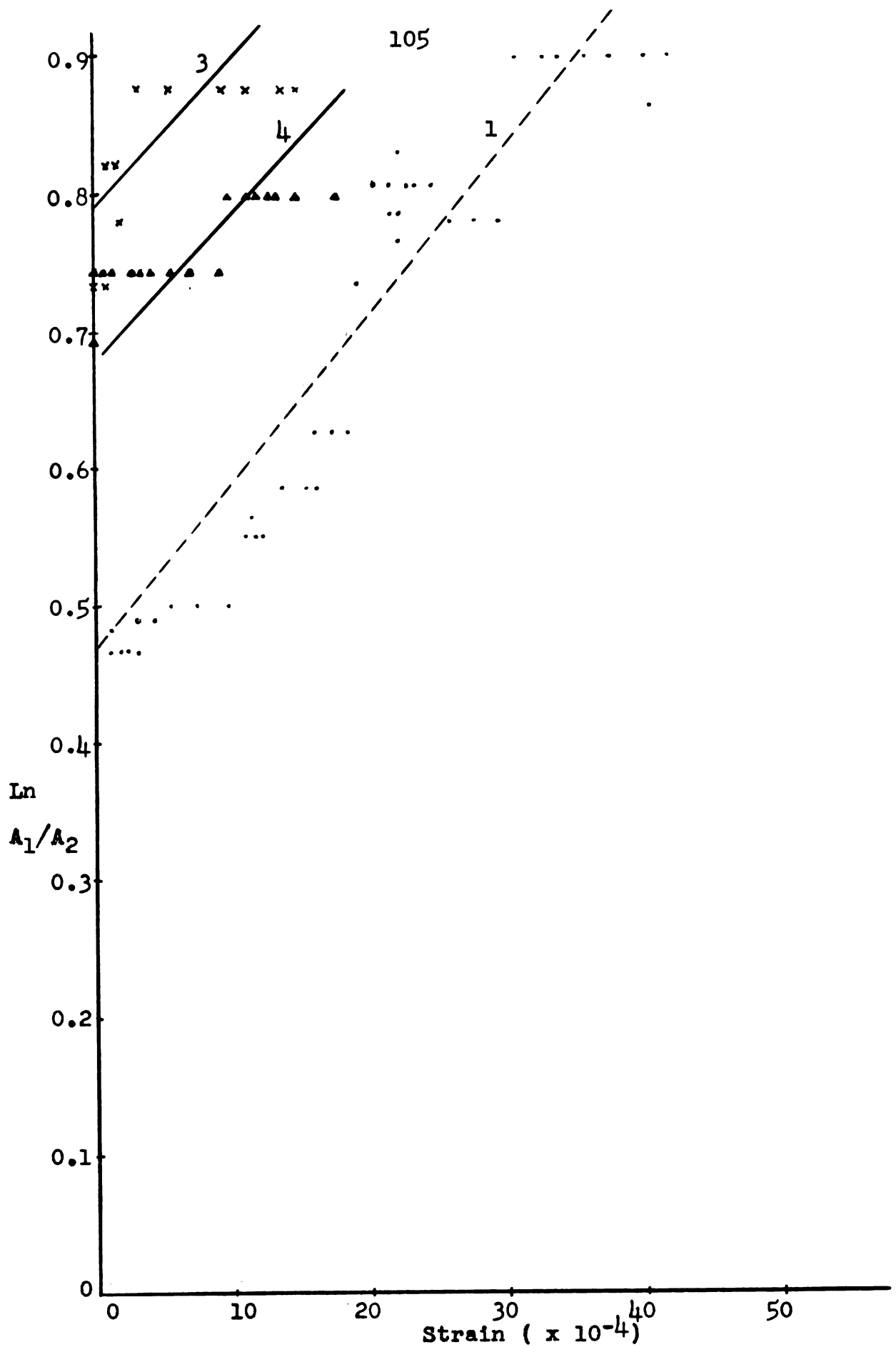


Figure 44. Logarithmic Decrement-strain Curve for Specimens 1, 3 and 4.

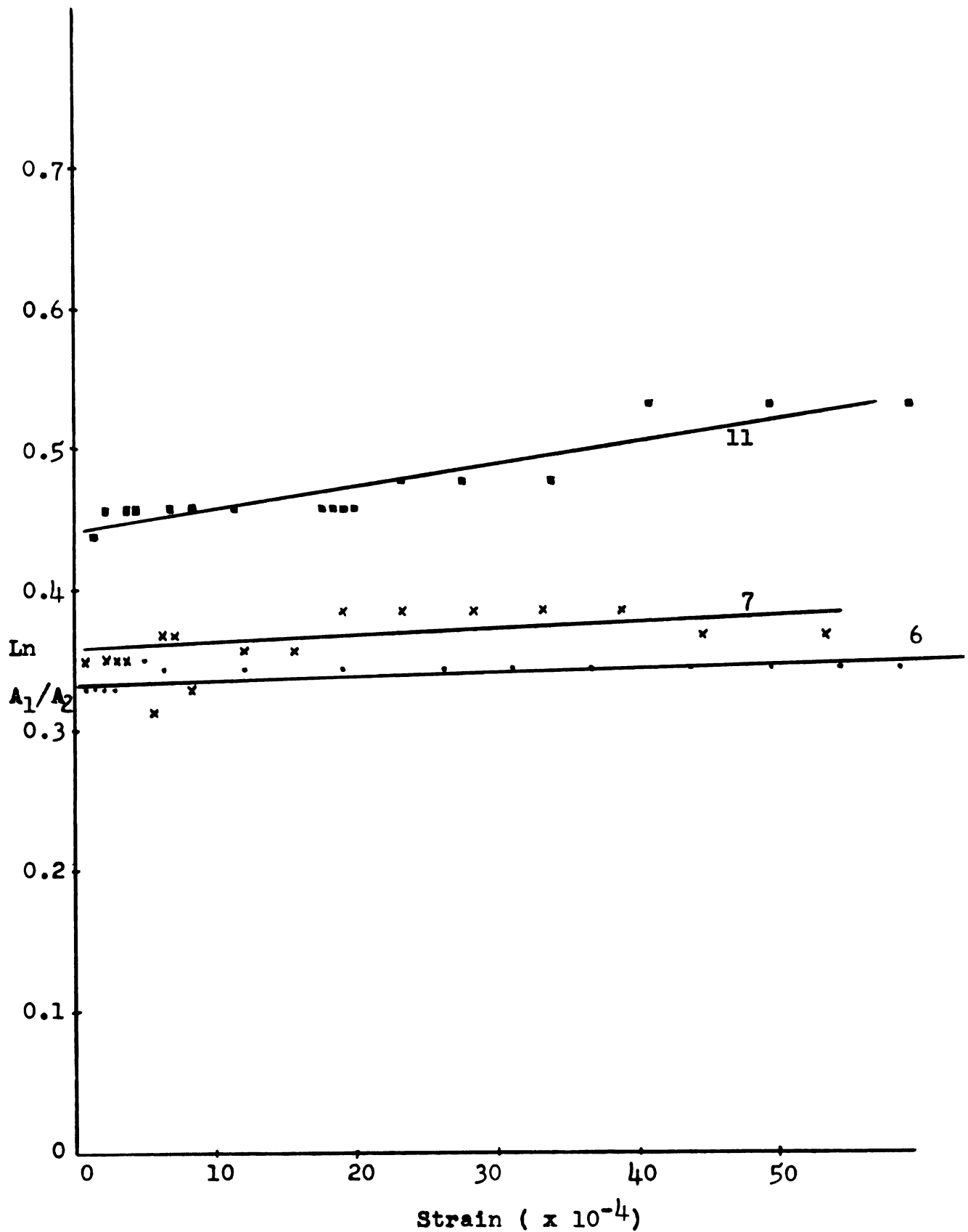


Figure 45. Logarithmic Decrement-strain Curve for Specimens 6, 7 and 11.

Appendix IV: Raw Data

- Notes:
- a. Units of stress are gm/mm^2 .
 - b. The value in the strain column must be multiplied by 10^{-4} .
 - c. The oscilloscope gain used in recording acoustic emission was 1000 MV/cm.
 - d. The background noise on the oscilloscope was $1/4$ cm, i.e. 250 MV.
 - e. The sweep speed was 50 micro-sec/cm.
 - f. The number or numbers directly under the column heading COUNTS/INCREMENT denote the trigger level setting used in counting the acoustic emissions.

Specimen 1

STRESS	STRAIN	$\text{LN}(A_1/A_2)$	COUNTS/INCREMENT 1/2 cm
8.43	0	0.444	0
8.43	0	0.482	0
8.43	1.23	0.482	0
8.43	1.23	0.482	0
8.43	1.23	0.466	4
11.24	1.85	0.466	0
14.05	2.46	0.466	1
19.67	3.08	0.466	0
25.29	3.08	0.489	13
30.91	4.32	0.489	9
36.53	5.55	0.502	41
42.15	7.40	0.502	22
50.06	9.86	0.502	9
56.20	11.10	0.549	130
64.63	11.71	0.549	95
75.87	12.33	0.549	89
87.11	13.57	0.585	25
109.59	15.42	0.585	16
120.83	16.03	0.585	48
132.07	16.03	0.626	43
148.93	17.27	0.626	36
165.79	18.50	0.626	43
179.84	19.10	0.733	52
191.08	20.35	0.805	39
219.18	21.60	0.805	27

Specimen 1 - continued

STRESS	STRAIN	$\ln(A_1/A_2)$	COUNTS/INCREMENT 1/2 cm
236.04	21.60	0.784	6
247.28	22.20	0.784	9
258.52	22.20	0.763	9
275.38	22.20	0.829	18
286.62	22.81	0.805	22
300.67	23.43	0.805	7
323.15	24.66	0.805	2
340.01	25.90	0.779	17
356.87	27.75	0.779	10
368.11	29.60	0.779	7
384.97	30.84	0.895	1
393.40	32.70	0.895	5
410.26	33.90	0.895	2
415.88	35.80	0.895	0
443.98	37.60	0.895	1
455.22	40.10	0.895	2
469.27	41.90	0.895	0

Specimen 2

0.70	0.62	0.405	0
1.41	1.23	0.405	0
2.11	1.23	0.405	0
2.81	1.23	0.405	0
4.22	1.23	0.405	0
5.62	1.23	0.405	0
7.73	1.23	0.405	0
9.84	1.23	0.405	0
12.65	1.23	0.405	0
16.15	1.23	0.405	1
20.40	1.23	0.405	4
23.90	1.85	0.405	10
26.70	2.47	0.405	23
29.50	3.70	0.405	22
34.40	4.94	0.405	17
38.60	6.17	0.405	27
43.50	7.40	0.405	38
47.10	8.63	0.405	22
50.60	9.86	0.405	21
54.80	11.10	0.405	11
61.10	12.33	0.405	4
65.40	13.57	0.405	16
72.40	15.43	0.405	15
76.60	17.90	0.405	3
80.10	20.36	0.405	8
81.50	25.30	0.425	0

Specimen 3

STRESS	STRAIN	$\text{LN}(A_1/A_2)$	COUNTS/INCREMENT 1/2 cm
0.35	0	0.652	0
1.76	0	0.652	0
3.16	0	0.652	0
5.62	0	0.732	0
8.43	0.93	0.732	0
10.53	0.93	0.732	0
13.34	0.93	0.820	1
16.86	1.54	0.820	3
21.80	1.85	0.779	0
26.00	1.85	0.779	5
31.60	3.08	0.875	2
36.50	3.08	0.875	10
44.90	3.08	0.875	13
52.30	5.55	0.875	6
60.00	5.55	0.875	17
69.30	9.25	0.875	20
76.10	11.10	0.875	8
87.40	13.56	0.875	30
90.60	14.80	0.875	12

Film Removed (H_2SO_4)

88.50	15.30	0.875	27
87.50	16.00	0.875	81
85.00	17.10	0.875	30
85.00	18.00	0.875	5
84.50	19.00	0.875	7
84.50	20.00	0.875	15
84.50	21.00	0.875	2

Specimen 4

STRESS	STRAIN	$\text{LN}(A_1/A_2)$	COUNTS/INCREMENT			
			1/2	3/4	1	2
5.51	0	0.742	0	0	0	0
8.26	0	0.742	0	0	0	0
8.26	0.65	0.742	0	0	0	0
13.77	0.65	0.742	0	0	0	0
19.30	1.36	0.742	0	0	0	0
24.80	1.36	0.742	0	0	0	0
30.40	1.36	0.742	16	8	8	5
38.50	2.77	0.742	0	0	0	0
47.00	2.77	0.742	1	1	1	0
52.30	3.48	0.742	2	1	0	0
57.90	4.19	0.742	0	0	0	0

Specimen 4 - continued

STRESS	STRAIN	LN(A ₁ /A ₂)	COUNTS/INCREMENT			
			1/2	3/4	1	2
68.80	5.60	0.742	1	0	0	0
79.80	7.00	0.742	4	3	0	0
93.80	9.10	0.742	1	0	0	0
104.50	9.85	0.798	0	0	0	0
121.00	11.25	0.798	2	1	1	0
137.50	12.00	0.798	3	2	2	2
154.00	12.70	0.798	2	2	2	0
176.00	13.40	0.798	0	0	0	0
201.00	14.80	0.798	6	3	3	2
223.00	17.60	0.798	76	47	45	24
245.00	19.00	0.798	42	22	22	10
267.00	23.30	0.798	124	58	56	28
284.00	24.60	0.798	34	17	17	8
306.00	26.10	0.693	26	12	9	3
328.00	27.50	0.798	62	39	39	23
342.00	28.90	0.798	23	16	15	9
357.00	29.60	0.798	6	3	3	2
379.00	31.00	0.798	29	18	18	9
396.00	31.80	0.798	28	18	18	9
393.00	31.80	0.798	158	92	91	55
416.00	31.80	0.798	64	41	40	21
447.00	32.40	0.798	68	39	36	15
465.00	33.80	0.798	7	4	3	0
482.00	34.60	0.798	25	14	14	10
498.00	36.00	0.798	20	13	13	5
520.00	36.00	0.798	6	0	0	0
536.00	36.70	0.798	23	14	13	9
556.00	37.40	0.798	14	7	6	3
585.00	39.50	0.798	31	17	17	5
590.00	42.40	0.798	12	5	5	3
618.00	43.80	0.798	5	4	4	1
630.00	45.90	0.798	21	13	13	8
638.00	48.70	0.798	13	8	7	2
646.00	51.50	0.798	4	3	3	1
646.00	54.40	0.798	3	2	2	1
646.00	57.90	0.798	2	1	1	0
646.00	60.70	0.867	0	0	0	0
646.00	65.00	0.867	2	2	2	0
646.00	68.50	0.867	0	0	0	0
646.00	71.30	0.867	0	0	0	0
646.00	74.10	0.867	0	0	0	0
646.00	78.40	0.867	2	1	1	1
646.00	84.00	0.867	0	0	0	0
646.00	87.50	0.867	1	0	0	0
649.00	91.80	0.867	0	0	0	0
652.00	97.30	0.811	1	0	0	0
655.00	101.00	0.867	0	0	0	0
666.00	105.10	0.867	0	0	0	0

Specimen 4 - continued

STRESS	STRAIN	LN(A ₁ /A ₂)	COUNTS/INCREMENT			
			1/2	3/4	1	2
675.00	110.00	0.867	2	0	0	0
689.00	113.80	0.867	2	0	0	0
697.00	119.30	0.867	3	1	1	1
708.00	124.30	0.944	1	0	0	0
717.00	129.20	0.944	4	2	2	1

Specimen 5

2.75	0	1.051	4	0	0	0
5.50	0.71	1.051	2	0	0	0
8.26	2.12	1.051	8	5	5	0
13.80	3.53	1.051	5	2	2	1
24.80	4.95	1.051	10	4	4	2
33.00	6.36	1.051	6	6	6	1
44.00	7.78	1.051	8	8	8	0
55.10	7.78	1.051	6	2	2	0
66.00	8.48	1.051	8	3	2	0
79.80	9.90	1.051	36	20	19	6
85.40	11.30	1.051	11	6	6	0
99.00	12.72	1.051	12	8	8	0
124.00	14.13	1.051	24	6	6	4
143.00	15.55	1.051	15	4	4	1
176.00	16.97	1.051	11	4	2	0
215.00	18.40	1.051	13	8	4	0
248.00	19.10	1.051	9	2	0	0

Film Removed (H₂O)

245.00	19.80	1.051	105	59	46	15
242.00	23.30	1.051	161	153	153	27
242.00	28.30	1.051	111	69	51	19
242.00	31.80	1.051	6	0	0	0

Specimen 6

STRESS	STRAIN	LN(A ₁ /A ₂)	COUNTS/INCREMENT			
			1/2			
2.75	0.71	0.329	1			
5.50	0.71	0.329	0			
5.50	1.41	0.329	0			
5.50	1.41	0.329	1			

Specimen 6 - continued

STRESS	STRAIN	$\ln(A_1/A_2)$	COUNTS/INCREMENT 1/2
5.50	2.12	0.329	0
8.26	2.82	0.329	0
10.95	2.82	0.329	3
13.78	2.82	0.329	0
19.30	2.82	0.329	0
24.80	2.82	0.329	0
30.23	2.82	0.329	1
35.80	6.36	0.344	0
41.30	12.00	0.344	0
46.80	19.10	0.344	1
52.25	26.20	0.344	1
57.90	31.10	0.344	1
63.20	36.80	0.344	0
74.20	43.80	0.344	3
85.40	49.50	0.344	0
96.40	54.40	0.344	2
107.20	58.60	0.344	0
118.30	64.30	0.344	0
132.00	70.00	0.289	0
146.00	76.30	0.289	0
162.20	82.00	0.289	1
176.00	89.00	0.289	1
193.00	96.70	0.289	1
201.00	98.20	0.289	0
215.00	106.60	0.289	2
231.00	112.20	0.289	1
242.00	117.20	0.344	0
253.00	125.00	0.344	3
270.00	131.00	0.344	0
284.00	138.00	0.344	3
300.70	148.00	0.344	1
316.00	156.00	0.300	0
333.00	163.00	0.300	1
350.00	170.00	0.300	3
364.00	178.00	0.300	0
379.00	185.00	0.300	0
385.00	192.00	0.300	0
410.00	198.00	0.300	0
427.00	202.00	0.300	1
438.00	208.00	0.300	1
452.00	210.00	0.300	1
462.00	217.00	0.300	0
474.00	222.00	0.365	1
495.00	225.00	0.365	0
506.00	231.00	0.365	2
518.00	235.00	0.365	2
525.00	242.00	0.365	1
548.00	249.00	0.340	1

Specimen 6 - continued

STRESS	STRAIN	$\ln(A_1/A_2)$	COUNTS/INCREMENT 1/2
560.00	253.00	0.340	0
570.00	259.00	0.340	1
581.00	262.00	0.340	0
587.00	267.00	0.340	0
598.00	271.00	0.340	0
604.00	278.00	0.340	0
612.00	284.00	0.340	0
618.00	290.00	0.340	0
624.00	296.00	0.340	0
624.00	304.00	0.340	2
629.00	310.00	0.340	0
629.00	319.00	0.340	2
629.00	326.00	0.385	0
635.00	335.00	0.385	0
640.00	340.00	0.385	1
640.00	350.00	0.385	1
646.00	357.00	0.385	1
651.00	368.00	0.385	0
651.00	376.00	0.385	0
655.00	383.00	0.385	0
660.00	388.00	0.385	1
666.00	392.00	0.385	0
666.00	394.00	0.451	0
666.00	398.00	0.451	0
677.00	401.00	0.451	1
680.00	405.00	0.451	0
685.00	406.00	0.451	2
675.00	409.00	0.451	2
691.00	410.00	0.451	0
691.00	412.00	0.451	3
691.00	414.00	0.451	1
680.00	417.00	0.451	10
685.00	418.00	0.451	0
680.00	421.00	0.451	5
685.00	422.00	0.451	5
682.00	425.00	0.451	0
677.00	426.00	0.451	7
674.00	428.00	0.451	7
671.00	431.00	0.451	1
671.00	433.00	0.451	0
666.00	435.00	0.451	6
666.00	436.00	0.451	5
666.00	437.00	0.451	0
655.00	439.00	0.451	5
655.00	440.00	0.451	4
649.00	440.00	0.451	4

Specimen 7

STRESS	STRAIN	LN(A ₁ /A ₂)	COUNTS/INCREMENT	
			1/2	Just Above Noise Level
2.75	0.71	0.351	0	0
2.75	2.12	0.351	0	0
5.50	2.83	0.351	0	0
8.26	2.83	0.351	0	0
11.00	3.54	0.351	0	0
16.50	4.95	0.351	0	0
19.25	5.65	0.315	0	0
24.47	6.36	0.368	1	1
33.00	7.07	0.368	0	1
44.00	8.48	0.329	0	4
55.10	12.00	0.357	0	2
66.00	15.55	0.367	2	4
74.40	19.10	0.385	1	2
85.50	23.30	0.385	2	6
93.60	28.30	0.385	0	0
104.50	33.20	0.385	0	0
115.50	38.90	0.385	0	2
126.50	49.50	0.368	0	3
137.80	55.90	0.368	0	0
148.50	61.50	0.368	0	0
159.50	68.60	0.405	0	0
168.00	77.00	0.405	1	1
184.40	86.20	0.405	0	0
198.00	93.20	0.405	0	0
209.00	99.00	0.405	0	1
226.00	106.70	0.405	1	4
242.00	114.50	0.405	0	2
259.00	120.00	0.405	1	3
270.00	124.50	0.405	0	0
287.00	132.00	0.405	1	8
302.00	139.00	0.405	0	1
319.00	144.00	0.405	0	0
336.00	150.00	0.405	1	2
352.00	157.00	0.438	1	7
369.00	163.00	0.438	0	5
388.00	168.00	0.438	0	0
410.00	175.40	0.438	0	1
430.00	181.00	0.393	0	0
445.00	185.00	0.393	0	1
465.00	191.00	0.393	0	2
487.00	197.00	0.393	0	0
503.00	203.00	0.393	0	0
517.00	206.00	0.393	0	1
525.00	214.00	0.393	0	0
548.00	218.00	0.393	0	0
565.00	223.00	0.393	0	0

Specimen 7 - continued

STRESS	STRAIN	LN(A ₁ /A ₂)	COUNTS/INCREMENT	
			1/2	Just Above Noise Level
581.00	231.00	0.393	0	0
598.00	235.00	0.393	0	0
613.00	242.00	0.393	0	0
624.00	245.00	0.393	0	0
640.00	250.00	0.393	0	1
652.00	253.00	0.393	0	0
669.00	259.00	0.393	0	0
677.00	263.00	0.393	0	0
695.00	270.00	0.393	0	0
710.00	275.00	0.393	0	0
725.00	280.00	0.393	0	0
742.00	286.00	0.393	0	0
754.00	290.00	0.393	0	0
767.00	296.00	0.393	0	0
781.00	300.00	0.393	0	0
792.00	304.00	0.393	0	0
804.00	309.00	0.404	0	0
817.00	313.00	0.405	0	0
829.00	318.00	0.405	0	0
840.00	321.00	0.405	0	0
855.00	326.50	0.427	0	1
860.00	331.00	0.427	0	1
877.00	337.00	0.438	0	0
888.00	340.00	0.438	0	0

Specimen 8

STRESS	STRAIN	LN(A ₁ /A ₂)	COUNTS/INCREMENT	
			1/2	
2.75	2.12	0.476	0	
5.51	2.83	0.476	0	
5.51	2.83	0.501	0	
8.26	2.83	0.501	0	
11.02	3.53	0.476	0	
19.25	3.53	0.476	0	
30.21	3.53	0.501	0	
46.76	4.95	0.501	0	
60.70	9.18	0.501	0	
68.85	12.01	0.501	0	
79.80	19.08	0.501	0	
88.23	26.14	0.432	0	

Specimen 8 - continued

STRESS	STRAIN	$\ln(A_1/A_2)$	COUNTS/INCREMENT 1/2
101.72	31.79	0.432	0
112.68	39.65	0.464	0
129.26	46.63	0.464	0
146.12	55.11	0.464	1
162.42	62.17	0.464	2
178.72	70.65	0.464	0
195.30	78.42	0.425	0
217.78	85.49	0.425	0
236.60	92.55	0.454	0
258.52	98.20	0.454	0
281.00	105.27	0.454	1
297.86	108.80	0.454	1
313.32	113.75	0.454	0
338.61	120.81	0.454	1
365.30	129.29	0.454	1
393.40	136.35	0.445	0
415.88	142.01	0.445	1
438.36	147.66	0.445	1
453.82	151.90	0.445	0
481.63	159.67	0.445	0
505.80	166.73	0.445	0
533.90	173.80	0.476	0
564.81	180.86	0.476	1
592.91	189.34	0.476	3
619.61	196.41	0.476	0
646.30	203.47	0.476	0
671.59	209.83	0.510	0
699.69	216.90	0.445	0
716.55	222.55	0.445	0
733.41	225.37	0.476	1
753.08	232.44	0.476	0
769.94	238.09	0.445	1
786.80	242.33	0.445	0
798.04	246.57	0.445	0
809.28	249.39	0.448	1
826.14	256.46	0.448	0
848.62	262.11	0.448	0
865.48	266.35	0.510	0
876.72	267.76	0.448	0
887.96	271.30	0.448	0
904.82	276.95	0.476	0
916.06	282.60	0.476	3
932.92	286.13	0.510	2
944.16	288.96	0.510	0

Specimen 9

STRESS	STRAIN	$\ln(A_1/A_2)$	COUNTS/INCREMENT 1/2
5.51	0.71	0.658	0
5.51	1.41	0.658	0
5.51	2.12	0.658	0
5.51	2.12	0.693	0
8.26	2.12	0.693	0
8.26	2.83	0.693	0
13.77	3.53	0.732	0
27.54	4.95	0.732	6
38.55	6.36	0.732	25
60.58	6.36	0.732	4
79.86	7.07	0.693	15
104.64	8.48	0.693	19
151.46	8.48	0.693	29
217.55	9.89	0.693	9
272.63	12.01	0.693	6
305.67	13.42	0.693	2
363.50	19.78	0.693	13
404.81	26.85	0.693	4
435.10	32.50	0.693	2
451.62	35.33	0.693	0
484.67	41.68	0.693	3

Removed Film (H_2O)

479.16	55.81	0.693	49
479.16	55.81	0.693	22
476.41	50.87	0.693	0
473.65	48.75	0.693	0
473.65	47.34	0.693	0
470.90	46.63	0.693	1
468.15	47.34	0.693	0

Specimen 10

5.51	0	0.693	0
5.51	0	0.658	0
8.26	0	0.658	0
11.02	0.71	0.658	0
16.52	1.41	0.658	0
22.03	2.12	0.658	0
30.29	2.83	0.655	0
41.31	4.24	0.693	0
57.30	9.19	0.654	0
74.35	16.96	0.654	0
85.37	24.02	0.655	0
99.14	33.21	0.655	0

Specimen 10 - continued

STRESS	STRAIN	$\ln(A_1/A_2)$	COUNTS/INCREMENT 1/2
112.91	40.98	0.693	0
123.92	49.46	0.693	0
137.69	56.53	0.693	0
151.46	63.59	0.652	0
167.98	73.48	0.655	1
187.26	81.95	0.693	2
206.54	91.14	0.637	0
228.57	99.62	0.652	1
247.84	107.39	0.693	2
267.12	117.28	0.673	0
289.15	127.17	0.673	1
311.18	135.65	0.637	0
335.96	144.13	0.654	0
357.99	152.60	0.693	0
374.52	156.84	0.654	0

Remove Film (H_2O)

369.01	160.38	0.654	17
357.99	165.32	0.654	5
352.37	163.91	0.654	0
346.75	162.50	0.652	7
341.42	162.50	0.654	2
338.61	161.08	0.652	3
335.80	161.08	0.652	0
330.46	161.79	0.652	0
327.65	161.08	0.693	16
327.65	161.08	0.693	0
327.65	161.08	0.652	0
327.65	161.08	0.652	1

Specimen 11

2.75	1.41	0.438	0
5.51	2.12	0.457	0
5.51	3.53	0.457	0
8.37	4.24	0.457	0
13.77	6.36	0.457	0
24.78	8.48	0.457	0
38.55	11.30	0.457	3
52.03	17.66	0.457	2
60.29	18.37	0.457	4
68.56	19.08	0.457	0
76.81	19.78	0.457	0

Specimen 11 - continued

STRESS	STRAIN	$\ln(A_1/A_2)$	COUNTS/INCREMENT 1/2
87.88	20.49	0.422	0
104.35	23.32	0.476	1
114.07	27.55	0.476	0
126.38	33.91	0.476	0
134.64	40.98	0.534	0
142.91	49.46	0.534	0
151.17	59.35	0.534	2
162.18	68.53	0.501	0
173.19	76.30	0.501	0
186.97	84.78	0.501	0
200.74	93.26	0.501	0
217.26	100.32	0.501	1
239.29	107.39	0.501	0
258.57	114.45	0.501	0
275.09	120.11	0.501	0
Removed Film (H ₂ O)			
269.58	128.58	0.501	26
269.58	131.41	0.501	18
269.58	134.24	0.501	5
266.83	136.35	0.501	5
264.07	137.06	0.501	9
264.07	137.06	0.501	24
264.07	134.23	0.501	0
261.32	131.41	0.501	0
258.56	129.29	0.501	0

MICHIGAN STATE UNIV. LIBRARIES



31293003838863